Modeling Relationships between Cycles in Psychology:

Potential Limitations of Sinusoidal and Mass-Spring Models

by

Elena Martynova

A Thesis Presented in Partial Fulfillment
of the Requirements for the Degree
Master of Arts

Approved April 2019 by the
Graduate Supervisory Committee:

Stephen G. West, Chair
Polemnia Amazeen
Jenn-Yun Tein

ARIZONA STATE UNIVERSITY

May 2019

ABSTRACT

With improvements in technology, intensive longitudinal studies that permit the investigation of daily and weekly cycles in behavior have increased exponentially over the past few decades. Traditionally, when data have been collected on two variables over time, multivariate time series approaches that remove trends, cycles, and serial dependency have been used. These analyses permit the study of the relationship between random shocks (perturbations) in the presumed causal series and changes in the outcome series, but do not permit the study of the relationships between cycles. Liu and West (2016) proposed a multilevel approach that permitted the study of potential between subject relationships between features of the cycles in two series (e.g., amplitude). However, I show that the application of the Liu and West approach is restricted to a small set of features and types of relationships between the series. Several authors (e.g., Boker & Graham, 1998) proposed a connected mass-spring model that appears to permit modeling of more general cyclic relationships. I showed that the undamped connected mass-spring model is also limited and may be unidentified. To test the severity of the restrictions of the motion trajectories producible by the undamped connected mass-spring model I mathematically derived their connection to the force equations of the undamped connected mass-spring system. The mathematical solution describes the domain of the trajectory pairs that are producible by the undamped connected mass-spring model. The set of producible trajectory pairs is highly restricted, and this restriction sets major limitations on the application of the connected mass-spring model to psychological data. I used a simulation to demonstrate that even if a pair of psychological time-varying

variables behaved exactly like two masses in an undamped connected mass-spring system, the connected mass-spring model would not yield adequate parameter estimates. My simulation probed the performance of the connected mass-spring model as a function of several aspects of data quality including number of subjects, series length, sampling rate relative to the cycle, and measurement error in the data. The findings can be extended to damped and nonlinear connected mass-spring systems.

TABLE OF CONTENTS

Page

LIST OF FIGURES

Figure Page

Figure Page

Figure Page

Figure Page

LIST OF TABLES

Table Page

Chapter 1

INTRODUCTION

For much of the history of psychology, researchers did not emphasize the importance of temporal processes underlying behavior. This longstanding neglect of the temporal aspect of psychological variables is understandable given the previous lack of technology available for the repeated assessment of behavior in everyday life (Trull & Ebner-Premier, 2013). Fortunately, since the 1990s technological developments have introduced devices like smartphones, activity trackers, smart watches, and PDAs (personal digital assistants) that permit intensive assessment of our daily lives. This technology, known as ambulatory assessment, dramatically improved our ability to collect intensive longitudinal data, permitting researchers "to study individuals (1) in their natural settings, (2) in real-time (or close to real-time), and (3) on repeated occasions" (Conner & Mehl, 2015). Ambulatory assessment guarantees ecological validity because it is embedded into individuals' daily lives and environments. Such assessment prevents distortions that may occur due to unrealistic laboratory settings (e.g. White, Schulman, McCabe, & Dey, 1989; Wilhelm & Grossman, 2010). Real-time measurement also minimizes cognitive bias resulting from the reconstruction of events in memory.

The number of ambulatory assessment studies in psychology has been rising exponentially since 1985 (Hamaker & Wichers, 2017; Mehl & Conner, 2012; Trull & Ebner-Priemer, 2013). These studies have produced two structures of data that have been previously uncommon in psychology. First are studies of single individuals with a large

number of observations over time (e.g., 50, 100, 1000, or more). Second are studies with a moderate to large number of observations in which data are collected on many participants (e.g., 100 or more). These new data structures require the use of statistical techniques that can address within-individual time series data.

Traditionally, time series data have been analyzed using multivariate (concomitant) time series analysis of the data for single individuals (Box, Jenkins, Reinsel, & Ljung, 2015; Hamilton, 1994; Lutkepohl, 2005). Data are collected at equally spaced observations on two variables, *X* and *Y*. *X* is typically treated as the presumed causal variable and *Y* is treated as the presumed outcome variable. Trends and cycles are removed from the *X* series (and possibly separately from the *Y* series) so that the series will become stationary (the series will have the same mean and variance over time). Time series data typically have a property known as serial dependency in which the observations at X_t and X_{t+d} may have a non-zero correlation, where *d* is the time delay between the two observations. This serial dependency is removed from the series through a transformation so that the standard errors of statistical tests will be proper. Following these transformations, the two series are correlated at the same time point *t* or with the observations in *Y* series lagged a fixed time delay *d* (e.g., 1 day) to examine relationships that take place over time. In the Box and Jenkins (1976) procedure, the trends and cycles are only removed from the *X* series. In the more conservative Haugh and Box (1977) procedure, the trends and cycles are removed from both the *X* and *Y* series. These procedures provide good estimates of the effects of random shocks (perturbations) of the *X*-series on the *Y*-series. However, in the traditional multivariate time series approach, the

cycles in the *X*-series and the cycles in the *Y*-series are treated as a confounder that needs to be removed from the data. However, little attention has been given in the traditional approach to the possibility that the cycles in the *X*-series may have a relationship to the cycles in the *Y*-series.

Within the individual time series area, less attention has been given to statistical methods that permit the investigation of cycles (Chow, Hamaker, Fujita, & Boker, 2009; Liu & West, 2016). In temporal data, cycles are series of measurements that reoccur periodically in the same magnitude order. In the behavioral sciences, cycles have been shown to occur in predictable patterns over fixed periods of time. Some examples include daily mood cycles (Rusting & Larsen, 1998), weekly cycles in sense of autonomy (Ryan, Bernstein, & Brown, 2010), monthly mate preference cycles in women (Wood, Kressel, Joshi, & Louie, 2014), seasonal affective disorder (Johansson et al., 2003), and circannual cycles in sex hormone rhythms (Assenmacher & Jallageas, 1980). Much of the intensive longitudinal data collected in clinical, health, personality, and social psychology has been in the form of daily reports.

Daily data in psychological studies often contain weekly cycles (Brown & Moskowitz, 1998; Larsen & Kasimatis, 1990; Ruscher, 2017). Human functioning has been shown to attune to two types of weekly cycles: (a) socially constructed calendar weekly cycles, and (b) circaseptan biological rhythms (e.g., Campbell, 1986; Halberg, 1983; Haus, Lakatua, Swoyer, & Sackett-Lundeen, 1983; Hilderbrandt & Geyer, 1984; Levi & Halberg, 1982). Psychologists tend to be concerned only with the calendar week cycles that characterize the lives of workers and students in industrial societies. Even

people who do not work or study may still follow weekly cycles because they adjust their lives to the community in which they live, which tends to follow consistent weekly schedules. Synchronized weekly cycles have been observed in mood (Cranford et al., 2006), arousal (McFarlane, Martin, & Williams, 1988), vitality (Sheldon, Ryan, & Reis, 1996), alcohol consumption (Studer et al., 2014), agreeableness, dominance, and submissiveness (Brown & Moscowitz, 1998), and sense of hurriedness, temperature and blood pressure (Tuomisto et al., 2006).

Although commonly synchronized among people, weekly cycles are not manifested identically within all people. Individuals have been shown to differ in their degree of entrainment to weekly cycles. For instance, Larsen and Kasimatis (1990) found that extraverts' day-to-day moods were less associated with 7-day cycles than introverts'. People have also been found to differ in the functional form of their cycles, typically reflected in the day of the week when a certain variable reaches its peak or trough. For example, Ram et al. (2005) found that for most people positive affect peaks on Saturdays, but that the day of the peak also varies from person to person. Similarly, Rossi and Rossi (1977) found that most men's positive affect peaked on Fridays, whereas most women's positive affect peaked on Saturdays. In the so called "blue Monday" phenomenon, negative affect was found to peak on Monday in some studies (e.g., Larsen & Kasimatis, 1990; Stone, Schneider, & Harter, 2012), whereas other studies found that negative affect was maximal at midweek (e.g., McFarlane, Martin, & Williams, 1988; Rossi & Rossi, 1977).

Another complexity attached to cyclical data is the units of time do not have a fully hierarchical structure. Although months are nested within years, days within months, hours within days, and minutes within hours, weeks are *not* nested inside of larger measurement units. This peculiarity of weekly cycles presents potential data analytic complexities when monthly, quarterly or yearly cycles are present in the data as the larger units of time do not represent simple multiples of weeks. Statistical techniques for modeling such cases have received little development, even though cyclic combinations of this kind may occur in our everyday lives. An important example is women's biological menstrual cycles, which are individually phased and thus unsynchronized across women. Rossi and Rossi (1977) have shown that women's weekly cycles combine with their biological menstrual cycles in terms of mood, emotional stability, desire for solitude, social group preference and physiological sensations. Attempts to compare men's and women's weekly cycles can be compromised by the complex pattern of confounding.

Even if a weekly or longer time cycle is theoretically of little interest with respect to a particular study topic, it still can be advantageous to model and remove the influence of the cycle. Ignoring a cycle creates the possibility of bias in the cross-correlation between the outcome and predictor series (Liu & West, 2016). Suppose a researcher is attempting to determine the relationship between daily diet and attention paid to significant others. In many households diet quality may be lower on weekdays and higher on weekends. Similarly, attention paid to significant others may be lower on weekdays and higher on weekends. Hence, if weekly cycles are ignored, a *spurious* positive

relationship between diet quality and attention paid to significant others will be detected in the data. In reality, a true causal relationship does not exist, but rather is produced in the data by a third variable of no theoretical interest to the researcher. Regular work hours can leave minimal time for both nutrition planning and relationship nurturing on weekdays, and hence contribute to the relationship between the two variables. Whenever the cyclical weekly structure affects two variables in the same direction, true positive relationships will be inflated, true negative relationships will be diminished, and non-existent true relationships may become spuriously existent and positive. In contrast, when the cyclical weekly structure affects the two variables in the opposite direction (e.g., stress is high on workdays and low on weekends, whereas alcohol consumption is low on weekdays and high on weekends), existing negative relationships may be inflated, existing positive relationships will be diminished, and non-existent relationships will become spuriously negative. Therefore, in order to ensure that the relationship between two time-dependent variables will be minimally biased, relevant cycles should be detected and controlled for in the analyses. Although many other issues related to everyday experience data, such as trends and serial dependency, have been largely addressed and resolved, methodological tools for modeling of cycles are in an earlier stage of development.

One important exception, which is applicable to cycle detection, is spectral analysis (e.g., Kagan, Reznick, & Snidman, 1987; Kirsch, Silva, Comey, & Reed, 1995; Larsen & Kasimatis, 1990; Warner, 1998). Spectral analysis is a statistical technique that decomposes sequenced data into sinusoidal waves of different amplitude and cycle

length. Spectral analysis helps to determine whether there are any cyclic patterns in the data, how many cyclic patterns exist, and what frequency or period they follow. In publications, spectral analysis is typically represented as a spectral density function (or power spectrum), which contains the average squared amplitude of the sinusoids plotted against ordered values of either the frequencies or periods. The higher the power (*Y* value) corresponding to a certain frequency or period, the larger proportion of variance in the series accounted for by the period (cycle length), and the more stable the cyclical component is that is associated with the particular frequency/period across the series. For instance, if weekly cycles were present in the daily time series, we would expect to see a peak at the period of 7 days, or at the frequency of about .143 (frequency is inverse of period, $1/7 \approx .143$). This method is available and is completely automated in standard statistical programs for time series data, leading to its popularity among psychologists.

Traditional Approaches to Controlling for and Modeling Cycles

When cycles are detected in single-subject data, they are traditionally analyzed using classical time-series methods (Box & Jenkins, 1976; Haugh & Box, 1977; Koopmans, 1995; Warner, 1998). The influence of cycles can be removed or modeled in time series involving a second variable. Once the influence of cycles is removed within each time series, contemporaneous or lagged relationships between two variables can be studied by investigating the relationships between the residuals of one variable (the predictor series) and the observed values of another variable (Box & Jenkins, 1976). Alternatively, the influence of cycles can be removed from both series or relationships between the two series can be investigated by studying the relationships between the

residuals of the two variables (Haugh & Box, 1977). The following four methods have been used in psychology to address cyclic patterns at the single subject time series (within-person) level in aggregated time series analyzed using the multilevel or SEM framework.

Differencing

When the period of the cycle is known (e.g. weekly), a new variable can be created by subtracting the observed measure at each time point from an observed measure at a corresponding time point in the next cycle. For example, if the cycle length is 7 days, a new transformed variable can be calculated by subtracting each Monday's observed value, from the next Monday's observed value, each Tuesday's value from the following Tuesday's value, and so forth, i.e. $Y_{trans(t+7)} = Y_{t+7} - Y_t$ (McCleary & Hay, 1980), where $Y_{trans(t+7)}$ is the transformed variable and Y_t is the observation on day *t*. The transformed variable is analyzed instead of the original variable, removing the impact of the weekly cycles. Some issues associated with this method include (a) the new variable is undefined for the first cycle of the series, so that the number of time points available for analysis is reduced, and (b) the potential introduction of serial dependency in some datasets, leading to biased standard errors (Judd & Kenny, 1981). Of importance, differencing removes cycles from the series, prohibiting the analysis of their potential effects.

Dummy variables

Dummy variables can be added to the regression equation to account for different segments of the cycle of interest. For instance, to account for weekly cycles six dummy

variables can be added to the regression equation to account for each day of the week (with the 7th day serving as the reference day), or a single dummy variable can be added to distinguish weekdays from weekends (Liu & West, 2016). Although this method usually provides a good model fit, it can be challenging to interpret as all of the coefficients are estimated with respect to the reference variable. This challenge can become overwhelming with longer cycles, denser dummy variables (e.g. a dummy variable scheme to account for each hour of the day would require 23 dummy variables), or more individualized cycles (e.g. additional between-individual variables). Thus, dummy variables can result in a cumbersome model that uses up an unreasonable number of degrees of freedom. Modeling the effects of multiple cycles, such as a women's monthly cycle and a weekly cycle is not plausible with dummy variables.

Sinusoid function model

Sine and/or cosine functions potentially provide a more efficient way of detecting and approximating consistent cycles. The basic model that incorporates cycles into a linear regression model can be written as

$$Y_t = b_0 + R[\cos(\omega t + \varphi)] + \varepsilon_t, \quad (1)$$

where Y_t is an observation for a single subject at time t (where $t = 0$ to T), R is the oscillation amplitude, $\omega = 2\pi/\tau$ is frequency of oscillations in radians where τ is their period in units of t, b_0 is the intercept of the time series, φ is the phase shift of the cycle or distance in radians from position at time 0 to the first positive peak, and ε_t is a residual value at time t.

Equivalently, equation (1) may be written in the following form:

$$Y_t = b_0 + b_1 \sin(\omega t) + b_2 \cos(\omega t) + \varepsilon_t, \quad (2)$$

where b_0 is again the intercept, b_1 and b_2 are the regression coefficients associated with the sine and cosine components, respectively, and ε_t is a residual value at time t. The oscillation amplitude R, and phase shift φ are now functions of the coefficients b_1 and b_2 that can be expressed respectively as

$$R = \sqrt{{b_1}^2 + {b_2}^2} \quad (3) \qquad \varphi = \tan^{-1}\left(\frac{-b_1}{b_2}\right) \quad (4)$$

Although parsimonious and convenient, this modeling technique has several limitations. First, not all functional forms of cycles can be represented. Equation (1) only addresses cycles that are symmetric. That is, the first half of the cycle has to be of identical length to the second half of the cycle, with the mean time series value always being crossed in the middle of the cycle. Moreover, the shape of the first half of the cycle, or where the peak of the cycle is, has to be identical to that of the second half of the cycle, where the trough is. Finally, the peaks and troughs can only be of one precise shape, which is defined and restricted by the sinusoid function, its frequency, and amplitude. These three properties are incompatible with a wide range of psychological data. For example, weekly cycles have been shown to generate a significant weekday versus weekend effect for numerous variables (Cranford et al., 2006; Larsen & Kasimatis, 1990; Reid, Towell, & Golding, 2000; Reis, Sheldon, Gable, Roscoe, & Ryan, 2000; Ryan et al., 2010; Ruscher, 2017; Sheldon, Ryan, & Reis, 1996; Stone, Hedges, Neale, & Satin, 1985), which is not fully compatible with the cycle being symmetrical around half its length (3.5 days). Second, having identically shaped peaks and troughs implies that people tend to respond to the opposite extremes of the cycle in exactly the

same way. For instance, it seems unlikely that the pattern of return to baseline from a highly stressful state would be the mirror image of the return to baseline from a highly serene state. Finally, most variables will not produce sinusoidally shaped peaks and troughs that will coincide with the specific peak width dictated by the amplitude and frequency of the oscillations. That is, subjects cannot dwell at the extremes, have transient flashes of extremes, or enter and exit the extremes asymmetrically because it is outside of the sinusoidal definition.

Seasonal trigonometric model

The seasonal trigonometric model from econometrics resolves many of the major problems of the simple sinusoid function model, but it is rarely used in psychology. Bowerman, O'Connell, and Koehler (2004) define a seasonal trigonometric model that allows for the modeling of more complex seasonal patterns:

$$Y_t = b_0 + b_1 \sin(\omega t) + b_2 \cos(\omega t) + b_3 \sin(2\omega t) + b_4 \cos(2\omega t) + \varepsilon_t, \quad (5)$$

where all the terms are the same as in the original sinusoid model, except for the additional sine and cosine components that have frequency that is twice the frequency of the dominant cycle. This seasonal trigonometric model permits the representation of symmetric and asymmetric cycles of many forms. Unlike the original sinusoid function model, it allows the mean value of the time series to be crossed at points other than the midpoint of the cycle. It allows one side of the cycle to be more extensive than the other, which is often more appropriate for modeling weekly cycles. However, several limitations related to the potential shapes of the peaks still remain. The shape of the peaks

does not have to be identical to that of troughs, but these shapes are still strictly determined by the amplitude, the frequency, and the sinusoidal nature of the function.

An Alternative Approach: The Single Mass-Spring Oscillator Model

The single mass-spring model was originally proposed in physics to describe time-dependent physical systems (Boker & Graham, 1998; Butner, Amazeen, & Mulvey, 2005; Hessler, Finan, & Amazeen, 2013). It has been introduced in psychology for the purpose of capturing the periodic dynamics of change in psychological processes. Unlike the sinusoid and dummy variable based models, mass-spring models can capture the frequency of the oscillating process without any prior knowledge about the structure of the process. Moreover, the single mass-spring model is designed to capture damping, if it is stable over time. For example, this model allowed Finan et al. (2010) to examine the decrease in the amplitude of fluctuations in chronic pain prediction accuracy with increased experience. The single mass-spring model can also potentially represent fluctuations whose form deviates from that of a classical sinusoid function. This can be accomplished by the addition of nonlinear escapement terms, which will be discussed in more depth at the end of this section. Mass-spring models are also associated with the visual representation of oscillation in a phase portrait, where position, or the value of a variable at a time point, is plotted against the velocity of the position change. Phase portraits can aid in detection of escapements that allow some energy to enter or escape the cycle, altering its general shape and amplitude (Abraham & Shaw, 1992). Finally, the single mass-spring model allows examination of how parameters representing damping, amplitude, and the form of fluctuation vary based on individual differences.

In this approach, derivatives are used to describe the rate of change of one variable with regard to time. For instance, if a person runs on a straight track and periodically records his/her position at that point in time, the person's rate of change in position with respect to time (a.k.a., *velocity*) can be calculated. To do that, the person's displacement over the time period is divided by the amount of elapsed time: $v_1 = (p_2 - p_1)/(t_2 - t_1)$, where p_1 and p_2 are position of the person at time 1 and time 2 respectively, t_1 and t_2 are time 1 and time 2, and v_1 refers to velocity at the first chosen time interval. Furthermore, the person's *acceleration*, the change in *velocity* over time, can be calculated. To estimate acceleration, the person's rate of change in velocity is divided by the amount of time that passed between the two velocity estimates. Two velocity estimates are needed for this calculation: one estimate at an arbitrary time interval, and the second at a consecutive time interval. The amount of time elapsed between the two velocity estimates is estimated by subtracting the time in the middle of the first interval from the time in the middle of the second interval. If the first velocity estimate is such as defined above (v_1), and the second velocity estimate is $v_2 = (p_3 - p_2)/(t_3 - t_2)$, where p_2 and t_2 are the same as in the equation of v_1, p_3 is the position of the person at some arbitrary but fixed time 3, and t_3 is time 3, the acceleration can be calculated with $a_i = (v_2 - v_1)/(t_{2.5} - t_{1.5})$, where a_i represents acceleration at time interval i, $t_{2.5}$ is time at the midpoint of the time interval between time 2 and time 3, and $t_{1.5}$ is time at the midpoint of the time interval between time 1 and time 2. Mathematically, if the person's position on the *Y*-axis is plotted against time on the *X*-axis, the result is a displacement trajectory, where the

first derivative represents the instantaneous linear slope of the trajectory at a given point, and the second derivative is a function of the acceleration at that given point.

The original expression, first derivative, and second derivative, respectively, represent the position/displacement, velocity, and acceleration. These three variables are needed for mass-spring/oscillator models. Position or displacement in the model can be a measure of any variable of interest, e.g., positive affect, alcohol consumption, or feeling of social acceptance. Following detrending, the first and second derivatives are then usually calculated by the method of local linear approximation (LLA; Boker, 2001; Boker & Graham, 1998). LLA is a generalization of the calculations described in the example above. LLA is the simplest reasonable technique for approximating local derivatives in non-continuous functions. The approximation of the first derivative is calculated by averaging the two slopes that surround the point of interest:

$$\frac{dx_{(t)}}{dt} \approx \frac{x_{(t+\tau)} - x_{(t-\tau)}}{2\tau\Delta t}, \tag{6}$$

where t is a time point at which the approximation is being estimated, Δt is the time interval between equally spaced observations, and τ is a selected time lag between the measures in units of Δt. As Δt approaches 0, the estimate approaches the true derivative of the function.

Local linear approximation of the second derivative can be similarly calculated by

$$\frac{d^2x_{(t)}}{dt^2} \approx \frac{x_{(t+\tau)} - 2x_{(t)} + x_{(t-\tau)}}{\tau^2\Delta t^2}. \tag{7}$$

The original expressions, first, and second derivatives of the variable of interest are then combined with linear motion coefficients to emulate the motion of a stably oscillating physical system. The two simplest physical systems that exhibit behavior of the kind are

a pendulum and a mass-spring. The physical basis of the second order oscillator model will be delineated in my thesis in terms of the mass-spring motion. All of the statements that I will make in relation to the physical basis of the oscillator model can be easily translated to the laws of motion of a pendulum or a pair of connected pendula. These physical systems are commonly used to illustrate the mass spring model as a representation for cyclical behavior in psychology.

A mass-spring oscillator consists of a weight attached to a spring fixed to a rigid wall at one end.

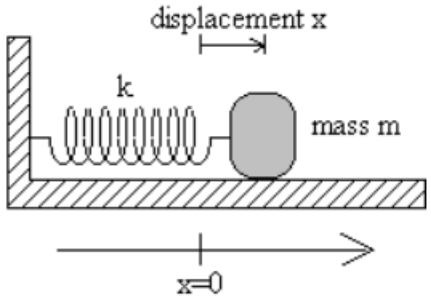

Figure 1. *A single mass-spring oscillator system.*

In an ideal, perfectly frictionless system, when the weight is displaced from its equilibrium position, it oscillates toward and away from the wall forever. In contrast, if there is friction between the mass and the surface, a decreasing oscillation amplitude will occur until the equilibrium position is reached. The force equation of the one-mass oscillator is a single 2nd order differential equation that is elaborated from Newton's second law of motion, which applies to unbalanced mechanical systems. The force equation states that exerted force equals to mass times acceleration ($F = ma$), where acceleration is the second derivative of position/displacement from the equilibrium (x) with respect to time ($a = d^2x/dt^2 = x''$). Whenever the weight is displaced from the

equilibrium, the compressed or stretched spring exerts a force that is opposite, and typically directly proportional to the displacement x (Hooke's law):

$$F_{spring} = - kx \,, \tag{8}$$

where *k* is a spring constant, or *stiffness* of the spring. The higher the stiffness, the more resistant to deformation the spring is, and the faster it will return to the equilibrium. The negative sign in (8) represents the opposing nature of the force.

Another force that is present in most mechanical systems is friction. It is modeled as a term proportionate to velocity:

$$F_{friction} = -b\frac{dx}{dt} = - bx', \tag{9}$$

where *b* is the *damping coefficient*, which represents intensity of the resistance of the surface to the movement of the mass, and *x'* represents the first derivative of *x* with respect to time. The negative sign in equation (9), as in the previous formula, reflects the opposing nature of the force.

The total equation representing the system (elaborated from the Newton's 2nd law) is:

$$F = F_{spring} + F_{friction} = - kx - bx' = mx'' = ma, \tag{10}$$

where x'' represents the second derivative of *x* with respect to time.

In psychology, mass-spring models have been typically used in a slightly different form that eliminates the explicit notion of mass from the formula, and which contains coefficients that relate more directly to the motion trajectory of the oscillations rather than the purely physical characteristics of the system. The motion trajectory is of

sinusoidal nature and is represented by Figure 2:

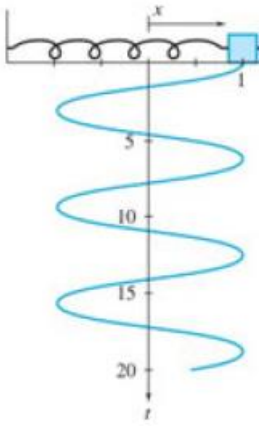

Figure 2. *Motion trajectory of an undamped mass-spring oscillator. Adapted from Nagle, Saff & Snider (2010).*

Equation (10) can be rearranged into:

$$\frac{d^2x}{dt^2} = -\omega^2 x - 2\zeta\omega\frac{dx}{dt}, \qquad (11)$$

where ω is *angular frequency* (equal to $\sqrt{k/m}$ radians/second, or $\sqrt{k/m}/2\pi$ periods/second), and ζ is *damping ratio* (equal to $\frac{b}{2\sqrt{mk}}$). The ω represents the frequency of the oscillations produced by the system in radians. To get the preferred frequency units used in the behavioral sciences, periods per time unit, ω has to be divided by 2π (perimeter of a unit circle in radians). Higher ω values indicate higher oscillation frequency. The damping ratio, ζ, represents the dissipation or gain in energy that is manifested in a constant increase or decrease in the amplitude of the fluctuations (see Figure 3). When $\zeta > 0$, the magnitude of the oscillation amplitude decreases; when $\zeta < 0$,

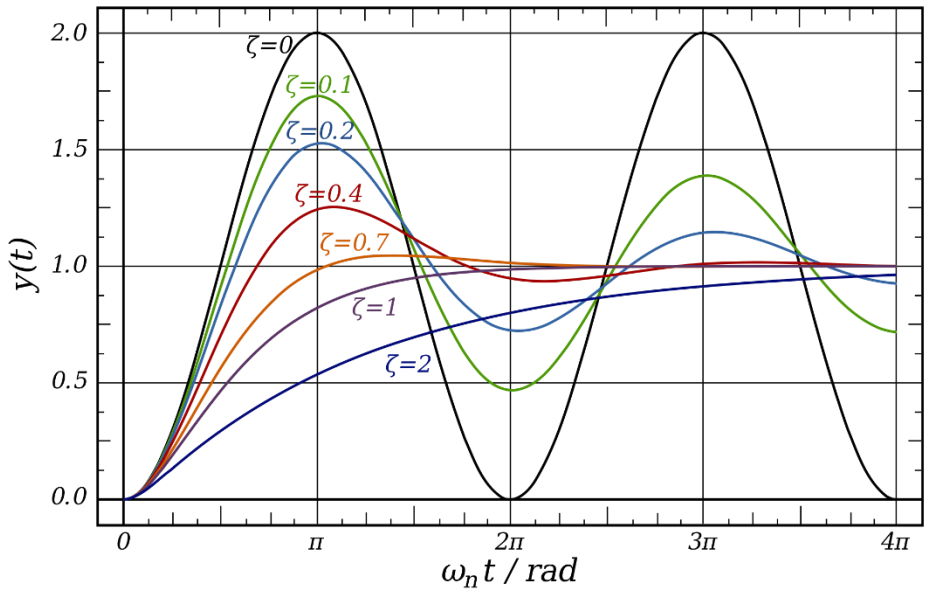

Figure 3. *The effect of the damping ratio on the oscillations produced by the mass-spring oscillator ("Damping ratio," n.d.).*

it increases; and when ζ = 0, the fluctuation amplitude remains constant (no damping). The shape of the motion trajectory of the mass over time is of sinusoidal nature, unless the system is critically damped (ζ = 1) or overdamped (ζ > 1, see Figure 3), in which case the motion trajectory is represented by a decaying exponential with no oscillation.

In order to capture fluctuations of different shapes, nonlinear terms, also called nonlinear escapements, can be added to the equation (Abraham & Shaw, 1992; Beek, Schmidt, Morris, Sim, & Turvey, 1995; Butner et al., 2005; Finan et al., 2012; Hessler et al., 2013). They represent influences on the system by some external process or object. Such external influences are potentially relevant to psychological processes because they are never isolated from other factors. A physical example of such an external influence would be the working of the grandfather clock: its pendulum never stops moving because the mechanism of the clock consistently injects energy at a certain point of its swing (see

Hessler et al., 2013). This influx of pulses of energy produces sudden changes in the amplitude and velocity of the oscillation, which makes the process nonlinear. In general, addition of any nonlinear term(s) to the mass spring model turns it into a nonlinear model.

There are four classical nonlinear terms that can be added to the mass spring model: two conservative and two nonconservative. The two conservative terms, Duffing and π-mix odd series, model the changes in the oscillatory cycles without affecting the overall energy of the system. They alter the motion trajectory of the oscillator while the sum of potential energy stored in the springs and kinetic energy of the moving masses remains the same at all times as it would be without the nonlinear terms. In contrast, the two nonconservative terms, Rayleigh and Van der Pol, capture cyclic shapes that require alterations in the system's total energy: positive values of the terms signify energy injection, whereas negative values signify energy removal. The four nonlinear terms are of higher order and are described by the cubed displacement (Duffing, δ), squared velocity multiplied by displacement (π-mix odd series, μ), cubed velocity (Rayleigh, ρ), and velocity multiplied by squared displacement (Van der Pol, ν). The 2nd order oscillator model with all four nonlinear terms included is presented in equation (12):

$$\frac{d^2x}{dt^2} = -\omega^2 x - 2\zeta\omega\frac{dx}{dt} + \delta x^3 + \mu\left[\frac{dx}{dt}\right]^2 x + \rho\left[\frac{dx}{dt}\right]^3 + \nu\left[\frac{dx}{dt}\right]x^2. \quad (12)$$

In equation (12), δ, μ, ρ, and ν are coefficients that correspond to the Duffing, π-mix odd series, Rayleigh, and Van der Pol nonlinear terms, respectively, and x is displacement from the equilibrium point, or deviation of the variable score from its mean value across the time series. It is extremely rare, however, for all the nonlinear terms to be needed in

the model. Usually only one or at most two terms suffice to describe the irregular shape of the oscillation trajectory. In physical and biological sciences the need for the particular nonlinear terms can often be determined from the theory of the physical processes modeled (e.g., Beek & Beek, 1988; Beek et al., 1995). In behavioral sciences, however, such theories are currently rare likely due to the recency of researchers' interest in the cyclic changes over time. Behavioral scientists tend to add nonlinear terms into the mass-spring model arbitrarily, retaining those that attain statistical significance or reach a desired effect size. Hypotheses are offered post hoc to explain the results of the fitted model (e.g., Finan et al., 2012).

Both the original linear oscillator model, and the extended nonlinear oscillator model can be written in the form of a regression equation, respectively:

$$x''_{(t)} = b_1 x_{(t)} + b_2 x'_{(t)} + e_{(t)}, \quad (13)$$

$$x''_{(t)} = b_1 x_{(t)} + b_2 x'_{(t)} + b_3 x^3_{(t)} + b_4 [x'_{(t)}]^2 x_{(t)} + b_5 [x'_{(t)}]^3 + b_6 x'_{(t)} x^2_{(t)} + e_{(t)}. \quad (14)$$

In equations (13) and (14), $b_1 = -\omega^2$, $b_2 = -2\zeta\omega$, $b_3 = \delta$, $b_4 = \mu$, $b_5 = \rho$, $b_6 = \nu$, and $e_{(t)}$ is the residual at time *t*.

Although estimated as a part of a simple regression equation, the terms have different interpretations from those in standard regression models. Rather than resulting in a linear functional form, the equation estimates the parameters of a periodic function that is likely to be produced by the motion of a mass-spring oscillator given some initial conditions. Some possible resulting functions are shown in *Figure 4*, panels *a* and *b*.

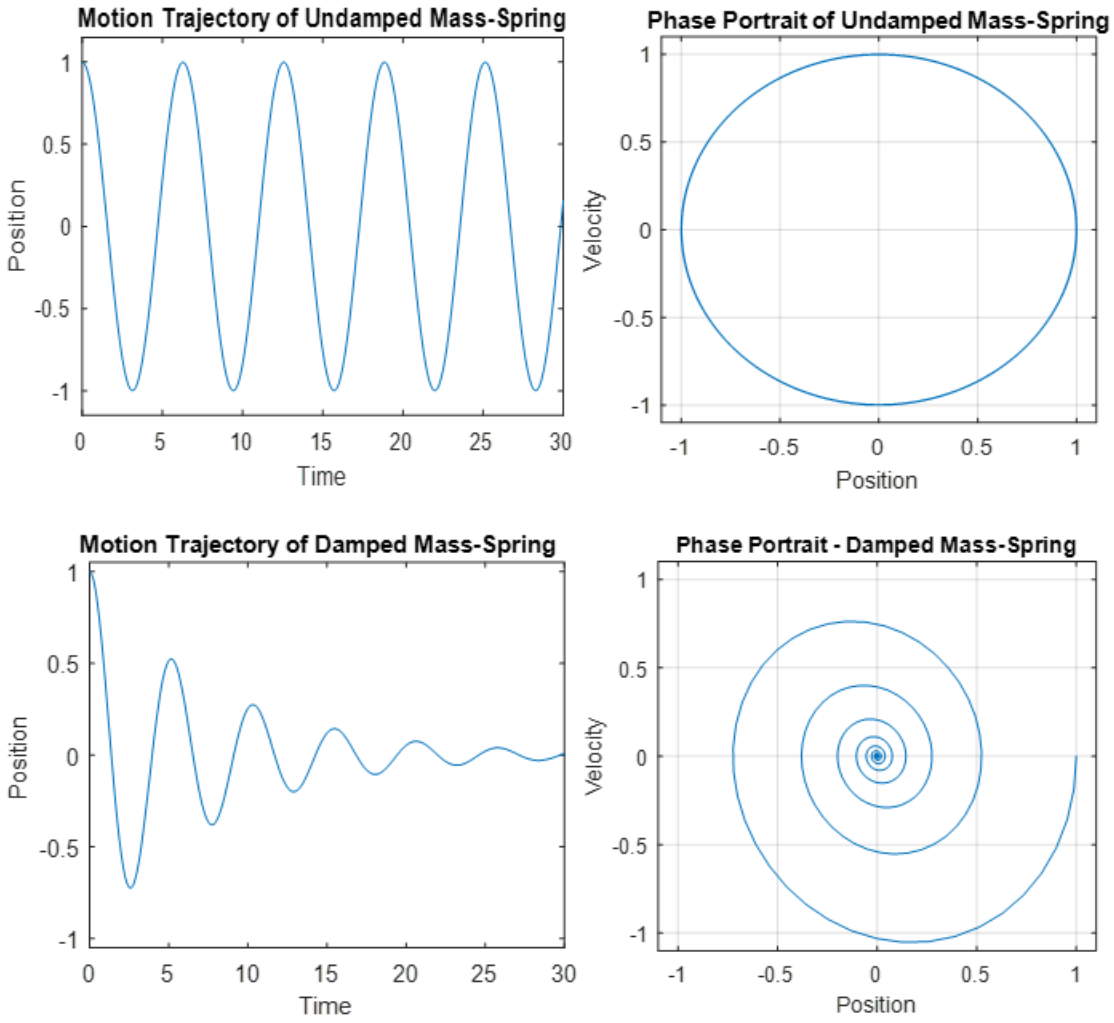

Figure 4a*. Motion trajectories and phase portraits of undamped and damped mass-springs.*

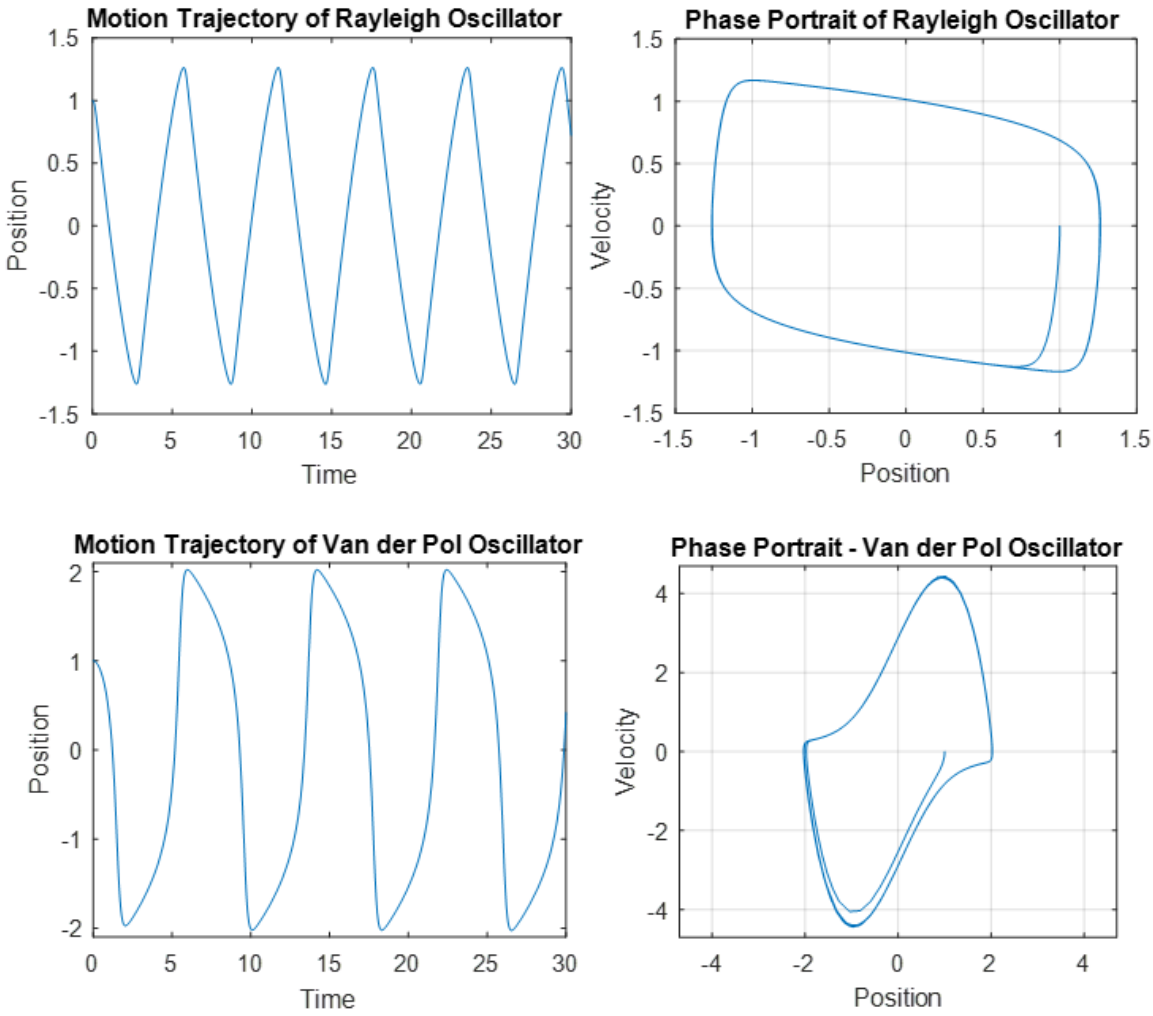

Figure 4b. *Motion trajectories and phase portraits of undamped Rayleigh and Van der Pol oscillators. (Note: Duffing and π-mix odd series oscillators are not plotted because they do not alter the shape of the movement trajectory, only the frequency with which it is traversed.)*

Single mass-spring oscillator models have typically been used in psychology to examine self-regulation. Typical questions the model was designed to answer were: (a) what is the baseline fluctuation frequency in different individuals, and (b) how is the model affected by internal self-regulation and external influences (e.g., Chow, Ram, Boker, Fujita, & Clore, 2005; Boker & Graham, 1998).

Connected Mass-Spring Oscillator Model

The single oscillator model, while suitable for modeling psychological rhythmicities for a single variable, needs to be extended (e.g., Boker & Graham, 1998; Butner et al., 2005; Hessler et al., 2013) to account for the oscillatory processes of two variables. The oscillatory processes of the two variables may be related, which is termed coupling. There are numerous psychological variables whose oscillatory change is coupled with the oscillatory change of at least one other variable. For instance, daily fluctuation in alcohol consumption has been shown to be related to the daily change in reported stress (Armeli, Carney, Tennen, Affleck, & O'Neil., 2000). Changes in reports of chronic pain have been shown to be related to reports of insomnia (Smith & Haythorntwaite, 2004; Kelly, Blake, Power, O'Keeffe, & Fullen, 2011), stress (Davis, Zautra, & Smith, 2004), and depression symptoms (Wilson et al., 2002). Changes in reported intimacy and disclosure in wives has been shown to be related to the reported intimacy and disclosure of their husbands (Boker & Laurenceau, 2007).

The coupled oscillator model can be described in terms of a physical system consisting of a mass-spring system with two weights that are each attached to a spring that is fixed to a wall and a spring that connects them to each other (see Figure 5). Both masses are free to move, therefore, the system can produce a variety of periodic and quasiperiodic motion trajectories given different initial displacement and velocity

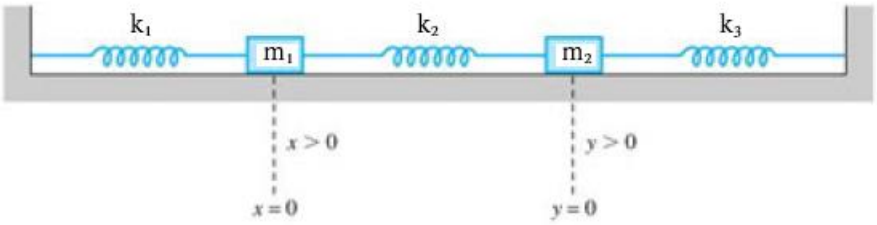

Figure 5. *Coupled mass-spring system with fixed ends (adapted from Nagle, Saff, & Snider, 2010).*

conditions. Since the system is comprised of two masses, the coupled oscillator model can be represented by the system of two 2nd order differential equations. These differential equations originate from Newton's second law of motion and Hooke's law. The simplest coupled oscillator model assumes no effects of friction or of gravity. If Newton's second law is applied to each of the weights in a coupled mass spring system, equations (15a) and (15b) result.

$$F_1 = m_1 a_1 = m_1 x'' \quad (15a)$$
$$F_2 = m_2 a_2 = m_2 y'' \quad (15b)$$

The total force of the first freely moving weight is equal to the product of its mass and acceleration, the second derivative of its displacement with respect to time. The total force of the second weight is equal to the product of its mass and its acceleration, the second derivative of its displacement with respect to time. Finally, the forces generated by the movement of springs (Hooke's law) need to be considered. For the left weight, consider the force of the spring that attaches it to the wall. As in the case of the single mass-spring model, this force can be written as:

$$F_{1\ spring1} = -k_1 x, \quad (16)$$

where $F_{1\ spring1}$ refers to the force that acts on the *first* mass due to the *first* spring (see Figure 5), k_1 is the stiffness of the *first*/leftmost spring. The formula describes the

opposing force produced by the spring when it is stretched or compressed, which is directly proportional to the displacement (Hooke's law). The second force, $F_{1\ \text{spring2}}$, acts on the *first* mass due to the *second*/middle spring that attaches the left weight to the right one. This force pulls the left weight proportionally to the displacement of the middle spring from its natural length ($y - x$):

$$F_{1\ spring2} = k_2 (y - x). \qquad (17)$$

That is, if the middle spring is stretched ($y - x > 0$), it will pull the left weight to the right, away from its wall, in the positive direction. If the middle spring is compressed ($y - x < 0$), it will push the left weight to the left, towards its wall, in the negative direction.

Considering now the *second*/right weight, it will be:

$$F_{2\ spring3} = -k_3 y \quad (18), \qquad F_{2\ spring2} = k_2 (x - y) \qquad (19).$$

Finally, considering the left and right weights together, the system can be defined by

$$\begin{cases} F_1 = m_1 a_1 = m_1 \mathrm{x}'' \\ F_2 = m_2 a_2 = m_2 \mathrm{y}'' \end{cases} \rightarrow \begin{cases} F_{1\_spring1} + F_{1\_spring2} = m_1 \mathrm{x}'' \\ F_{2\_spring3} + F_{2\_spring2} = m_2 \mathrm{y}'' \end{cases} \rightarrow$$

$$\begin{cases} m_1 \mathrm{x}'' = -k_1 x + k_2 (y - x) \\ m_2 \mathrm{y}'' = -k_3 y + k_2 (x - y) \end{cases} \qquad (20)$$

and then rearranged into

$$\begin{cases} \frac{d^2 x}{dt^2} = -\omega_1^2 x + \kappa_1 (\mathrm{y} - \mathrm{x}) \\ \frac{d^2 y}{dt^2} = -\omega_2^2 y + \kappa_2 (\mathrm{x} - \mathrm{y}) \end{cases} . \qquad (21)$$

In equation set (21), ω_1 is the natural angular frequency of the first mass ($= \sqrt{k_1/m_1}\,/2\pi$ periods/s), ω_2 is the natural angular frequency of the second mass

(= $\sqrt{k_3/m_2}\,/2\pi$ periods/s), κ_1 is the coupling coefficient that describes the influence of the displacement of the right mass on the movement of the left mass (= k_2/m_1), and κ_2 is the coupling coefficient that describes the influence of the displacement of the left mass on the movement of the right mass (= k_2/m_2). Since there are two coupling coefficients, and they can vary from each other, the influence of one weight on the other and vice versa can be asymmetric. In the physical model, the asymmetry comes from the different mass of the weights. If one weight is 1 kg and the other 1 g, the heavier weight will have much more influence on the lighter weight than vice versa. In the case of psychological variables, such a result would imply that there is a bidirectional causal relationship between two variables with, for instance, daily stress influencing mood more than mood influencing daily stress.

Illustrations of motion trajectories produced by the movement of the coupled mass-springs are depicted in Figure 6. In addition to the dependence on the physical parameters of the system, motion trajectories also depend on the initial conditions (initial position and velocity) of the masses. Both pairs of trajectories depicted in Figure 6 are periodic and symmetric. However, asymmetric and quasiperiodic trajectory pairs can also

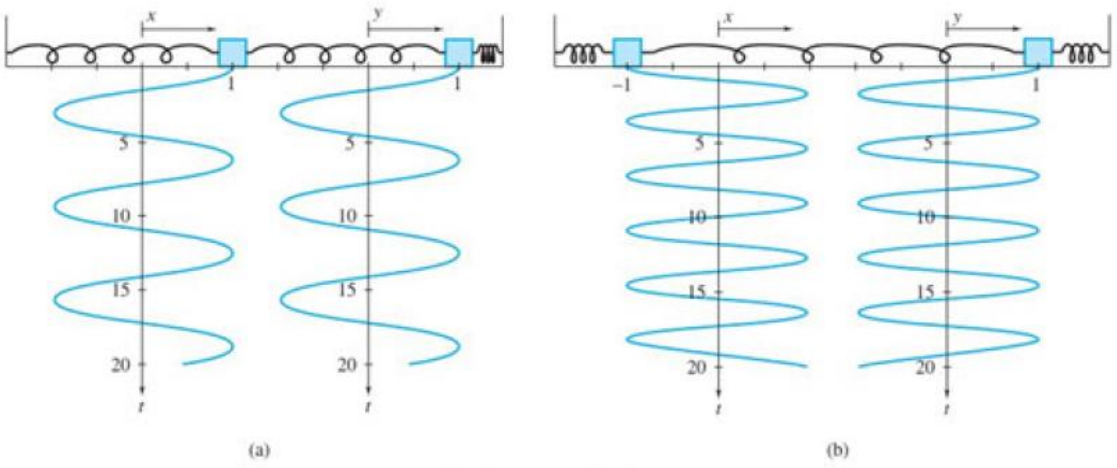

Figure 6. *Motion trajectories produced by a coupled mass-spring oscillator with two identical masses and three identical springs, but different initial conditions (taken from Nagle, Saff, & Snider, 2010).*

be produced. An example of a quasiperiodic pattern in the context of weekly cycles in two variables would occur if similar, but slightly different trajectories were observed from week to week. These weekly trajectory changes represent carryover effects from the interaction of the two variables during the previous week.

The basic coupled oscillator model considered above is the simplest version, in which only the position of the two masses is considered. Researchers in psychology have also suggested extensions of the coupled oscillator model that include friction in the definition of displacement of both individual masses, but not in their coupling terms (see model 22; Butner et al., 2005), and that include friction in the definition of displacement of both individual masses, and in their coupling terms (see model 23; Boker & Graham, 1998). The addition of the nonlinear terms to all three types of coupled models, represented by equation systems (21), (22), and (23), has also been suggested as an

option in the literature (e.g. Butner et al., 2005; Boker & Graham, 1998; Hessler et al., 2013).

$$\begin{cases} \frac{d^2x}{dt^2} = -\omega_1^2 x - 2\zeta\omega_1 \frac{dx}{dt} + \kappa_1(\mathrm{y} - \mathrm{x}) \\ \frac{d^2y}{dt^2} = -\omega_2^2 y - 2\zeta\omega_2 \frac{dy}{dt} + \kappa_2(\mathrm{x} - \mathrm{y}) \end{cases} \tag{22}$$

$$\begin{cases} \frac{d^2x}{dt^2} = (-\omega_1^2 x - 2\zeta\omega_1 \frac{dx}{dt}) + \kappa_1(-\omega_2^2 y - 2\zeta\omega_2 \frac{dy}{dt}) \\ \frac{d^2y}{dt^2} = (-\omega_2^2 y - 2\zeta\omega_2 \frac{dy}{dt}) + \kappa_2(-\omega_1^2 x - 2\zeta\omega_1 \frac{dx}{dt}) \end{cases} \tag{23}$$

Statistical Estimation of Oscillator Models

Two closely related statistical methods for the estimation of the parameters in the mass-spring oscillator models, especially the coupled ones, have been proposed: multilevel models (Butner, Amazen, & Mulvey, 2005; Hessler, Finan, & Amazeen, 2013) and structural equation models (Boker & Graham, 1998; Boker et al., 2008; Chow et al., 2005). In my thesis I focus on the multilevel approach. Multilevel models permit partitioning the data to separately represent both intra- and inter-individual effects. If connected oscillator models operate in ways that psychology researchers claim they do, the multilevel approach can represent potential individual differences in intra-individual oscillatory processes when data are available for multiple participants. The multilevel approach can represent each of the effects as either fixed or random, which means that oscillation frequencies, damping rates and the presence/absence and level of nonlinear escapements can be modeled as stable (fixed) across individuals, or varying for different individuals with an assumed underlying normal distribution. Furthermore, nonlinear escapements as well as other predictor or moderator variables, if they are theoretically relevant, can be added to either level of the multilevel model.

Returning to the simple undamped single oscillator model originally presented in equation (11), this model can be estimated as a multilevel model as follows:

$$\frac{d^2x_{ti}}{dt^2} = \eta_i x_{ti} + \varphi_i \frac{dx_{ti}}{dt} + e_{ti}, \quad \text{Level 1} \tag{24}$$

where $\eta_i = -\omega_i^2$ or the negative squared angular frequency for person *i*, and $\varphi_i = -2\zeta_i\omega_i$ or negative product of the damping ratio and angular frequency for person *i*. The displacement, first (velocity), and second (acceleration) derivatives of variable *x* are typically calculated by using the local linear approximation method described above. Note that *x* now has the subscript *t* that identifies the time at which the observation was made and the subscript *i* that identifies the individual on whom the observations were made. Note also that an additional term e_{ti} is included reflecting the error of prediction. e_{ti} is assumed to be normally distributed with mean 0, and a common variance across individuals of σ^2, $\sim N(0, \sigma^2)$.

At level 2 of the multilevel model, potential random effects can be represented as:

$$\begin{aligned} \eta_i &= \gamma_1 + u_{1i} \\ \varphi_i &= \gamma_2 + u_{2i}. \end{aligned} \quad \text{Level 2} \tag{25}$$

In equation (25), γ_1 and γ_2 represent the mean negative squared angular frequency across individuals and the mean damping ($-2\zeta_i\omega_i$) across individuals, respectively. u_1 represents the interindividual variation in γ_1 and u_2 represents the interindividual variation in γ_2. u_1 and u_2 are assumed to have a bivariate normal distribution with means 0, variances τ_0, τ_1, and covariance τ_{01}. The level 1 equation can be extended to include nonlinear and other terms that have not been utilized in the psychological literature, but that may make

sense on a mechanical level for the model underlying system (Boker & Graham, 1998; Butner et al., 2005).

Extending the multilevel approach to the coupled oscillator model, a three level multilevel model is needed in the general case in which there are random effects (Butner et al. 2005). The 1st level equation (corrected version[1] of the equation 8 in Butner et al., 2005) in any case would be:

$$\frac{d^2x_{pit}}{dt^2} = \beta_{1it}(D1_{pit}) + \beta_{2it}(D2_{pit}) + r_{pit}\ . \qquad \text{Level 1} \tag{26}$$

In equation (26), $\frac{d^2x_{pit}}{dt^2}$ represents the acceleration of the variable (mass) p in individual i at time t. β_{1it} is the random slope for indicator variable $D1_{pit}$, which is also the acceleration of mass 1 at time t in individual i. β_{2it} is the random slope for indicator variable $D2_{pit}$, which is the acceleration of mass 2 at time t in individual i. Given that this is a no intercept model, $D1_{pit}$ is an indicator variable that is coded 1 if the data point belongs to the differential definition of the first variable/mass, analogous to the first equation in the equation system 21 (p=1), and 0 if it belongs to the definition of the

[1] In the Level 1 equation (26) a subscript p that refers to the process equation number was added to the error coefficient (r_{ij} in Butner et al., 2005, where i refers to time) as the vector length and, accordingly, the subscript structure of the level-1 outcome variable and the level-1 error term in a multilevel model must align (Raudenbush & Bryk, 2002). In the Level 1 equation (26) and Level 2 equations (27) and (28), a subscript t that refers to time was added to the random slope coefficients (β_{1j} and β_{2j} in Butner et al., 2005, where subscript j refers to individual) and the error coefficients (e_{1j} and e_{2j}in Butner et al., 2005) as the Level 2 outcome variable vector length and, accordingly, the subscript structure must align with those of the error terms and predictor variables in the level 2 equations (Raudenbush & Bryk, 2002). Based on the same justification, subscripts i and t that refer to individual and time, respectively, were added to the predictor variables that represent displacement and velocity in Level 2 equations (27) and (28), ($disp_1$, $disp_2$, vel_1, vel_2 in Butner et al., 2005). All the corrections were made in accordance with the authors' intentions expressed in the text surrounding the corrected models.

second variable/mass, analogous to the second equation in the equation system 21 (p=2). r_{pit} is the level 1 error term for individual i at time t, again assumed to be $\sim N(0, \sigma^2)$.

The 2nd level of the multilevel model then contains the two equations that describe the motion of the two masses/variables. The simplest coupled mass-spring model without any damping, that includes a coupling term that depends solely on displacement, such as described by the equation system (21), would be defined at level 2 of the connected mass-spring multilevel model by

$$\beta_{1it} = \eta_1 x_{1it} + \kappa_1(x_{2it} - x_{1it}) + e_{1it} \quad \text{Level 2}$$
$$\beta_{2it} = \eta_2 x_{2it} + \kappa_2(x_{1it} - x_{2it}) + e_{2it}. \quad (27)$$

In Equation set (27), η_1 and η_2 represent the mean negative squared angular frequency across individuals and time points of mass/variable 1, and mass/variable 2, respectively. κ_1 and κ_2 represent the mean coupling influence across individuals and time points of mass/variable 2 on mass/variable 1, and mass/variable 1 on mass/variable 2, respectively. e_{1it} represents the interindividual residual variation in the force estimate of the first mass, and e_{2it} represents the interindividual residual variation in the force estimate of the second mass. e_{1it} and e_{2it} are assumed to have a bivariate normal distribution with means 0, variances τ_0, τ_1, and covariance τ_{01}.

Butner et al. (2005) suggest that damping terms and nonlinear terms can be added to the level 2 equations, if needed. For example, if both masses/variables are known to oscillate over time with a decrease in amplitude, and an irregularity in motion that resembles the one produced by the inclusion of the π-mix odd series term, level 2 of the connected mass-spring model would be defined by

$$\beta_{1it} = \eta_1 x_{1it} + \varphi_1 \frac{dx_{1it}}{dt} + \mu_1 \left[\frac{dx_{1it}}{dt}\right]^2 x_{1it} + \kappa_1(x_{2it} - x_{1it}) + e_{1it} \qquad \text{Level 2}$$

$$\beta_{2it} = \eta_2 x_{2it} + \varphi_2 \frac{dx_{2it}}{dt} + \mu_2 \left[\frac{dx_{2it}}{dt}\right]^2 x_{2it} + \kappa_2(x_{1it} - x_{2it}) + e_{2it}. \qquad (28)$$

In equation set (28), φ_1 and φ_2 represent the mean damping ($-2\zeta\omega$) across individuals and time points of mass/variable 1, and mass/variable 2, respectively, and μ_1 and μ_2 represent the mean π-mix odd series term across individuals and time points in mass/variable 1, and mass/variable 2, respectively.

Finally, if any of the coefficients vary across individuals, level 3 terms can be added to define them the same way as it was done in equation (25). For instance, if in the model whose level 2 is defined by equation set (27) the coupling varies across individuals, they could be defined in the level 3 as

$$\kappa_1 = \theta_1 + v_{1i}$$

$$\kappa_2 = \theta_2 + v_{2i}\,. \qquad \text{Level 3} \qquad (29)$$

In equation (29), θ_1 and θ_2 represent the mean coupling influence across individuals of mass/variable 2 on mass/variable 1, and mass/variable 1 on mass/variable 2, respectively. v_{1i} and v_{2i} represent the interindividual variation in the coupling terms κ_1 and κ_2, respectively. v_1 and v_2 are assumed to have a bivariate normal distribution with means 0, variances τ_0, τ_1, and covariance τ_{01}.

Connection of Motion Trajectories to the Existent Psychological Models

Although the mass-spring oscillator model coefficients describe the properties of the physical system, the motion trajectory of the masses is a function that directly describes the behavior of the masses (or variables of interest) over time, given certain

initial conditions. The motion trajectory (see Figures 2 and 6 for illustrations) is a function that approximates the distribution of the data points of the time series with the *X*-axis representing time and *Y*-axis being the position of the mass, or, in a psychological context, the magnitude of the score on the variable. The motion trajectory of a classical mass-spring system has a sinusoidal functional form. When inserted into a regression equation, it can model cyclic behaviors of variables together with their cyclic relationships. The traditional sinusoid model and seasonal trigonometric model from time series analysis discussed above are equivalent to the motion trajectories of two specific mass-spring systems. The sinusoid model corresponds to the trajectory produced by an undamped single mass-spring system with ω of the mass-spring system equal to the ω in the sinusoid model (Equation 2). The seasonal trigonometric model corresponds to the motion trajectory of one mass of a connected mass-spring system, with ω_1 and ω_2 of the force equations equal to the ω in the seasonal model, and the sum of the coupling coefficients $\kappa_1 + \kappa_2 = 3\omega^2$.

This analysis implies that the sinusoid model models a variable over time that is isolated from other variables and has no cyclic relations with them. When it is used in a multilevel model as suggested in Liu and West (2016) to model cycles in both the predictor and the outcome variable, cycles are modeled separately in the predictor and the outcome variable. A sinusoidal form is chosen by the researchers separately for each variable without any consideration of how the cycling pattern of the predictor variable might be affecting the cycling of the outcome variable and vice versa. If the cycles interact, then the linear relationships detected between the predictor variables and the

outcome will be inaccurate. A physical analogy of this would be attempting to model the motion of the two masses in the undamped connected mass-spring system with two separate single mass-spring oscillators. Motion trajectories of each of the masses in the undamped connected mass-spring system consist of a combination of two different frequencies, which, if not nested within each other, can produce cyclic patterns that vary within each period. Motion trajectories of the masses in single undamped mass-spring systems consist of symmetric sinusoids of one set frequency that are identical within each period. Therefore, modeling trajectories of the masses from an undamped connected mass-spring system with the trajectory patterns expected from two distinct single mass-spring systems would yield inaccurate estimates due to model misspecification. A very simplified abstract visual example for a pair of cycles without a cyclic interaction, and for a pair of cycles with a cyclic interaction is depicted in Figure 7.

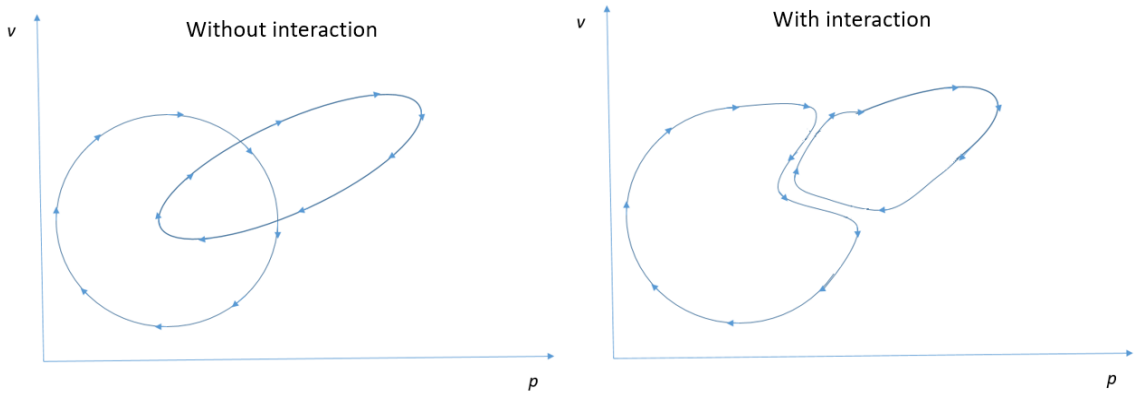

Figure 7. *Hypothetical phase portraits of two processes that cycle independently (without interaction) versus two cycles whose cycling interacts, with position on the x-axis and velocity on the y-axis.*

Some features of cyclic interactions that are uncommon in linear relationships include: 1) cyclic interactions being able to produce patterns that vary over time; 2) interacting cycles typically having asymmetric bidirectional relationships; 3) interacting

cyclic variables influencing each other's position, velocity, and acceleration over time; 4) interacting cyclic variables influencing the amplitudes of each other's position fluctuations over time; 5) interacting cycles producing alterations in the frequencies of both cycles.

Below I present four hypothetical examples of cyclic interactions between time-dependent self-reported stress and alcohol consumption.

1. Drinking potentially slows down individuals' reaction times, and consequently reduces the *acceleration* of their stress level to its peak values. Alcohol consumption impairs information processing and slows down reaction times (Maylor & Rabbitt, 1993). When exposed to a stressful event, an individual who has consumed a significant amount of alcohol might take longer to process the situation and develop a different reaction to it than he/she would in a sober state. In terms of the motion trajectory of stress, when the consumed alcohol is taking effect, the stress level upon the exposure to the stressful event might be escalating to the peak more slowly than it would in a sober state.

2. Drinking potentially intensifies individuals' perception of stress and serenity (lack of stress), increasing the *amplitudes* of the self-reported stress fluctuations at the peaks and troughs of the cycle. That is, in addition to altering acceleration of stress to its peaks, the amount of consumed alcohol might as well change the height of the peaks. For instance, an individual who has been physically pushed might take it more seriously if intoxicated, creating a higher perceived level of stress for himself/herself.

3. Drinking potentially increases the time dwelling at the extremes of stress and lack of stress, making self-reported stress oscillations flatter around the peaks and

troughs. Intoxicated individuals tend to have slower reaction times and cognitive processing, which is likely to impede and delay their transition between mental states, such as the transition from a high stress to a low stress state. Hence, changes in drinking might change the *form* of the oscillations in stress.

4. Extended periods of high stress might, in turn, increase the *frequency* of excessive drinking periods. People tend to seek out alcoholic beverages to temporarily relieve the discomfort produced by stressful experiences. It is possible that when stressful events are experienced especially intensely and for longer periods of time, the individual may tend to consume alcohol more frequently to reduce stress. In conjunction with the first three examples, such an effect would produce a causal *asymmetrical bidirectional* relationship between reported stress and alcohol consumption.

Using models with separate non-interacting cycles, such as the classic sinusoid model (that only represents symmetric cycles), limits the patterns of relationships between two cycles that can be represented. The seasonal trigonometric model is more flexible mathematically, but requires that the coupling coefficients κ_1 and κ_2 sum to $3\omega^2$ $(= 3\omega_1^2 = 3\omega_2^2)$, allowing only for a very narrow subset of possible relationships, and currently provides no theoretical justification for this restriction. For instance, if we are dealing with 7-day cycles, $\omega = \frac{2\pi}{7} \approx \sqrt{0.8}$, and $\kappa_1 + \kappa_2 = 3\omega^2 \approx 3*0.8=2.4$, which means that the cyclic relationship between two time series will be detected correctly by the model only if their coupling coefficients sum to 2.4, a very specific restriction that is highly unlikely to be met with real data. These considerations imply that none of the phenomena of the sort described above can be adequately represented.

An Alternative Approach: Connected Mass-Spring Models

By representing any psychological time series data that are expected to be cyclical as connected mass-spring models (e.g., Hessler et al., 2013; Boker & Graham, 1998), researchers make an assumption that any pair of trajectories can be represented by the connected mass-spring system. If this were the case, researchers could use a two-stage approach to represent undamped cyclic time series data together with their cyclic interactions and linear trends. The first stage would be to input the position and acceleration of the two detrended time dependent potentially cycling variables into a multilevel connected mass-spring model (Butner et al., 2005). This model permits estimation of the major/natural frequencies of the two fluctuating variables, as well as their coupling terms on the within-individual (Level 1 equation) level. In the second step, the system of the two differential force equations that describe the connected mass-spring model need to be solved for *x(t)* and *y(t)*, which represent position over time for the first mass/variable and the second mass/variable, respectively. The solutions of a model without friction/damping terms will be a sum of imaginary exponents of *e*. When split into sine and cosine components by Euler's formula ($e^{\theta it} = \cos\theta t + \mathrm{i}\sin\theta t$) and projected onto the real plane, they will result into general definitions of motion trajectories of the two masses/variables from the connected mass-spring model with the major frequencies and coupling terms detected in the first step. The resulting equations will be of a form similar to the seasonal trigonometric model in that each trajectory will consist of two pairs of sine and cosine functions with two different frequencies. When the natural angular frequencies of the two masses/variables are equal, the first a pair of sine

and cosine functions will represent the major frequencies of the masses/variables, and the second pair of sine and cosine functions will represent the secondary frequencies produced by the cyclic interaction. When the natural angular frequencies of the two masses/variables are unequal, the two frequencies will have a more complex meaning and composition. Each of the trigonometric terms will have a coefficient that is free to vary and is dependent on the initial position and velocity of the two masses. Some of the sine and cosine components will have additional coefficients composed of the angular frequencies and/or the coupling coefficients of the corresponding model. The connection between the system parameters estimated by the connected mass-spring model and the motion trajectories simplifies to have a convenient universal general solution that can be directly input into the sinusoid regression or multilevel model without additional calculation. Thus, this process of estimating coupling coefficients through the multilevel connected mass-spring model, and solving for *x(t)* and *y(t)* turns them into a model analogous to the seasonal trigonometric model, but without the restriction that the coupling coefficients sum to $3\omega^2$.

The connected mass-spring model can potentially address all of the limitations of the sinusoid model and the seasonal trigonometric model. The model can potentially detect cycles together with their relationships and model them in a familiar and convenient sinusoid form and be successfully estimated using a hierarchical linear model. The major frequencies of the cyclic variables can (a) be estimated using an exploratory approach through inputting time series data into the multilevel connected mass-spring model, or (b) alternatively, if theory exists that specifies the major frequencies, they can

be specified in the connected mass-spring model. The coupling terms and their translation to the motion trajectories will determine the directional causal influence of one cyclic variable on the other (and vice versa) allowing us to detect and explain complicated relationships, as were exemplified earlier in the example using alcohol consumption and stress. Finally, cyclic effects can be modeled and/or removed together with their cyclic relationships, preventing model misspecification that might arise in the existing cyclic models due to the neglect of potential cyclic relationships.

Given that Boker, Butner, Amazeen, Hessler, Finan and others are correct about the implied assumption that trajectories produced by the connected mass-spring system can represent the majority of the possible cyclical patterns of psychological variables, the two-stage model delineated above should provide a general representation of the relationships between cycles in two time series. But, does the coupled mass-spring model provide a fully adequate representation or does it have its own limitations?

Critique of the Connected Mass-Spring Model Approach

The connected mass-spring system, as depicted in Figure 5, is a closed system (Cook & Campbell, 1979) that obeys a set of strict laws of mechanics. Since each of the laws adds restrictions to the motion trajectory of the masses (variables), the connected mass-spring system may be too physically restricted to be able to represent the full range of possible combinations of paired cyclic trajectories.

One physical law that applies to any *closed* mechanical system, including the basic coupled mass-spring system (without nonlinear escapements), is the law of conservation of energy. This law states that the total energy of a closed system is

conserved over time. In case of the isolated mass-spring system, this property means that the kinetic and potential energies of the system fluctuate, but that their sum must remain constant at all times. Kinetic energy (E_K), also termed the energy of motion, is contained in moving objects that have mass. In mass-spring systems, kinetic energy is contained in the moving weights, and can be calculated with equation (30), where *m* is the mass of the weight and *v* is its movement velocity. Potential energy (E_P) is the stored energy of an object that is produced by its relative position to other objects or parts of the system. To illustrate, when a bowstring is pulled back, a bow stores potential energy due to its position. When the arrow is released, potential energy of the bow is converted into kinetic energy, and transmitted to the arrow that is propelled into motion. In the mass-spring system, potential energy is contained in the springs that are either stretched or compressed. The potential energy of each individual spring can be calculated by using Equation (31), where *k* stands for the stiffness of the spring, and *x* is displacement or deformation of the spring.

$$E_K = \frac{mv^2}{2} \quad (30) \qquad E_P = \frac{kx^2}{2} \quad (31)$$

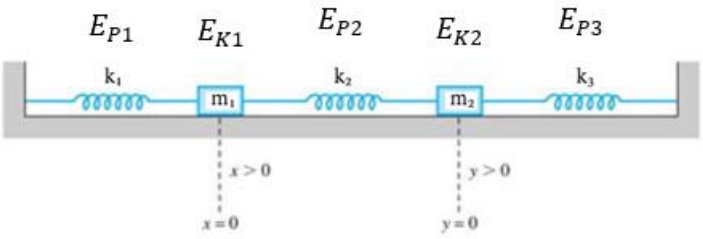

Figure 8. *Kinetic and potential energy distribution in the connected mass-spring system.*

Suppose we have two cyclically oscillating time dependent variables, both of which fluctuate synchronously producing a pattern described by the simplest form (see Figure 9) of the seasonal trigonometric model, i.e. sin(ωt) + cos(ωt) + sin(2ωt) + cos(2ωt). Such a

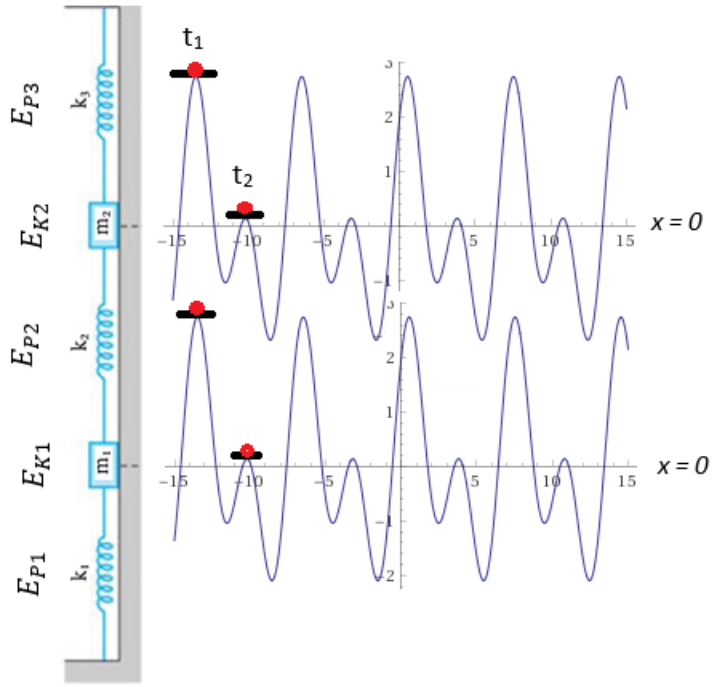

Figure 9. *Motion trajectories of a hypothetical connected mass-spring system that coincide with the function sin(ωt) + cos(ωt) + sin(2ωt) + cos(2ωt).*

motion trajectory combination is possible with two psychological variables. Now, if this motion trajectory combination is producible by the connected mass-spring system, it must obey the law of conservation of energy. In terms of the physics of the system, the sum of all potential and kinetic energies of the system has to be equal at all times. To simplify the case, consider two time points, one at the first peak of the trajectories (t_1), and the second at the second peak of the trajectories (t_2, see Figure 9), and compare the sum of energies at these two time points. If this trajectory combination is producible by the

system, equation (32) should be true given the closed system property.

$$E_{P1}(t_1) + E_{P2}(t_1) + E_{P3}(t_1) + E_{K1}(t_1) + E_{K2}(t_1) = E_{P1}(t_2) + E_{P2}(t_2) + E_{P3}(t_2) + E_{K1}(t_2) + E_{K2}(t_2). \quad (32)$$

Recall that the trajectories in this example are synchronous, which means that they move perfectly in accord with each other, implying that the distance between the two masses never changes. Consequently, the middle spring is never stretched or compressed. Under these conditions it will store no potential energy:

$$E_{P2}(t_1) = E_{P2}(t_2) = 0 \quad (33)$$

To further simplify equation (32), consider the kinetic energy terms. Since we chose t_1 and t_2 at the peaks of the trajectories, that is, when the masses change their direction of movement, velocity at these two time points is 0. Velocity can be visualized as the slope of the tangent line to the trajectories at t_1 and t_2 (see Figure 9). Hence, from the definition of kinetic energy:

$$E_{K1}(t_1) = E_{K2}(t_1) = E_{K1}(t_2) = E_{K2}(t_2) = 0 \quad (34)$$

We are left with:

$$E_{P1}(t_1) + E_{P3}(t_1) = E_{P1}(t_2) + E_{P3}(t_2) \quad (35)$$

After plugging in the definitions of potential spring energy (see Equation 31) and multiplying by 2 we get the following result:

$$k_1 * x(t_1)^2 + k_3 * x(t_1)^2 = k_1 * x(t_2)^2 + k_3 * x(t_2)^2, \quad (36)$$

where k_1 and k_3 are stiffness of the side springs (see Figure 8 and Figure 9), and x is displacement of the masses from the equilibrium $x = 0$ (see Figure 9). Since movement of the two masses is identical, their displacement is also identical at all time points, and

hence can be marked with the same letter for simplicity. Now we rearrange (36) into:

$$(k_1 + k_3) * x(t_1)^2 = (k_1 + k_3) * x(t_2)^2, \quad (37)$$

and since stiffness of the side springs cannot be negative, and is obviously not 0, we divide both sides by $k_1 + k_3$ and end up with:

$$x(t_1)^2 = x(t_2)^2 \quad (38) \quad \rightarrow \quad |x(t_1)| = |x(t_2)| \quad (39)$$

The final equation (39) states that the displacement magnitude of the masses at t_1 and t_2 is the same, which *cannot* be true (see Figure 9) and therefore proves by *contradiction* that the defined pair of motion trajectories is not producible by the connected mass-spring system. This analysis suggests that the connected mass-spring model may not be identified. A unique solution for the coefficients may not exist.

The key problem is this: If the trajectory pair is not in the range of the physical possibility of the mass-spring system, then there simply is no unique matching set of connected mass-spring model parameters to accommodate it. Unless there are a pair of trajectories that are producible by the coupled mass-spring system and are which very close to the improducible pair, the frequency coefficients (ω_1^2, ω_2^2) detected by the connected mass-spring model will be biased, whereas the coupling coefficients (κ_1, κ_2) would be expected to be arbitrary. This results in three possibilities, which I describe below.

1) The demonstrated pair of improducible trajectories is a special case. Such trajectory combinations can be expected to be very rare, and will have no material detrimental effect on the functionality of the connected mass-spring model. In this case, the non-damped connected mass-spring model will be applicable to virtually any

psychological variable pair that cycles over time. If this were the case, the two-stage model proposed above would be fully functional in the psychological context and could be successfully used to model or remove cyclic behaviors of psychological variables together with their bivariate cyclic relationships.

2) There is a subset of improducible trajectory pairs that limit the application of the non-damped connected mass-spring model, and therefore the proposed two-stage approach. However, it could potentially be overcome by easy fixes, such as coupling coefficient scaling.

3) The number of trajectory pairs producible by the non-damped connected mass-spring system is very restricted, and cannot accommodate the majority of cyclic trajectory pairs present in psychological data. None of the connected mass-spring models (undamped and, without loss of generality, damped) proposed in the literature cited above will be suitable for usage with psychological data, as they do not have a unique solution (underidentified). Connected mass-spring model coefficients reported in the published literature will not be trustworthy.

The purpose of my master's thesis was to find evidence for one of the three scenarios above, and to demonstrate my findings through analytic work, and through simulation.

Chapter 2

METHOD

Analytic work

I mathematically defined the restrictions that apply to the pairs of movement trajectories of the classical connected mass-spring system with no damping, no nonlinear escapements, and with a set natural angular frequency of both masses that corresponds to a weekly cycle. The findings/conclusions, without loss of generality, logically extend to any other pairs of natural angular frequencies, and to models with damping and nonlinear escapements. If the basic model is underidentified, the more complex models will also be underidentified. No additional information will be available with which to estimate the additional parameters.

To solve this problem, I used the elimination method for 2 × 2 differential systems with constant coefficients (Nagle, Saff & Snider, 2010, p. 263) to find the general solution of the system. Because the motion trajectories of an undamped mass-spring model are composed of nonfading cyclic components (on average, there is no decrease in the amplitude of fluctuations over time), the general solution is composed of imaginary exponentials of *e*. Imaginary exponentials of *e* were decomposed into the sums and of sines and cosines by the Euler's formula ($e^{\theta it} = \cos\theta t + \mathrm{i}\sin\theta t$), and projected onto the real plane by removing the imaginary coefficients. This approach resulted in general definitions of the motion trajectories of the two connected masses with their elements defined in terms of the natural angular frequencies of the mass spring system (ω_1, ω_2), the coupling terms of the connected mass-spring system (κ_1, κ_2), and the initial

condition dependent coefficients (C_1, C_2, C_3, C_4). General definitions of the two motion trajectories allowed visualization of the general pattern of their relationship and the restrictions on their relationships.

Simulation Study

The simulation study estimated parameters of motion trajectories producible by the undamped connected mass-spring system with equal major frequencies (see equation set 40 below). The trajectories of the two masses in the undamped connected mass-spring model with equal natural angular frequencies (the two side springs having the same stiffness to mass ratio, $\frac{k_1}{m_1} = \frac{k_2}{m_2}$, and thus having the same natural frequency), according to the results of my analytic work (see Appendix A for derivation), follow:

$$\begin{cases} y(t) = C_1 \cos(\omega_1 t) + C_2 \sin(\omega_1 t) + C_3 \cos\left(\sqrt{\omega_1^2 + \kappa_1 + \kappa_2}\, t\right) + C_4 \sin\left(\sqrt{\omega_1^2 + \kappa_1 + \kappa_2}\, t\right) \\ x(t) = C_1 \cos(\omega_1 t) + C_2 \sin(\omega_1 t) - C_3 \frac{\kappa_1}{\kappa_2} \cos\left(\sqrt{\omega_1^2 + \kappa_1 + \kappa_2}\, t\right) - C_4 \frac{\kappa_1}{\kappa_2} \sin\left(\sqrt{\omega_1^2 + \kappa_1 + \kappa_2}\, t\right) \end{cases} \quad (40)$$

In the equation system represented in the Equation set (40), t stands for time, $x(t)$ represents position over time of mass 1, $y(t)$ represents position over time of mass 2, ω_1 represents the angular frequency of the side springs, $\sqrt{\omega_1^2 + \kappa_1 + \kappa_2} = \omega_{secondary}$ represents angular frequency of the middle spring, and κ_1 and κ_2 are coupling coefficients. κ_1 represents the influence of mass 2 on mass 1, and κ_2 represents the influence of mass 1 on the mass 2. C_1, C_2, C_3, C_4 are coefficients that depend on the initial conditions (initial position and velocity of the masses).

Equation system (40) was used to generate pairs of trajectories that, according to my analytic work, are producible by the connected mass-spring system, and therefore

should be properly represented by the multilevel connected mass-spring model. Pairs of trajectories were generated for each individual. Uncorrelated residuals were generated and added at each time point within each individual within each trajectory. Acceleration values of the position trajectories were calculated using the local linear approximation method (Boker, 2001; Boker & Graham, 1998).

The multilevel connected mass-spring model defined in the equation set (41) below was then be applied to the generated data.

$$\begin{aligned} \frac{d^2x_{mit}}{dt^2} &= \beta_{1it}(D1_{mit}) + \beta_{2it}(D2_{mit}) + r_{mit}\ . && \text{Level 1} \\ \beta_{1it} &= \eta_1 x_{1it} + \kappa_1(x_{2it} - x_{1it}) + e_{1it} && \text{Level 2} \\ \beta_{2it} &= \eta_2 x_{2it} + \kappa_2(x_{1it} - x_{2it}) + e_{2it}\ . \end{aligned} \qquad (41)$$

In equation set (41), x_{mit} represents position of mass *m* in subject *i* at time *t*, and $\frac{d^2x_{mit}}{dt^2}$ represents the 2nd derivative of the position of mass *m* in subject *i* at time *t* (or acceleration of mass *m* in subject *i* at time *t*). $D1_{mit}$ is an indicator variable coded 1 when *m*=1, and coded 0 when *m*=2, whereas $D2_{mit}$ is an indicator variable coded 0 when *m*=1, and coded 1 when *m*=2. β_{1it} is the random slope for indicator variable $D1_{mit}$, which is also acceleration of mass 1 at time *t* in individual *i*. β_{2it} is the random slope for indicator variable $D2_{mit}$, which is also acceleration of mass 2 at time *t* in individual *i*. η_1 and η_2 represent the mean negative squared angular frequency across individuals and time points of mass 1, and mass 2, respectively. κ_1 and κ_2 represent the mean coupling influence across individuals and time points of mass 2 on mass 1, and mass 1 on mass 2, respectively. r_{mit} is the level 1 error term for mass *m* individual *i* at time *t*, assumed to be $\sim N(0, \sigma^2)$. e_{1it} represents the variation in the force estimate of mass 1 across individuals

and time points, and e_{2it} represents the residual variation in the force estimate of mass 2 across individuals and time points. e_{1it} and e_{2it} are assumed to have a bivariate normal distribution with means 0, variances τ_0, τ_1, and covariance τ_{01}.

The multilevel connected mass-spring model implemented in SAS estimated (a) the mean negative squared angular frequency of the left-most spring (ω_1 in equation *x(t)*), (b) the mean negative squared angular frequency of the right-most spring (ω_1 in equation *y(t)*), (c) κ_1 and (d) κ_2, together with their standard errors. I evaluated the bias of the estimates of ω_1, ω_2, $\omega_{secondary}$ ($= \sqrt{\omega_1^2 + \kappa_1 + \kappa_2}$) , κ_1, κ_2, and κ_1/κ_2 by calculating the relative parameter bias, where $relative\ bias = \frac{estimate - true\ value}{true\ value}$. Values of parameter bias which did not exceed 10 percent were considered adequate (Muthén & Muthén, 2002).

a) Angular Frequency Values: Primary

The precise sets of values that were tested in my simulation are:

$\omega_1 = \frac{2\pi}{7}, \frac{2\pi}{14}, \frac{2\pi}{35}, \frac{2\pi}{70}$;

The primary angular frequency values presented above represent the theoretical fluctuation frequencies generated by the side springs. They are equivalent to the fluctuation frequency of each of the two independent mass-springs that would be produced by removing the middle spring of the connected mass-spring system. In this simulation study, they also determine the sampling frequency[2] of the generated

[2] Having sampling rate as an independent manipulated variable, separate from the theoretical frequency ω_1 would be redundant. For instance, having a sampling rate of 7 measures per cycle where the theoretical major frequency ω_1 is $\frac{2\pi}{7}$, and having a sampling rate of 7 measures per cycle where the theoretical major

trajectories *x(t)* and *y(t)*. The first frequency, 7 measures per cycle, is equivalent to 7 daily diary measures in the data with expected weekly cycles. The second frequency, 14 measures per cycle, is equivalent to two equally spaced daily measures in the data with expected weekly cycles. Analogously, the third frequency represents 5 measures, and the fourth frequency 10 measures per day in the same context. The findings can be generalized to any major frequencies and sampling rates that are in the range of the listed values. According to my pilot simulation, lower frequencies are too sparse for the cycles to be detected correctly by the multilevel connected mass-spring model, whereas higher frequencies produce acceleration terms that are overly sensitive to error (more discussion on that below).

b) Angular Frequency Values: Secondary

$\omega_{secondary}$

When $\omega_1 = \frac{2\pi}{7}$: $\omega_{secondary} = \frac{2\pi}{3.5}, \frac{2\pi}{4}, \frac{2\pi}{5}, \frac{2\pi}{6}$;

When $\omega_1 = \frac{2\pi}{14}$: $\omega_{secondary} = \frac{2\pi}{4}, \frac{2\pi}{7}, \frac{2\pi}{10}, \frac{2\pi}{13}$;

When $\omega_1 = \frac{2\pi}{35}$: $\omega_{secondary} = \frac{2\pi}{4}, \frac{2\pi}{10}, \frac{2\pi}{17.5}, \frac{2\pi}{25}, \frac{2\pi}{34}$;

When $\omega_1 = \frac{2\pi}{70}$: $\omega_{secondary} = \frac{2\pi}{4}, \frac{2\pi}{20}, \frac{2\pi}{35}, \frac{2\pi}{50}, \frac{2\pi}{69}$.

Secondary frequency values represent the angular frequency of the middle spring. Equations (40) constrain the sum $\kappa_1 + \kappa_2$ to a fixed value because $\sqrt{\omega_1^2 + \kappa_1 + \kappa_2} = \omega_{secondary}$. The secondary frequency values are presented above in the same format as

frequency ω_1 is $\frac{2\pi}{70}$ would yield identical results. The two sampling rates represent the same pattern, but are measured on a different time scale (Δt, which does not affect model estimates).

the major frequencies ω_1. Given that ω_1 represents both the theoretical major frequency and the sampling frequency, the numeric values in the denominator of $\omega_{secondary}$ represent the length of the secondary cycle in terms of the equally spaced observation points as well as the number of observation points per each secondary cycle (e.g., $\omega_{secondary} = \frac{2\pi}{4}$ means that the secondary cycle is completed after 4 observations, and that there are 4 observations per each full secondary cycle). For instance, in the case where $\omega_1 = \frac{2\pi}{7}$ and $\omega_{secondary} = \frac{2\pi}{4}$, the following *x(t)* and *y(t)* trajectories (with some fixed C_1, C_2, C_3, C_4 and $\frac{\kappa_1}{\kappa_2}$) will be generated:

$$\begin{cases} x(t) = C_1 \cos\left(\frac{2\pi}{7}t\right) + C_2 \sin\left(\frac{2\pi}{7}t\right) + C_3 \cos\left(\frac{2\pi}{4}t\right) + C_4 \sin\left(\frac{2\pi}{4}t\right) \\ y(t) = C_1 \cos\left(\frac{2\pi}{7}t\right) + C_2 \sin\left(\frac{2\pi}{7}t\right) - C_3 \frac{\kappa_1}{\kappa_2} \cos\left(\frac{2\pi}{4}t\right) - C_4 \frac{\kappa_1}{\kappa_2} \sin\left(\frac{2\pi}{4}t\right) \end{cases}$$

and sampled at the rate of 7 equally spaced measurements per cycle, where the cycle length is 2π radians.

All the selected $\omega_{secondary}$ values were larger than the corresponding ω_1 values as the impact of the middle spring cannot physically generate secondary frequencies that are lower than the major frequencies. In mathematical terms, $\omega_{secondary} = \sqrt{\omega_1^2 + \kappa_1 + \kappa_2} > \omega_1$ because $\kappa_1 = \frac{k_{middle}}{m_1}$ and $\kappa_2 = \frac{k_{middle}}{m_2}$ with the k_{middle} (stiffness of the middle spring), m_1 (mass of the left weight) and m_2 (mass of the right weight). These values will always be positive because stiffness and mass cannot be negative or zero in the classical mechanics of the mass-spring system. The lowest secondary frequency in case of each ω_1 was chosen to be the value that is closest to the minimal

boundary value (i.e. $1\omega_1$), with 2π in the numerator (to maintain the standard format) and a whole number in the denominator (for convenience).

The frequency of the secondary cyclic component, $\omega_{secondary}$, is always higher than the major frequency ω_1. According to my pilot simulation, in order to avoid empirical underidentification, at the very least 4 equally spaced observations are needed per each cyclic component. For that reason, the highest secondary frequency in case of each ω_1 (except for $\omega_1 = \frac{2\pi}{7}$) was selected to be $\frac{2\pi}{4}$. In case of $\omega_1 = \frac{2\pi}{7}$, a higher secondary frequency, $\frac{2\pi}{3.5}$, was also tested because together with $\omega_1 = \frac{2\pi}{7}$ it corresponds to the frequency composition of the seasonal trigonometric model ($\omega_{secondary} = 2\omega_1$), which is of interest. A secondary frequency that together with the corresponding ω_1 proportionally corresponds to the seasonal trigonometric model was included among the $\omega_{secondary}$ values for each ω_1.

The rest of the values were selected to be easily interpretable (whole numbers in the denominator) and approximately equally spaced between the set boundaries of $\omega_{secondary}$ values given the four selected major frequencies ω_1.

c) Coupling Ratios

1. κ_1/κ_2 = 1/100, 1/40, 1/10, 1/2, 1; $0 < \kappa_1/\kappa_2 \leq 1$
2. $\kappa_1/\kappa_2 = m_2/m_1$ = 2/1 = 2 $\kappa_1/\kappa_2 > 1$

   $\kappa_1/\kappa_2 = m_2/m_1$ = 10/1 = 10

$\omega_1 = \frac{2\pi}{70}$; $\omega_{secondary} = \frac{2\pi}{20}$; $n = 50$; series length = 7 cycles;

$\frac{\sigma_{error}^2}{\sigma_{signal}^2+\sigma_{error}^2} = 0.0000002; \quad p_1 = 1,\ p_2 = -10,\ v_1 = 10,\ v_2 = -1$

The majority of coupling ratios κ_1/κ_2 were bounded by $0 < \kappa_1/\kappa_2 \leq 1$. The minimum boundary of 0 comes from the aforementioned equalities $\kappa_1 = \frac{k_{middle}}{m_1}$ and $\kappa_2 = \frac{k_{middle}}{m_2}$. Redefining the coupling ratio in terms of stiffness and mass gives $\kappa_1/\kappa_2 = \frac{k_{middle}}{m_1} : \frac{k_{middle}}{m_2} = \frac{m_2}{m_1}$. In classical mechanics mass cannot be negative and hence, $\kappa_1/\kappa_2 \geq 0$. Having mass being 0 would undermine the physical structure of the connected mass-spring system, and hence, $\kappa_1/\kappa_2 > 0$. The upper boundary excluded cases where $m_2 > m_1$. Setting this boundary eliminates the consideration of identical systems to those that are spanned by the κ_1/κ_2 between 0 and 1, but with m_2 and m_1 exchanged.

By looking at the equation system of $x(t)$ and $y(t)$, and knowing that $x(t)$

$$\begin{cases} y(t) = C_1\cos(\omega_1 t) + C_2\sin(\omega_1 t) + C_3\cos\left(\sqrt{\omega_1^2+\kappa_1+\kappa_2}t\right) + C_4\sin\left(\sqrt{\omega_1^2+\kappa_1+\kappa_2}t\right) \\ x(t) = C_1\cos(\omega_1 t) + C_2\sin(\omega_1 t) - C_3\frac{\kappa_1}{\kappa_2}\cos\left(\sqrt{\omega_1^2+\kappa_1+\kappa_2}t\right) - C_4\frac{\kappa_1}{\kappa_2}\sin\left(\sqrt{\omega_1^2+\kappa_1+\kappa_2}t\right) \end{cases}$$

always represents the trajectory of m_1, whereas $y(t)$ always represents the trajectory of m_2, at first glance one might argue that given the structure of the last two terms of the equations, m_2 and m_1 cannot produce identical (but reversed) motion trajectory pairs when exchanged. However, this apparent result occurs only because the initial condition dependent coefficients (C_1, C_2, C_3, C_4) were represented here by single coefficients for simplicity. The C_1, C_2, C_3, C_4 values in terms of other coefficients were derived by solving $p_1 = x(0),\ p_2 = y(0),\ v_1 = x'(0),\ v_2 = y'(0)$ in a single equation system. The

derivation shows that C_1 to C_4 can be fully expressed in terms of initial position (p_1, p_2),

$$C_1 = \frac{v_2 + \frac{\kappa_2}{\kappa_1} v_1}{\omega_1 \left(1 + \frac{\kappa_2}{\kappa_1}\right)} \quad C_2 = \frac{p_2 + \frac{\kappa_2}{\kappa_1} p_1}{1 + \frac{\kappa_2}{\kappa_1}} \quad C_3 = \frac{v_2 - v_1}{\omega_{secondary} \left(1 + \frac{\kappa_1}{\kappa_2}\right)} \quad C_4 = \frac{p_2 - p_1}{1 + \frac{\kappa_1}{\kappa_2}} \qquad (42)$$

$$C_1 = \frac{v_2 + \frac{m_1}{m_2} v_1}{\omega_1 \left(1 + \frac{m_1}{m_2}\right)} \quad C_2 = \frac{p_2 + \frac{m_1}{m_2} p_1}{1 + \frac{m_1}{m_2}} \quad C_3 = \frac{v_2 - v_1}{\omega_{secondary} \left(1 + \frac{m_2}{m_1}\right)} \quad C_4 = \frac{p_2 - p_1}{1 + \frac{m_2}{m_1}} \qquad (43)$$

initial velocity (v_1, v_2), primary and secondary frequencies, and either the coupling ratio (Equation set 42), or the mass ratio (Equation set 43). In this form, it becomes evident that exchanging m_2 and m_1, exchanging initial position and initial velocity terms, and setting them to their additive inverses (i.e, $p_1 = -p_2$, $p_2 = -p_1$, $v_1 = -v_2$; $v_2 = -v_1$) will yield identical motion trajectories to those produced by the initial system, but reversed and mirror reflected (i.e. the mirror image of *x(t)* of the initial system will equal *y(t)* of the rearranged system, and the mirror image of *y(t)* of the initial system will equal *x(t)* of the rearranged system).

I included two κ_1/κ_2 values larger than 1 (together with a fixed set of other coefficients) to test my statements about the consequences of exchanging of m_2 and m_1. More precisely, to test whether the trajectory pairs produced with κ_1/κ_2 = 2/1 , and κ_1/κ_2 = 10/1 are the mirror images of exchanged *x(t)* and *y(t)* of the systems where κ_1/κ_2 = 1/2 and κ_1/κ_2 = 1/10, respectively. All the other parameters (except for C_1, C_2, C_3, C_4) were fixed, and C_1, C_2, C_3, C_4 were adjusted in accordance with the changes in initial position and velocity proposed above. The set of fixed parameters (ω_1, $\omega_{secondary}$, n, series length, $\frac{\sigma_{error}^2}{\sigma_{signal}^2 + \sigma_{error}^2}$) were selected so that, according to the pilot simulation, the parameters of the corresponding connected mass-spring system could be

detected correctly by the multilevel model. The set of initial position and velocity values was chosen from the manipulated sets of initial condition values (see next section) such that initial position and velocity values would be different for mass 1 and mass 2, and have the highest predicted convergence rate based on the pilot simulation (set 8). The initial position and velocity values from this set were exchanged, and set to their additive inverses, as discussed above (i.e, $p_1 = -p_2$, $p_2 = -p_1$, $v_1 = -v_2$; $v_2 = -v_1$). If the position values of the two masses are the same, the fourth term of the motion trajectories (see equations sets 42 and 43) is cancelled out. If the velocity values of the two masses are the same, the third term of the motion trajectories cancels out. Testing conditions where all four trajectory equation terms were present permitted the simultaneous examination of all four motion trajectory terms.

The highest κ_1/κ_2 value in the $0 < \kappa_1/\kappa_2 \leq 1$ range was chosen to coincide with the upper boundary of 1, where the two coupling terms (and, equivalently, the two masses) are equal. The lowest κ_1/κ_2 value (1/100) in the $0 < \kappa_1/\kappa_2 \leq 1$ range was chosen to be close to the lower boundary and represents the case where one coupling coefficient is 100 times stronger than the other. The κ_1/κ_2 values between the two extremes were chosen to be easily interpretable and representative of the range of the values between the extremes.

d) Initial Position and Velocity: p_1, p_2, v_1, v_2

The ten conditions below represent different sets of values for the initial position and velocity of each mass. The state of the system that is represented by each condition is described below the list of conditions. The choice of initial values for the position and

velocity of each mass were subject to the constraints of equation sets (42) and (43). A variety of values were chosen to represent the performance of the system given a range of initial values.

1. $p_1 = p_2 \quad v_1 = v_2 = 0 \quad \rightarrow \quad p_1 = 10,\ p_2 = 10,\ v_1 = 0,\ v_2 = 0$
2. $p_1 = p_2 = 0 \quad v_1 = v_2 > 0 \quad \rightarrow \quad p_1 = 0,\ p_2 = 0,\ v_1 = 10,\ v_2 = 10$
3. $p_1 = p_2 > 0 \quad v_1 = v_2 < 0 \quad \rightarrow \quad p_1 = 1,\ p_2 = 1,\ v_1 = -1,\ v_2 = -1$
4. $p_1 > 0 \ \ p_2 > 0 \quad v_1 = v_2 > 0 \quad \rightarrow \quad p_1 = 1,\ p_2 = 10,\ v_1 = 5,\ v_2 = 5$
5. $p_1 < 0 \quad p_2 > 0 \quad v_1 > 0 \quad v_2 < 0 \quad \rightarrow \quad p_1 = -10,\ p_2 = 1,\ v_1 = 10,\ v_2 = -1$
6. $p_1 > 0 \quad p_2 < 0 \quad v_1 < 0 \quad v_2 > 0 \quad \rightarrow \quad p_1 = 1,\ p_2 = -10,\ v_1 = -1,\ v_2 = 10$
7. $p_1 < 0 \quad p_2 > 0 \quad v_1 < 0 \quad v_2 > 0 \quad \rightarrow \quad p_1 = -1,\ p_2 = 10,\ v_1 = -10,\ v_2 = 1$
8. $p_1 > 0 \quad p_2 < 0 \quad v_1 > 0 \quad v_2 < 0 \quad \rightarrow \quad p_1 = 10,\ p_2 = -1,\ v_1 = 1,\ v_2 = -10$
9. $p_1 > 0 \quad p_2 > 0 \quad v_1 < 0 \quad v_2 > 0 \quad \rightarrow \quad p_1 = 10,\ p_2 = 10,\ v_1 = -10,\ v_2 = 10$
10. $p_1 > 0 \quad p_2 > 0 \quad v_1 > 0 \quad v_2 < 0 \quad \rightarrow \quad p_1 = 5,\ p_2 = 5,\ v_1 = 1,\ v_2 = -10$

The ten combinations of initial conditions presented above correspond to ten different major cases of initial position and velocity parings that produce different types of motion patterns. The exact initial position and/or velocity values were chosen to be equal in the first four and the last two combinations in order to test the motion trajectory pairs where the third (4), the fourth (9, 10), or both the third and the fourth (1, 2, 3) terms of *x(t)* and *y(t)* are 0, as $C_3 = \frac{v_2 - v_1}{\omega_{secondary}\,(1 + \frac{\kappa_1}{\kappa_2})}$ and $C_4 = \frac{p_2 - p_1}{1 + \frac{\kappa_1}{\kappa_2}}$ (see Equations 42 and 43). The condition where all the initial position and velocity values are equal to 0 yields a motionless system and was not considered.

The first initial position and velocity value combination represents the case where both masses are pulled away from their equilibrium by an equal distance in the same direction and then released. The second combination represents the case where both masses are positioned at their equilibria, and then pushed in the same direction inducing the same initial velocity in both masses. The third combination represents both masses being pulled away from their equilibria by an equal distance towards the right wall and then pushed towards the left wall (in the direction in which both would move if released freely) with equal initial velocity. The fourth combination represents both masses being pulled away from their equilibria towards the right wall and then pushed towards the right wall (in the opposite direction from the one they would move if released freely) with equal initial velocity. The fifth combination represents an instance where both masses are pulled to the sides and then pushed towards the center of the system (in the direction in which they would move if released freely). The sixth combination represents an instance where both masses are pulled towards the center of the system and then pushed to the sides (in the direction in which they would move if released freely). The seventh combination represents the two masses being pulled to the sides and then pushed to the sides (against the direction in which they would move if released freely). The eighth combination represents an instance where the two masses are pulled towards the center of the system and then pushed towards the center of the system (against the direction in which they would move if released freely). The ninth combination is an instance where the two masses are pulled to the right, and then the left mass is pushed to the left (in the direction in which it would move if released freely), whereas the right mass is pushed to

the right (against the direction in which it would move if released freely). The tenth combination represents an instance where the two masses are pulled to the right side, and then the left mass is pushed to the right (against the direction in which it would move if released freely), whereas the right mass is pushed to the left (against the direction in which it would move if released freely). All the cases presented above are possible in psychological data, they represent a relatively comprehensive set of the possible trajectory pattern types producible by the connected mass-spring system.

As mentioned above, the initial position and/or velocity values were chosen to be equal in the first four combinations in order to test the motion trajectory pairs where the third, the fourth, or both the third and the fourth terms of $x(t)$ and $y(t)$ are 0. Furthermore, the numeric values that satisfy the ten conditions described above were selected in a way that allowed testing of whether the magnitudes of initial position and velocity values have an effect on the adequacy of the parameter estimates. Each initial value combination defined above was assigned one magnitude pattern (corresponding initial value combination number is in parentheses):

- All values small (3.)
- All values large (9.)
- Zero position values, large velocity values (2.)
- Large position values, zero velocity values (1.)
- Contrasting position values, equal medium velocity values (4.)
- Equal medium position values, contrasting velocity values (10.)

- Contrasting position values, contrasting velocity values with low $p_1,\ v_1$ and high $p_2,\ v_2$ (6.)
- Contrasting position values, contrasting velocity values with low $p_2, v_2,$ and high p_1, v_1 (5.)
- Contrasting position values, contrasting velocity values with low $p_1, v_2,$ and high v_1, p_2 (7.)
- Contrasting position values, contrasting velocity values with low $v_1, p_2,$ and high p_1, v_2 (8.)

Zero values indicate the absence of the term, low values indicate values with magnitude of 1, medium values correspond to the magnitude of 5, and large values indicate values with magnitude of 10. Whole numbers between 0 and 10 were chosen for simplicity. They do not carry any fixed meaning in terms of psychological variables: Any psychological variable that fluctuates over time can be scaled to have initial position and velocity between 0 and 10. Initial position and velocity values can be changed by scaling the oscillation amplitude of a variable, and/or Δt.

Each of the 10 initial value combinations were used to calculate C_1, C_2, C_3, C_4 by using equation set (41). Calculated C_1, C_2, C_3, C_4 values were used in combination with all the other manipulated variables to generate motion trajectories *x(t)* and *y(t)*.

e) Sample Size

n = 50;

According to the pilot simulation, when all the other manipulated variables are held constant, the mean estimates of the parameters of interest do not change across sample sizes (in terms of the number of subjects) that are common in daily diary studies in psychology (n = 15 to 150). Variation in n affects only the standard error of the estimates. A larger number of subjects results in smaller standard errors. As the main purpose of this simulation was to test whether the generated motion trajectories are being linked by the multilevel model to the set of parameters that define the corresponding physical system that produced them, varying n to explore standard errors would provide no meaningful information. Hence, n is fixed at the value of 50, which is a common number of subjects in daily diary studies and, according to the pilot simulation, produces reasonable standard error patterns.

f) Series length

7 full cycles;

Variation in series length in terms of the number of traversed cycles affects parameter estimates analogously to the variation in sample size n. According to the pilot simulation, when all other manipulated variables are held constant, the mean estimates of the parameters of interest remain the same across series lengths that are common in daily diary studies in psychology (3 to 15 full cycles). Variation in series length affects only the standard error of the estimates, with longer series resulting in smaller standard errors. For the same reasons as sample size above, series length was held constant in this simulation study at the value of 7 full cycles, a value that is representative of several

daily diary studies. According to the pilot simulation, having 7 full cycles produces reasonable standard error patterns.

g) Error Magnitude

$\frac{\sigma^2_{error}}{\sigma^2_{signal}+\sigma^2_{error}} * 100\% = 0.00002\%$, 10% , where

σ^2_{signal} is the variance of the *x(t)* or *y(t)* trajectory generated without error for each individual, and σ^2_{error} is the variance of the normal distribution that the residual terms are generated from for each individual at each time point. 10% error corresponds to reliability of .90 since reliability = $\frac{\sigma^2_{signal}}{\sigma^2_{signal}+\sigma^2_{error}}$ (the variance due to the signal is equivalent to the true score variance).

Generated error magnitudes are listed above in terms of the proportion of the error variance to the total variance of the generated position values (*x(t)* and *y(t)*). According to the pilot simulation, the error variance proportion of 0.00002% should yield adequate estimates for all the sets of manipulated parameter values. This observation assumes that no problems of identification exist. Error variance proportion of 10%, according to the pilot simulation, was expected to yield inadequate parameter estimates for all the sets of manipulated parameter values. In addition, error variance proportion of 10% relates to psychological measurement as it reflects high reliability (ρ_{xx} = .90) of a questionnaire.

Design

All the listed manipulated variable values, except for those that were listed together with their own specific combinations of the remaining manipulated variable

values, were combined in a factorial structure. This resulted in a general 18 (combinations of ω_1 and ω_2) × 5 (coupling ratios, κ_1/κ_2) × 10 (initial position and velocity combinations) × 2 (error magnitudes) design. The factorial design was supplemented with the examination of 2 additional special conditions, coupling ratios >

Evaluation

As described in parts e) and f), the mean estimates of the parameters of interest remain constant across different sample sizes and series lengths that are common in daily diary studies in psychology. Based on the pilot simulation, taking the mean of 30 parameter estimate sets appeared to be sufficient to achieve stable estimates, so 30 replications of each possible combination of the manipulated parameters listed above were generated. The parameters of the connected mass-spring system that produced them were estimated in the multilevel connected mass-spring model defined above.

The multilevel connected mass-spring model implemented in SAS estimated the mean negative squared angular frequency of the left-most spring (ω_1 in equation *x(t)*), the mean negative squared angular frequency of the right-most spring (ω_1 in equation *y(t)*), κ_1 and κ_2, together with the standard errors of each parameter. I evaluated the relative bias of the means of ω_1, ω_2, $\sqrt{\omega_1^2 + \kappa_1 + \kappa_2} = \omega_{secondary}$, κ_1, κ_2, and κ_1/κ_2 across the 30 simulated replications of each manipulated parameter set by calculating the mean parameter bias ($relative\ mean\ bias = \frac{mean\ estimate - true\ parameter\ value}{true\ parameter\ value}$) . I considered estimates whose mean parameter bias did not exceed 10 percent to be adequate (a criterion suggested in Muthén & Muthén, 2002).

Expected Results

It was not expected that all the trajectory pairs generated in accordance with the Equation system (40) would be detected by the multilevel SAS model correctly.

1. With higher density of the measures, acceleration terms become very small and overly susceptible to distortions due to the error in the position trajectories. Higher density of the time series implies smaller steps in time between the measures. Smaller steps in time between the measures imply smaller changes in velocity for each step. Smaller changes in velocity per step imply a smaller magnitude of acceleration for each step. Since acceleration terms are derived from the position trajectories, errors that are negligible in the context of position can potentially lead the estimate of acceleration to be very unreliable. This pattern also depends on the ratio κ_1/κ_2. If one coupling coefficient is very small relative to the other, the amplitude of its position trajectory will be small. Accordingly, the acceleration magnitudes of the corresponding mass will be small, and susceptible to distortions due to measurement error in the measure of position trajectory (*x(t)* or *y(t)*). Thus, it is reasonable to expect that there is a range of combinations of frequencies (ω_1 and ω_2), error rates ($\frac{\sigma^2_{error}}{\sigma^2_{signal}+\sigma^2_{error}}$), and coupling ratios (κ_1/κ_2) that separates trajectory pairs whose parameters are accurately estimated by the multilevel model, and trajectory pairs whose parameters are not estimated accurately by the multilevel model due to the noise in the acceleration terms.

2. With lower density of measurement, the number of the potential theoretical trajectories that accommodate the observed data increases, increasing the number of parameter combinations that would be expected to yield good model fit. When the

measures have a low sampling rate, multiple potential continuous time series models can be constructed that could potentially coincide with those measures. If any of those continuous time series trajectory pairs could theoretically be produced by the connected mass-spring system, they can potentially be detected by the multilevel model. The sparser the measures, the higher the likelihood of the existence of multiple continuous time series that can be producible by a connected mass-spring system, and the more likely that the multilevel model will detect a set of parameters that define a system other than the one that was used to generate the measures. For instance, if the theoretical trajectories have small cyclical fluctuations between sparse empirical measurements, the multilevel model would be likely to detect the parameters of a system that produces trajectories with smooth connections instead of fluctuations, in turn neglecting the secondary frequency.

Chapter 3

RESULTS

Checks on Adequacy of Solutions

Solution Quality

All (100%) of the replications yielded SAS warning messages that included "NOTE: Estimated G matrix is not positive definite. NOTE: Asymptotic variance matrix of covariance parameter estimates has been found to be singular and a generalized inverse was used. Covariance parameters with zero variance do not contribute to degrees of freedom computed by DDFM=SATTERTH." They reflect an error in the definition of the multilevel connected mass-spring model presented in Butner et al. (2005). However, they do not undermine the quality of the *fixed effect* estimates of the model that are of interest in this study.

To model the connected mass-spring system Butner et al. (2005) use a multivariate multilevel model, wherein Level-2 contains two equations that define the connected mass-spring system, and Level-1 rearranges the data related to these two equations into a univariate form using indicator variables. Such a model contains only one actual hierarchical level (Level 2), whereas Level 1 is present just for the variable arrangement into the univariate form, and contains the same equations as Level 2, one at a time, depending on the values of the indicator variables. Given such a structure of the multivariate multilevel model, the error term(s) can be estimated either at Level 1, or at Level 2, but not both, as they would be identical and inestimable (for example, see Ryu,

West, & Sousa, 2012). In the Butner et al. (2005) model[3] (see Equation set 44 below), however, error terms are present at both levels. Under such circumstances, when subscript *m* is equal to 1, the combined multilevel equation is presented in Equation (45),

$$\begin{aligned} \frac{d^2x_{mit}}{dt^2} &= \beta_{1it}(D1_{mit}) + \beta_{2it}(D2_{mit}) + r_{mit}\ . && \text{Level 1} \\ \beta_{1it} &= \eta_1 x_{1it} + \kappa_1(x_{2it} - x_{1it}) + e_{1it} && \text{Level 2} \\ \beta_{2it} &= \eta_2 x_{2it} + \kappa_2(x_{1it} - x_{2it}) + e_{2it}\ . \end{aligned} \tag{44}$$

and when subscript *m* is equal to 2, the combined multilevel equation is presented in Equation (46). Now technically, there are 4 error terms at the same hierarchical level ($e_{1it}, e_{2it}, r_{1it}, r_{2it}$) being estimated in the system of 2 equations (45 and 46). 4 unknowns

$$\frac{d^2x_{1it}}{dt^2} = \eta_1 x_{1it} + \kappa_1(x_{2it} - x_{1it}) + e_{1it} + r_{1it} \tag{45}$$

$$\frac{d^2x_{2it}}{dt^2} = \eta_2 x_{2it} + \kappa_2(x_{1it} - x_{2it}) + e_{2it} + r_{2it} \tag{46}$$

cannot be estimated from 2 equations, regardless of whether the covariance term between e_{1it} and e_{2it} is estimated or not (which Butner et al., 2005, find of importance).

SAS warnings reflect the issue by stating that the "asymptotic variance matrix of covariance parameter estimates has been found to be singular" and the "Estimated G matrix is not positive definite." To permit estimation of the model, SAS PROC MIXED automatically sets one of the three error variance components to 0 and estimates the remaining model. As a result, the model misspecification in the Butner et al. (2005)

[3] The corrected Butner et al. (2005) model with variable subscripts corrected to be consistent with the standard multilevel model notation of Raudenbush and Bryk (2001). The corrections were previously explained in the text. The original error term subscripts presented in Butner et al. were retained.

model is automatically corrected by the program, and correct fixed model estimates are produced.

As a check on the adequacy of the fixed effect estimates in the models that I ran in this simulation, I reran subsets of models across different manipulated parameter sets with the error term present in the Level 1 of the model (r_{mit}), and Level 2 error terms (e_{1it} and e_{2it}) absent from the model. Such a model formulation would be expected to produce no SAS warnings and yield identical fixed effect estimates to the originally defined model, as e_{1it} and e_{2it} are uncorrelated in my simulation. All the conditions (50) across different manipulated parameter sets that I reestimated in this way yielded fixed parameter estimates identical to those that were produced by the original model and evoked no SAS warnings.

If researchers wanted to define the multivariate multilevel connected mass-spring model in SAS PROC MIXED correctly from the start by removing the Level 1 residual term (which would be necessary if the covariance between the level 2 error terms was present), they could use a `repeated / subject = time(subject) type=un` statement instead of the `random d1 d2 / subject = time(subject) type=un` statement. I reexamined multiple conditions across different manipulated parameter sets with this replacement, and in all cases the fixed model estimates were identical to the ones estimated in the original model that produced SAS warnings. In an analogous model, Ryu et al. (2012) fixed Level 1 residual variance to a very small number to circumvent this issue.

Convergence

In the 0.00002% error variance conditions, 279 of the 27,000 replications did not converge. 236 of the non-converged replications occurred in the sampling frequency/major frequency of $\frac{2\pi}{70}$. The remaining 43 nonconverged replications were spread out across the other sampling/major frequencies with 24 instances at $\frac{2\pi}{35}$, 10 instances at $\frac{2\pi}{14}$, and 9 instances at $\frac{2\pi}{7}$. Nonconvergence tended to be more likely when there were extreme secondary frequencies ($\frac{2\pi}{4}$ and $\frac{2\pi}{69}$), initial value sets in which both velocity terms were large in magnitude (sets 2 and 9). In the 10% error variance conditions, all of the 27,000 replications converged. All the nonconverged replications in the 0.000002% error variance conditions were regenerated until a total of 27,000 converged replications in the condition were achieved.

Relative Bias

I evaluated the relative bias of the means of the estimates of (a) ω_1, (b) ω_2, (c) κ_1, (d) κ_2, (e) κ_1/κ_2, and (f) $\sqrt{\omega_1^2 + \kappa_1 + \kappa_2} = \omega_{secondary}$ across the 30 simulated replications of each manipulated parameter set. In the connected mass-spring system, I studied the population values of ω_1 ($=\frac{k_1}{m_1}$) for the mass of the first spring and ω_2 ($=\frac{k_2}{m_2}$) for the mass of the second spring were set equal. I used the mean estimate of ω_1 and ω_2 in computing the relative bias of $\omega_{secondary}$ (f). The true parameter values of κ_1 and κ_2 were fully defined by the remaining manipulated variables and were calculated by $\frac{\omega_{secondary}^2 - \omega_1^2}{1+\frac{1}{coupling\ ratio}}$ and $\frac{\omega_{secondary}^2 - \omega_1^2}{1+\ coupling\ ratio}$, respectively. Relative bias was calculated as:

$relative\ bias = \frac{mean\ estimate - true\ parameter\ value}{true\ parameter\ value}$. Following Muthén and Muthén (2002), I considered any parameter having more than 10% relative bias to be unacceptable.

In Tables 1 to 4, I report a summary of the percentage of replications that satisfied the 10% bias criterion for each of the manipulated conditions in the study. In the Tables, in addition to the six parameters of interest (a) to (f) identified above, I include columns (g) and (h). Column (g) contains assessment of the approximate equality of the ω_1 and ω_2 estimates. Approximate equality of the estimates is considered to be satisfied if an ω_2 estimate is within $\pm$10% of the corresponding ω_1 estimate. Column (h) indicates whether all seven parameters (a)-(h) met the criterion of acceptable relative bias (<10%).

Breakdown of Adequate Estimates by Condition for 0.00002% Error Rate

Manipulated Conditions for Major Frequencies ω_1 and ω_2

Table 1. Proportion of adequate estimates by manipulated value of major frequency ω_1 /sampling frequency.

	(a)	**(b)**	**(c)**	**(d)**	**(e)**	**(f)**	**(g)**	**(h)**
$\boldsymbol{\omega_1}$	$\boldsymbol{\omega_1}$	$\boldsymbol{\omega_2}$	$\boldsymbol{\kappa_1}$	$\boldsymbol{\kappa_2}$	$\boldsymbol{\kappa_1/\kappa_2}$	$\boldsymbol{\omega_{secondary}}$	$\boldsymbol{\omega_1 = \omega_2}$	**Whole**
2π/70	0.98	0.98	0.488	0.532	0.7	0.544	0.984	0.488
2π/35	0.98	0.98	0.54	0.544	0.736	0.544	0.984	0.54
2π/14	0.98	0.98	0.51	0.51	0.74	0.51	0.985	0.51
2π/7	0.98	0.98	0	0.005	0.74	0.17	0.985	0

As shown in Table 1, major frequencies ω_1 and ω_2 were detected adequately in 98% of replications across all the manipulated major frequencies/sampling frequencies. The estimated ω_1 and ω_2 were approximately equal in close to all cases (> 98%) across all the manipulated major frequencies/sampling frequencies. Individual coupling terms

(κ_1 and κ_2) were detected correctly in approximately 52% of the cases with manipulated major frequencies between $\frac{2\pi}{14}$ and $\frac{2\pi}{70}$ (higher sampling rates). When the manipulated major frequency was equal to $\frac{2\pi}{7}$, κ_1 and κ_2 estimates were virtually never accurate (< 1%). Coupling ratio κ_1/κ_2 estimates were consistently adequate across all the manipulated major frequencies at a similar rate of about 73%. Estimates of secondary frequencies were adequate at an approximate rate of 53% across the manipulated major frequency values between $\frac{2\pi}{14}$ and $\frac{2\pi}{70}$. When the manipulated major frequency was equal to $\frac{2\pi}{7}$, estimates of secondary frequencies were acceptable in 17% of the cases. The entire set of the estimated parameters was detected correctly in about 52% of cases with manipulated major frequencies between $\frac{2\pi}{14}$ and $\frac{2\pi}{70}$ (higher sampling rates), and in 0% of cases with the manipulated major frequency of $\frac{2\pi}{7}$ (lowest sampling rate).

Manipulated Conditions for Secondary Frequency $\omega_{secondary}$

Table 2. Proportion of adequate estimates by manipulated value of secondary frequency $\omega_{secondary}$ in combination with the corresponding major frequency.

		(a)	(b)	(c)	(d)	(e)	(f)	(g)	(h)
ω_1	$\omega_{secondary}$	ω_1	ω_2	κ_1	κ_2	κ_1/κ_2	$\omega_{secondary}$	$\omega_1 = \omega_2$	Whole
2π/70	**2π/4**	0.98	0.98	0	0	0.74	0	1	0
2π/70	**2π/20**	0.98	0.98	0.68	0.68	0.74	0.68	0.98	0.68
2π/70	**2π/35**	0.98	0.98	0.68	0.68	0.74	0.68	0.98	0.68
2π/70	**2π/50**	0.98	0.98	0.66	0.68	0.72	0.68	0.98	0.66
2π/70	**2π/69**	0.98	0.98	0.42	0.62	0.56	0.68	0.98	0.42
2π/35	**2π/4**	0.98	0.98	0	0	0.74	0	1	0
2π/35	**2π/10**	0.98	0.98	0.68	0.68	0.74	0.68	0.98	0.68
2π/35	**2π/17.5**	0.98	0.98	0.68	0.68	0.74	0.68	0.98	0.68
2π/35	**2π/25**	0.98	0.98	0.68	0.68	0.74	0.68	0.98	0.68
2π/35	**2π/34**	0.98	0.98	0.66	0.68	0.72	0.68	0.98	0.66
2π/14	**2π/4**	0.98	0.98	0	0	0.74	0	1	0
2π/14	**2π/7**	0.98	0.98	0.68	0.68	0.74	0.68	0.98	0.68
2π/14	**2π/10**	0.98	0.98	0.68	0.68	0.74	0.68	0.98	0.68
2π/14	**2π/13**	0.98	0.98	0.68	0.68	0.74	0.68	0.98	0.68
2π/7	**2π/3.5**	0.98	0.98	0	0.02	0.74	0	0.98	0
2π/7	**2π/4**	0.98	0.98	0	0	0.74	0	1	0
2π/7	**2π/5**	0.98	0.98	0	0	0.74	0	0.98	0
2π/7	**2π/6**	0.98	0.98	0	0	0.74	0.68	0.98	0

As shown in Table 2, major frequencies ω_1 and ω_2 were detected adequately in 98% of replications across all the manipulated secondary frequencies in combination with all the manipulated major frequencies/sampling frequencies. Estimated ω_1 and ω_2 were approximately equal in virtually all of the cases (98%) across all the manipulated secondary frequencies/sampling frequencies with the exception of $\frac{2\pi}{4}$, which produced equal ω_1 and ω_2 estimates in 100% of the cases. Individual coupling terms (κ_1 and κ_2) were detected correctly in approximately 68% of cases across all the primary and secondary frequency combinations with the exception of the fastest secondary frequency

of $\frac{2\pi}{4}$ and the fastest major frequency of $\frac{2\pi}{7}$, where estimate adequacy rate was 0%, and the frequency combination of $\frac{2\pi}{70}$ and $\frac{2\pi}{69}$, where estimate adequacy rate was 42% and 62% for κ_1 and κ_2, respectively. Coupling ratio κ_1/κ_2 estimates were consistently adequate across all the manipulated primary and secondary frequency combinations at the rate of 74%, except for the low major frequency combinations with the lowest secondary frequencies, $\frac{2\pi}{70}$ with $\frac{2\pi}{69}$, $\frac{2\pi}{70}$ with $\frac{2\pi}{50}$, and $\frac{2\pi}{35}$ with $\frac{2\pi}{34}$, where estimate adequacy rates were 56%, 72%, and 72%, respectively. Secondary frequency estimates were adequate at the rate of 68% across all the manipulated primary and secondary frequency combinations, where manipulated secondary frequencies were lower than $\frac{2\pi}{6}$. When manipulated secondary frequencies were faster than $\frac{2\pi}{6}$, 0% of the secondary frequency estimates were accurate. The entire set of the estimated parameters was detected correctly in 68% of cases with manipulated major frequencies between $\frac{2\pi}{70}$ and $\frac{2\pi}{14}$ in combination with manipulated secondary frequencies between $\frac{2\pi}{35}$ and $\frac{2\pi}{7}$. In cases with manipulated primary and secondary frequency combinations of $\frac{2\pi}{70}$ with $\frac{2\pi}{69}$, $\frac{2\pi}{70}$ with $\frac{2\pi}{50}$, and $\frac{2\pi}{35}$ with $\frac{2\pi}{34}$, the estimates of adequacy rates were 66%, 42%, and 66%, respectively. In the remaining cases, with secondary frequency of $\frac{2\pi}{4}$ or primary frequency of $\frac{2\pi}{7}$, the entire set of model parameters was never estimated correctly.

Manipulated Conditions for Coupling Ratio κ_1/κ_2

Table 3. Proportion of adequate estimates by manipulated value of coupling ratio κ_1/κ_2.

	(a)	(b)	(c)	(d)	(e)	(f)	(g)	(h)
κ_1/κ_2	ω_1	ω_2	κ_1	κ_2	κ_1/κ_2	$\omega_{secondary}$	$\omega_1 = \omega_2$	Whole
1/100	1.00	1.00	0.39	0.42	0.67	0.47	1.00	0.39
1/40	1.00	1.00	0.41	0.42	0.68	0.47	1.00	0.41
1/10	0.90	0.90	0.36	0.37	0.59	0.40	0.92	0.36
1/2	1.00	1.00	0.42	0.43	0.70	0.47	1.00	0.42
1	1.00	1.00	0.42	0.42	1.00	0.47	1.00	0.42

As shown in Table 3, major frequencies ω_1 and ω_2 , as well as their approximate equality were estimated adequately in 100% of replications across all the manipulated coupling ratios except for $\frac{\kappa_1}{\kappa_2} = 1/10$, where the adequacy rate was around 90%. Secondary frequencies were detected accurately in 40% of replications with the manipulated coupling ratio of 1/10, and in 47% of cases across all the remaining manipulated coupling ratios. Estimated coupling ratio approximately coincided with the theoretical one in 100% of cases when the manipulated coupling ratio was equal to 1, in approximately 68% of cases when the manipulated coupling ratio was equal to 1/2, 1/40 or 1/100, and in 59% of cases when the manipulated coupling ratio was 1/10. κ_2 was detected adequately in 37% of replications with the manipulated coupling ratio of 1/10, and in approximately 42% of cases across all the remaining manipulated coupling ratios. κ_1 estimates were adequate in approximately 41.5% of cases when manipulated coupling ratios were 1/40, 1/2, or 1, in 39% of cases when manipulated coupling ratio was equal to 1/100, and in 36% of cases when the manipulated coupling ratio was 1/10. Adequacy rates of the entire set of the estimated parameters were identical to the κ_1 adequacy rates.

Manipulated Conditions for Initial Value Sets

Table 4. Proportion of adequate estimates by initial value sets (1 through 10).

Initial Value Set (p_1,p_2,v_1,v_2)	(a) ω_1	(b) ω_2	(c) κ_1	(d) κ_2	(e) κ_1/κ_2	(f) $\omega_{secondary}$	(g) $\omega_1 = \omega_2$	(h) Whole
1. (10,10,0,0)	1.00	1.00	0.00	0.00	0.20	0.00	1.00	0.00
2. (0,0,10,10)	1.00	1.00	0.00	0.00	0.20	0.00	1.00	0.00
3. (1,1,-1,-1)	1.00	1.00	0.00	0.00	0.20	0.00	1.00	0.00
4. (1,10,5,5)	1.00	1.00	0.53	0.60	0.94	0.67	1.00	0.53
5. (-10,1,10,-1)	1.00	1.00	0.60	0.61	0.99	0.67	1.00	0.60
6. (1,-10,-1,10)	0.80	0.80	0.47	0.48	0.79	0.53	0.84	0.47
7. (-1,10,-10,1)	1.00	1.00	0.60	0.61	0.99	0.67	1.00	0.60
8. (10,-1,1,-10)	1.00	1.00	0.61	0.61	1.00	0.67	1.00	0.61
9. (10,10,-10,10)	1.00	1.00	0.57	0.61	0.97	0.67	1.00	0.57
10. (5,5,1,-10)	1.00	1.00	0.61	0.61	1.00	0.67	1.00	0.61

Note. p_1 = initial position of mass 1, p_2 = initial position of mass 2, v_1 = initial velocity of mass 1, and v_2 = initial velocity of mass 2.

As shown in Table 4, major frequencies ω_1 and ω_2 , as well as their approximate equality were estimated adequately in 100% of replications across all the initial value sets except 6, where the adequacy rate was around 80%. Initial value sets 1, 2, and 3 did not yield any other adequate estimates except for the 20% adequacy rate of the estimated coupling ratio. Initial value sets 4, 5, 7, 8, 9, and 10 yielded adequate estimates of κ_1, κ_2, κ_1/κ_2, $\omega_{secondary}$, and the entire model (Whole) in approximately 58%, 61%, 98%, 67%, and 58% of cases, respectively, with initial value sets 4 and 9 having slightly lower rates than the sets 5, 7, 8, and 10. These estimate adequacy rates were about 15% for the initial value set 6.

Adequate Estimates for 0.00002% Error Rate

In total, 882 replications out of 900 (98%) yielded adequate ω_1 and ω_2, estimates. In 886 cases (98.4%) out of 900 they were adequately detected to be equal. 408 replications out of 900 (45.3%) yielded adequate $\omega_{secondary}$, estimates. 359 replications out of 900 (39.9%) yielded adequate κ_1 estimates, and 372 replications out of 900 (41.3%) yielded adequate κ_2 estimates. 655 replications out of 900 (72.8%) yielded adequate κ_1/κ_2 ratio estimates. 359 replications out of 900 (39.9%) yielded adequate estimates for all model parameters (Whole). 288 (32%) replications did not yield adequate estimates for the whole model parameter set due to selected parameter values combining into multiple trajectory coefficients of zero, 350 (38.9%) replications due to empirical underidentification caused by undersampling, and 15 (1.7%) replications due to oversensitivity of acceleration terms due to high density of observations, with some of the replications having overlapping causes for nonconvergence.

0% of the parameter sets with initial value sets 1, 2, and 3 produced adequate whole model estimates, and 0% of the parameter sets with initial value set 6. together with κ_1/κ_2 ratio of 1/10 produced adequate whole model estimates. The initial value pattern in those conditions completely cancelled out either primary or secondary frequency from the trajectory equations. Then, due to the statistical structure of the connected mass-spring model, which requires both frequencies to be present in the trajectories to detect the two coupling coefficients, the adequate detection of all the parameters is impossible (see Discussion chapter). If the delineated parameter sets that produce single frequency motion trajectories are removed, and only parameter

combinations that produce trajectories with both, primary and secondary frequencies present in them are considered, then the estimate adequacy pattern would look like the one in Table 5.

Table 5. *Proportion of adequate estimates by manipulated value of secondary frequency* $\omega_{secondary}$ *in combination with the corresponding major frequency with single frequency trajectories producing parameter sets removed.*

		(a)	(b)	(c)	(d)	(e)	(f)	(g)	(h)
ω_1	$\omega_{secondary}$	ω_1	ω_2	κ_1	κ_2	κ_1/κ_2	$\omega_{secondary}$	$\omega_1 = \omega_2$	Whole
2π/70	**2π/4**	1	1	0	0	1	0	1	0
2π/70	**2π/20**	1	1	1	1	1	1	1	1
2π/70	**2π/35**	1	1	1	1	1	1	1	1
2π/70	**2π/50**	1	1	0.97	1	0.97	1	1	0.97
2π/70	**2π/69**	1	1	0.62	0.91	0.74	1	1	0.62
2π/35	**2π/4**	1	1	0	0	1	0	1	0
2π/35	**2π/10**	1	1	1	1	1	1	1	1
2π/35	**2π/17.5**	1	1	1	1	1	1	1	1
2π/35	**2π/25**	1	1	1	1	1	1	1	1
2π/35	**2π/34**	1	1	0.97	1	0.97	1	1	0.97
2π/14	**2π/4**	1	1	0	0	1	0	1	0
2π/14	**2π/7**	1	1	1	1	1	1	1	1
2π/14	**2π/10**	1	1	1	1	1	1	1	1
2π/14	**2π/13**	1	1	1	1	1	1	1	1
2π/7	**2π/3.5**	1	1	0	0	1	0	1	0
2π/7	**2π/4**	1	1	0	0	1	0	1	0
2π/7	**2π/5**	1	1	0	0	1	0	1	0
2π/7	**2π/6**	1	1	0	0	1	1	1	0

With the single frequency trajectories producing parameter sets removed (parameter sets that include initial value sets 1, 2, 3, or a combination of initial value set 6 with a coupling ratio of 0.1), the remaining parameter estimate adequacy pattern becomes

interpretable (Table 5). As predicted, whole parameter sets were fully adequate (Whole = 1) unless:

a) The sampling rate was too low with $\omega_1 = \frac{2\pi}{7}$, which corresponds to 7 observations per full cycle, and/or $\omega_{secondary} < \frac{2\pi}{7}$, which corresponds to fewer than 7 observations per secondary cyclic component. Under those conditions the coupling coefficients, and in turn the whole model parameter set were never estimated adequately (Whole = 0).

b) The sampling rate was high ($\omega_1 = \frac{2\pi}{70}$, i.e. 70 observations per full cycle with $\omega_{secondary} = \frac{2\pi}{69}\ or\ \frac{2\pi}{50}$, i.e. 69 or 50 observations per secondary cyclic component, and $\omega_1 = \frac{2\pi}{35}$ with $\omega_{secondary} = \frac{2\pi}{34}$) in combination with small κ_1 and/or κ_2 values that emerge from the small difference between ω_1 and $\omega_{secondary}$ (as $\sqrt{\omega_1^2 + \kappa_1 + \kappa_2} = \omega_{secondary} \rightarrow \kappa_1 + \kappa_2 = \omega_{secondary}^2 - \omega_1^2$), small coupling ratio (e.g. κ_1/κ_2 = 1/100) and/or cancellation of one of the secondary frequency representing motion trajectory terms due to the set of initial conditions (see Discussion section). In particular, combinations of $\omega_1 = \frac{2\pi}{70}$, $\omega_{secondary} = \frac{2\pi}{50}$, $\frac{\kappa_1}{\kappa_2}$ = 1/100, initial value set 4 (p_1=1, p_2=10, v_1=5, v_2=5), and $\omega_1 = \frac{2\pi}{35}$, $\omega_{secondary} = \frac{2\pi}{34}$, $\frac{\kappa_1}{\kappa_2}$ = 1/100, initial value set 4 (p_1=1, p_2=10, v_1=5, v_2=5) did not yield adequate κ_1 estimates, and consequently whole model estimates. 13 replications that did not yield adequate whole model estimates with $\omega_1 = \frac{2\pi}{70}$ and

$\omega_{secondary} = \frac{2\pi}{69}$ were found in combination with all the coupling ratios and multiple initial value sets.

Summary for 0.00002% Error Rate

In general, parameter sets that had all their parameters estimated adequately had following features:

1) Had both, primary and secondary frequency represented in the motion trajectories (i.e. the set of initial conditions did not produce $C_1 = 0$ and $C_2 = 0$, or $C_3 = 0$ and $C_4 = 0$).
2) Had primary frequencies $\omega_1 = \frac{2\pi}{14}, \frac{2\pi}{35}$ or $\frac{2\pi}{70}$, which corresponds to the sampling rate of 14, 35, and 70 observations per full cycle.
3) Had secondary frequencies $\omega_{secondary} = [\frac{2\pi}{50}, \frac{2\pi}{7}]$, which corresponds to the sampling rate of 7 through 50 observations per secondary cyclic component.

The remaining parameter sets did not yield adequate estimates of all parameters due to: a) selected parameter values combining into multiple trajectory coefficients of zero (initial value sets 1, 2, and 3, and 6 with $\frac{\kappa_1}{\kappa_2} = \frac{1}{10}$); b) empirical underidentification caused by undersampling ($\omega_1 = \frac{2\pi}{7}$, and/or $\omega_{secondary} < \frac{2\pi}{7}$); c) oversensitivity of acceleration terms due to high density of observations ($\omega_1 = \frac{2\pi}{70}$ with $\omega_{secondary} = \frac{2\pi}{69}$) .

Breakdown of Adequate Estimates by Condition for 10% Error Rate

In Tables 5 to 8, I report a summary of the percentage of replications that satisfied the 10% bias criterion for each of the manipulated conditions in the study.

Manipulated Conditions for Major Frequencies ω_1 and ω_2

Table 6. Proportion of adequate estimates by manipulated value of major frequency ω_1/sampling frequency.

	(a)	(b)	(c)	(d)	(e)	(f)	(g)	(h)
ω_1	ω_1	ω_2	κ_1	κ_2	κ_1/κ_2	$\omega_{secondary}$	$\omega_1 = \omega_2$	Whole
2π/70	0	0	0.032	0.004	0.2	0	0.576	0
2π/35	0	0	0.032	0.008	0.208	0.004	0.588	0
2π/14	0	0.015	0.07	0.115	0.24	0.015	0.725	0
2π/7	0.98	0.96	0.06	0.045	0.36	0.235	0.925	0.015

As shown in Table 6, manipulated major frequencies of $\frac{2\pi}{70}$ and $\frac{2\pi}{35}$, which correspond to the sampling rates of 70 and 35 observations per cycle, respectively, yielded adequate parameter estimates in virtually 0% of cases, except for the coupling ratio estimates, which were estimated adequately in about 20% of cases. Although individual primary frequencies ω_1 and ω_2 were never detected correctly with the manipulated major frequencies of $\frac{2\pi}{70}$ and $\frac{2\pi}{35}$, they were correctly estimated to be approximately equal in about 58% of cases.

Manipulated major frequency condition of $\frac{2\pi}{14}$ in most cases yielded slightly higher parameter estimates, with ω_2 being detected adequately at the rate of 1.5%, κ_1 at the rate of 7%, κ_2 at the rate of 11.5%, κ_1/κ_2 ratio at the rate of 24%, and $\omega_{secondary}$ 1.5%.

However, the estimates in these conditions never correctly reproduced ω_1; consequently, in no replication was the entire set of model parameters (h) detected correctly.

Manipulated major frequency condition of $\frac{2\pi}{7}$ generated adequate estimates of ω_1, ω_2 and their equality in most cases (98%, 96%, and 92.5%, respectively). Coupling ratio estimates and secondary frequency estimates yielded adequate estimates in 36% of cases, and 23.5% of the cases, respectively. These rates were higher than in the rest of the manipulated major frequencies/sampling rate conditions. The remaining estimates, κ_1, κ_2 and the combined adequacy of the entire model were as low as in other manipulated major frequency conditions, with the whole set of model parameters being adequate in only 1.5% of cases.

Manipulated Conditions for Secondary Frequency $\omega_{secondary}$

Table 7. Proportion of adequate estimates by manipulated value of secondary frequency $\omega_{secondary}$ in combination with the corresponding major frequency.

		(a)	(b)	(c)	(d)	(e)	(f)	(g)	(h)
ω_1	$\omega_{secondary}$	ω_1	ω_2	κ_1	κ_2	κ_1/κ_2	$\omega_{secondary}$	$\omega_1 = \omega_2$	Whole
2π/70	**2π/4**	0	0	0.16	0	0.2	0	1	0
2π/70	**2π/20**	0	0	0	0	0.22	0	0.46	0
2π/70	**2π/35**	0	0	0	0.02	0.28	0	0.54	0
2π/70	**2π/50**	0	0	0	0	0.18	0	0.48	0
2π/70	**2π/69**	0	0	0	0	0.12	0	0.4	0
2π/35	**2π/4**	0	0	0.14	0	0.2	0	1	0
2π/35	**2π/10**	0	0	0	0.02	0.24	0	0.46	0
2π/35	**2π/17.5**	0	0	0.02	0.02	0.28	0	0.52	0
2π/35	**2π/25**	0	0	0	0	0.22	0	0.44	0
2π/35	**2π/34**	0	0	0	0	0.1	0.02	0.52	0
2π/14	**2π/4**	0	0	0.04	0	0.28	0	1	0
2π/14	**2π/7**	0	0	0.16	0.34	0.3	0.06	0.58	0
2π/14	**2π/10**	0	0	0.08	0.08	0.28	0	0.56	0
2π/14	**2π/13**	0	0.06	0	0.04	0.1	0	0.76	0
2π/7	**2π/3.5**	0.98	0.98	0.04	0.02	0.38	0	0.98	0
2π/7	**2π/4**	0.98	0.98	0.12	0	0.38	0	1	0
2π/7	**2π/5**	0.98	0.94	0.02	0	0.36	0.62	0.96	0
2π/7	**2π/6**	0.98	0.94	0.06	0.16	0.32	0.32	0.76	0.06

The entire set of model parameters was estimated correctly only in 3 cases out of 900; all of these cases included the manipulated primary and secondary frequency combination $\frac{2\pi}{7}$ with $\frac{2\pi}{6}$. As shown in Table 6, ω_1 and ω_2 were adequately estimated in most cases (~97%) with the manipulated primary frequency of $\frac{2\pi}{7}$. In case of all the remaining manipulated frequency combinations, ω_1 and ω_2 estimates were almost never adequately estimated (~0%). The criterion for the equality of ω_1 and ω_2 was satisfied in

approximately 50% of the replications, with the exception of the manipulated secondary frequency of $\frac{2\pi}{4}$, which yielded adequate equality estimates in 100% of the replications. The manipulated frequency combinations of $\frac{2\pi}{14}$ with $\frac{2\pi}{13}$, and $\frac{2\pi}{7}$ with $\frac{2\pi}{6}$, also yielded adequate estimates in 76% of the cases, and the manipulated frequency combinations of $\frac{2\pi}{7}$ with $\frac{2\pi}{3.5}$, and $\frac{2\pi}{7}$ with $\frac{2\pi}{5}$, which produced equal primary frequency estimates in approximately 97% of the cases. $\omega_{secondary}$ was detected adequately in 62% of the replications with the manipulated frequency combination of $\frac{2\pi}{7}$ with $\frac{2\pi}{5}$, in 32% of cases with the manipulated frequency combination of $\frac{2\pi}{7}$ with $\frac{2\pi}{6}$, and in close to 0% of the replications in the remaining manipulated frequency combinations. κ_1 and κ_2 estimates were adequate in a very low proportion of replications across all the manipulated frequency combinations except of $\frac{2\pi}{14}$ with $\frac{2\pi}{7}$, in which case they were adequate at higher rates of 16% and 32%, respectively. Coupling ratio estimates were adequate in ~20% of cases across all the major frequencies higher than $\frac{2\pi}{7}$. In case of manipulated major frequency of $\frac{2\pi}{7}$ it was estimated correctly in ~35% of cases.

Manipulated Conditions for Coupling Ratio κ_1/κ_2

Table 8. Proportion of adequate estimates by manipulated value of coupling ratio κ_1/κ_2.

	(a)	(b)	(c)	(d)	(e)	(f)	(g)	(h)
κ_1/κ_2	ω_1	ω_2	κ_1	κ_2	κ_1/κ_2	$\omega_{secondary}$	$\omega_1 = \omega_2$	Whole
1/100	0.22	0.23	0.01	0.02	0.04	0.03	0.59	0.00
1/40	0.22	0.22	0.01	0.04	0.03	0.04	0.59	0.00
1/10	0.20	0.21	0.07	0.03	0.02	0.04	0.62	0.00
1/2	0.22	0.21	0.10	0.05	0.24	0.08	0.72	0.01
1	0.22	0.22	0.05	0.05	0.90	0.09	0.93	0.01

The entire set of model parameters was estimated correctly only in 3 out of 900 replications, with 2 of the successful replications occurring with the manipulated coupling ratio of 1/2 and 1 occurring with the manipulated coupling ratio of 1. As shown in Table 8, primary frequency estimates ω_1 and ω_2 were detected adequately in approximately 22% of cases across all the manipulated coupling ratios, with the manipulated coupling ratio of 1/10 producing slightly lower rates of adequate estimates of both ω_1 and ω_2. The approximate equality of the estimated primary frequencies was satisfied in approximately 60% of the replications with the manipulated coupling ratios of 1/100, 1/40, and1/10, in approximately 72% of the replications with the coupling ratio of ½, and in 93% of cases with the manipulated coupling ratio of 1. As the two coupling coefficients became more similar, the adequacy of the estimates increased. Adequacy rates of the estimates of the individual coupling coefficients as well as adequacy rates of the estimates of the secondary frequency were very low (ranging from 1% to 10%). The higher adequacy rates occurred at the higher manipulated coupling ratios. The estimated coupling ratios were adequate in approximately 3% of the replications across the

manipulated coupling ratios of 1/100, 1/40, and 1/10. With the manipulated coupling ratio of ½, the estimated coupling ratio adequacy rose to 24%, and with the manipulated coupling ratio of 1 the estimated coupling ratio was adequate at the rate of 90%.

Manipulated Conditions for Initial Value Sets

Table 9. Proportion of adequate estimates by initial value sets (1 through 10).

Initial Value Set (p_1,p_2,v_1,v_2)	(a) ω_1	(b) ω_2	(c) κ_1	(d) κ_2	(e) κ_1/κ_2	(f) $\omega_{secondary}$	(g) $\omega_1 = \omega_2$	(h) Whole
1. (10,10,0,0)	0.22	0.22	0.01	0.00	0.20	0.00	1.00	0.00
2. (0,0,10,10)	0.22	0.22	0.01	0.00	0.20	0.00	1.00	0.00
3. (1,1,-1,-1)	0.22	0.22	0.01	0.00	0.20	0.00	1.00	0.00
4. (1,10,5,5)	0.22	0.26	0.01	0.03	0.21	0.09	0.52	0.00
5. (-10,1,10,-1)	0.22	0.22	0.07	0.04	0.20	0.08	0.57	0.01
6. (1,-10,-1,10)	0.18	0.13	0.06	0.07	0.37	0.06	0.46	0.00
7. (-1,10,-10,1)	0.22	0.22	0.06	0.04	0.21	0.08	0.57	0.00
8. (10,-1,1,-10)	0.22	0.22	0.09	0.08	0.28	0.09	0.56	0.00
9. (10,10,-10,10)	0.22	0.22	0.04	0.04	0.30	0.09	0.64	0.01
10. (5,5,1,-10)	0.22	0.22	0.11	0.08	0.30	0.09	0.59	0.01

Note. p_1 = initial position of mass 1, p_2 = initial position of mass 2, v_1 = initial velocity of mass 1, and v_2 = initial velocity of mass 2.

The entire set of model parameters was detected correctly in only 3 replications out of 900, with one of them with initial value set 5, one with the initial value set 9, and one with the initial value set 10. ω_1 and ω_2 were estimated correctly in approximately 22% of the replications across all of the initial value sets, except for the initial value set 7, where estimate adequacy rates were lower, at 18% and 13%, respectively. Approximate equality of the two major frequencies was detected correctly in 100% of cases across initial value sets 1, 2, and 3, in 64% of cases with the initial value set 9, in approximately 55% of cases across initial values sets 4,5,7,8, and 10, and in 46% of cases with the initial

value set 6. Initial value sets 1, 2, and 3 produced identical estimate adequacy rates for all the estimated parameters, with κ_2 and $\omega_{secondary}$ never being detected correctly, κ_1 detected adequately in 1% of cases and coupling ratio detected adequately in 20% of the cases. In all of the remaining initial value set conditions, individual coupling coefficients as well as $\omega_{secondary}$ were rarely detected adequately: adequacy rates ranged from 1% to 11%. The coupling ratio was detected correctly in approximately 20.5% of cases with initial value sets 3, 4, 5, and 7, in 28% of cases with the initial value set 8, in 30% of cases with initial value sets 9 and 10, and in 37% of cases with the initial value set 6.

Summary for 0.10% Error Rate Conditions

With an error rate of 10%, only in 3 replications out of 900 was the entire set of mass-spring system parameters detected correctly. Such an outcome was consistent with the pilot simulation. Statistical theory also leads to the expectation that the 10% error rate in position values will generate highly biased acceleration values, and in turn biased parameter estimates.

The three replications that yielded all model parameter estimates adequate were:

1. $\omega_1 = \frac{2\pi}{7}$, $\omega_{secondary} = \frac{2\pi}{6}$, $\frac{\kappa_1}{\kappa_2} = \frac{1}{2}$, initial value set 5 ($p_1$ = -10, p_2 = 1, v_1 = 10, v_2 = -1);
2. $\omega_1 = \frac{2\pi}{7}$, $\omega_{secondary} = \frac{2\pi}{6}$, $\frac{\kappa_1}{\kappa_2} = \frac{1}{2}$, initial value set 9 ($p_1$ = 10, p_2 = 10, v_1 = -10, v_2 = 10);
3. $\omega_1 = \frac{2\pi}{7}$, $\omega_{secondary} = \frac{2\pi}{6}$, $\frac{\kappa_1}{\kappa_2} = 1$, initial value set 10 ($p_1$ = 5, p_2 = 5, v_1 = 1, v_2 = -10).

Although all three of them share the same primary and secondary frequency, they did not form a single coherent cluster in the space of the remaining manipulated parameter values. In addition, replications with these parameter sets did not yield adequate whole model parameter estimates with the error rate of 0.00002%. Thus, it is most likely that the adequacy of these three particular cases emerged as a result of a serendipitous combination of manipulated parameters, together with a beneficial systematic interpretation of the distorted acceleration terms by the statistical structure of the connected mass-spring model. Hence, to sum up, as was predicted, the error rate that is common in psychology (10%, comparable to reliability = .90), yields estimates that are profoundly affected by the error of measurement. With such an error rate, the undamped connected mass-spring model cannot recover the parameters of the underlying physical system adequately even when the motion trajectories inserted into the model are producible by the connected mass-spring system.

Auxiliary Question: Coupling ratio $\kappa_1/\kappa_2 < 1$ versus $\kappa_1/\kappa_2 > 1$

All the coupling ratios in the factorial design delineated above contained κ_1 lower than or equal to κ_2. The reverse pattern of the coupling coefficients (i.e. κ_1 higher than κ_2) was not considered, as exchanging κ_1 and κ_2 along with exchanging initial position and initial velocity terms, and setting them to their additive inverses (i.e, $p_1 = -p_2,\ p_2 = -p_1,\ v_1 = -v_2;\ \ v_2 = -v_1$) should yield identical motion trajectories to those produced by the initial system, but reversed and mirror reflected (i.e. the mirror image of *x(t)* of the initial system will equal *y(t)* of the rearranged system, and the mirror image of *y(t)* of the initial system will equal *x(t)* of the rearranged system). If this is

correct, multilevel connected mass-spring model estimates of the original and the reversed case should yield identical set of parameter estimates, but with ω_1 and ω_2 estimates reversed, and κ_1 and κ_2 estimates reversed.

With a fixed manipulated value set of $\omega_1 = \frac{2\pi}{70}$, $\omega_{secondary} = \frac{2\pi}{20}$, $n = 50$, series length = 7 cycles , $\frac{\sigma^2_{error}}{\sigma^2_{signal}+\sigma^2_{error}}$ = 0.0000002, and initial value set 8, motion trajectories with two pairs of coupling rates were generated and estimated in the multilevel connected mass-spring model. The estimates are shown in Table 10.

Table 10. Main parameter estimates with coupling ratio reversed.

κ_1/κ_2	ω_1	ω_2	κ_1	κ_2
1/2	0.0897	0.0897	0.0299	0.0599
2/1	0.0897	0.0897	0.0599	0.0299
1/10	0.0897	0.0897	0.0082	0.0817
10/1	0.0897	0.0897	0.0817	0.0082

The model converged in 100% of cases across all replications and yielded adequate estimates of all parameters. As predicted, exchanging coupling terms (together with the pairs of initial values) produced identical, but exchanged parameter estimates in both pairs of cases (see Table 10).

Chapter 4

DISCUSSION

Although estimate adequacy rates may appear to be distributed quite randomly across Tables 1 through 4, the manipulated parameter sets that produced inadequate estimates are quite systematic and predictable. Some of these sets yielded inadequate parameter estimates due to the cancellation of the motion trajectory terms as a result of specific manipulated values combining into 0 coefficients. Manipulated parameter sets that included conditions with low number of observations per each cyclic component yielded estimates that were undermined by empirical underidentification resulting from undersampling. Another cluster of inadequate estimates stemmed from the high sampling rate conditions yielding imprecise estimates of acceleration terms.

Motion Trajectory Term Cancellation due to Manipulated Values Combining into 0 Coefficients

Initial value sets 1, 2, and 3. Initial value sets 1, 2, and 3 did not yield a single adequate coupling term or secondary frequency estimate, although the primary frequency related estimates, ω_1, ω_2 , and $\omega_1 = \omega_2$, were all accurate in 100% of cases. Initial value combinations 1, 2, and 3 were purposefully selected to have their pairs of initial positions and initial velocities to be equal, i.e. $p_1=p_2$ and $v_1=v_2$. Both initial position and initial velocity terms being equal results in the third and the fourth terms of the trajectory equations being equal to zero. When 3rd and 4th terms are not present, there are no remaining terms that represent the second frequency, so they are cancelled out (see

Figure 10 for illustration). In addition, the remaining terms do not contain any individual coupling terms (κ_1 or κ_2), only their ratio. Hence, the resulting motion trajectories do not

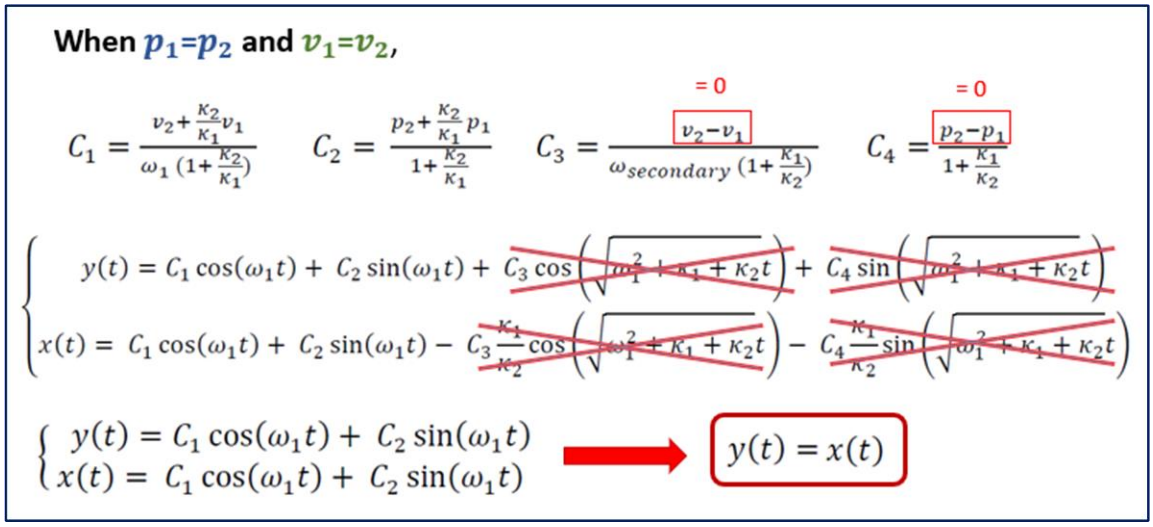

Figure 10. *Cancellation of secondary frequency representing motion trajectory terms in case of equal initial position and initial velocity terms.*

include terms that represent the secondary frequency or individual coupling value magnitudes. Moreover, as it is apparent from the illustration in Figure 10, the *x(t)* and *y(t)* trajectories are identical. In the multilevel connected mass-spring model κ_1 and κ_2 are estimated as the regression coefficients of the difference between the position values of the two masses at each time point (see Figure 11). When the two position trajectories are identical, the difference between them is just the difference between the error terms at each time point. Accordingly, for initial value sets 1-3 SAS PROC MIXED produces a warning that states that "A linear combination of covariance parameters is confounded

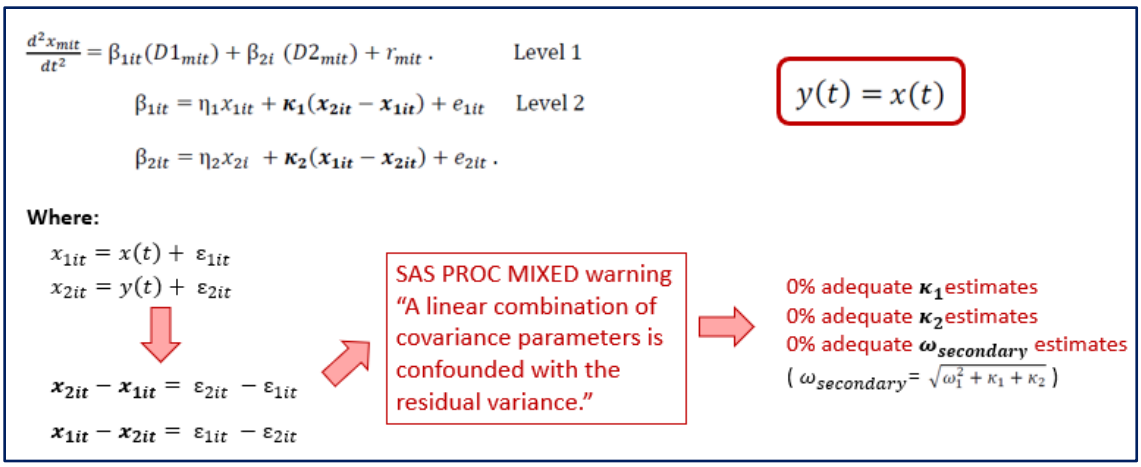

Figure 11. *Effect of the cancellation of the secondary frequency terms from the motion trajectories on statistical structure of multilevel connected mass-spring model.*

with the residual variance." As a consequence, under the circumstances where initial position and initial velocity pairs are equal, individual coupling terms cannot be estimated correctly. The secondary frequency that is estimated by $\sqrt{\omega_1^2 + \kappa_1 + \kappa_2}$ cannot be detected accurately either, as it needs both the κ_1 and κ_2 estimates to be correct in order to yield adequate estimates. In conclusion, the connected mass-spring model cannot be used when the two time-varying variables of interest have the same starting value positions along with the equal initial rate of change. By definition, this includes any cases where two variables are oscillating over time in an identical manner. This result reflects a boundary condition for the mass-spring model.

Initial value set 6 ($p_1 = 1,\ p_2 = -10,\ v_1 = -1,\ v_2 = 10$) in combination with the manipulated coupling ratio $\frac{\kappa_1}{\kappa_2}$ *= 1/10* never produced adequate estimates of ω_1, ω_2, $\omega_{secondary}$, κ_1, or $\frac{\kappa_1}{\kappa_2}$. This occurs due to the combination of the initial position and initial velocity values present in initial value set 6 producing zero C_1 and C_2 coefficients

when combined with the coupling ratio of 1/10 (see Figure 12). Hence, such an initial value and coupling ratio combination cancels out both terms that represent the primary

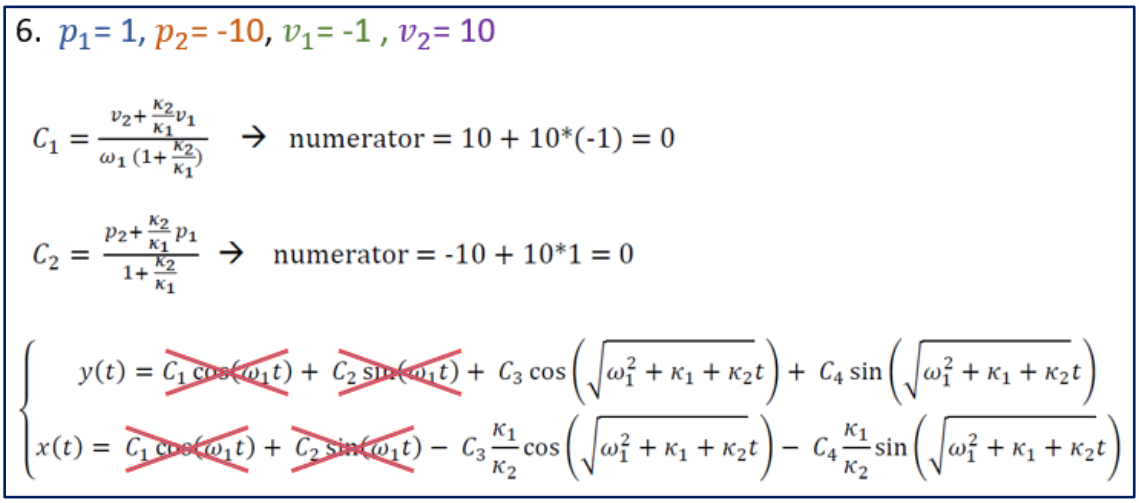

Figure 12. *Cancellation of primary frequency representing motion trajectory terms in case of initial value set 6 in combination with the coupling ratio of 1/10.*

frequency in the trajectory equations $x(t)$ and $y(t)$. Therefore, the primary frequency is nonexistent in the motion of the two masses (see Figure 12), and is impossible to detect from such generated trajectories. More precisely, the absence of the primary frequency representing terms renders both regression predictor pairs in the Level 2 of the multilevel model collinear, which can be seen in Figure 13 below.

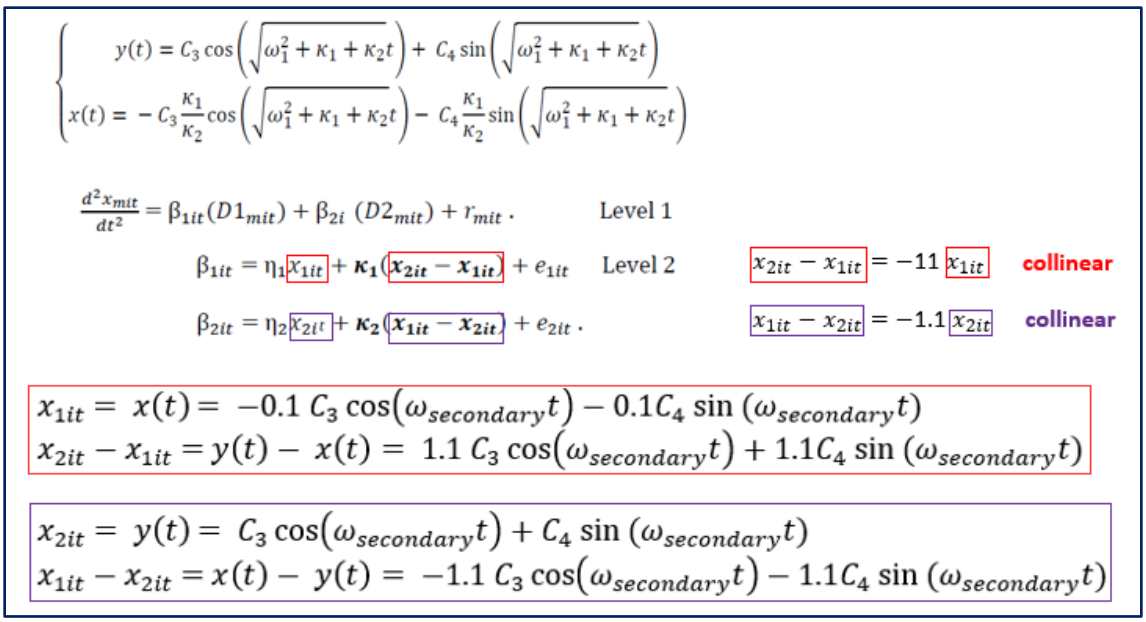

Figure 13. *Effect of the cancellation of the primary frequency terms from the motion trajectories on statistical structure of multilevel connected mass-spring model.*

Since the two pairs of regression predictors are collinear, they are confounded with the error variance and cannot yield correct model estimates. This is confirmed by the SAS PROC MIXED warning that "A linear combination of covariance parameters is confounded with the residual variance." Therefore, the connected mass-spring model is not applicable when initial position and velocity values of two time varying variables combine with their coupling ratio in a way that $v_2 + \frac{\kappa_2}{\kappa_1} v_1 = 0$ and $p_2 + \frac{\kappa_2}{\kappa_1} p_1 = 0$. This also means that whenever the two time varying variables are oscillating completely in phase, multilevel connected mass-spring model will not yield correct estimates.

Empirical Underidentification due to Undersampling

Primary frequency of $\frac{2\pi}{7}$. The primary frequency of $\frac{2\pi}{7}$ (sampling rate of 7 equally spaced observations per cycle) never yielded adequate estimates for the entire set of

connected mass-spring model parameters. Such an outcome was expected: The pilot simulation indicated that 7 equally spaced observations per cycle would yield data that are too sparse to accurately capture a trajectory pattern of two interacting cycles. As was presented above, with lower density of measurement, the number of the potential theoretical trajectories that accommodate the observed data increases, increasing the number of parameter combinations that would be expected to yield good model fit. When the measures have a low sampling rate, multiple potential continuous time series models can be constructed that could potentially represent those measures. If any of those continuous time series trajectory pairs could theoretically be produced by the connected mass-spring system, they can potentially be detected by the multilevel model. The sparser the measures, the higher the likelihood of the existence of multiple continuous time series that can be potentially produced by a connected mass-spring system. Consequently, the likelihood increases that the multilevel model will detect a set of parameters that define a system *other* than the one that was used to generate the data. For instance, if the theoretical trajectories have small cyclical fluctuations between sparse empirical measurements, the multilevel model would be likely to detect the parameters of a system that produces trajectories with smooth connections instead of fluctuations, failing to detect the secondary frequency. This example approximately coincides with the adequacy pattern produced by the sampling frequency of 7 measures per cycle (manipulated $\omega_1 = \frac{2\pi}{7}$). When the initial value and coupling ratio combinations did not cancel out an entire frequency from the motion trajectories, the primary frequencies ω_1 and ω_2 were detected adequately in 100% of cases with the manipulated $\omega_1 = \frac{2\pi}{7}$. In contrast, the coupling

terms κ_1 and κ_2 were always underestimated so that the detected secondary frequency was always underestimated. An illustration of this process with $\omega_1 = \frac{2\pi}{7}$ and $\omega_{secondary} = \frac{2\pi}{2}$ is presented in Figure 14 (a high $\omega_{secondary}$ was chosen to produce a clear illustration; lower secondary frequencies produce patterns that are less visually discernable).

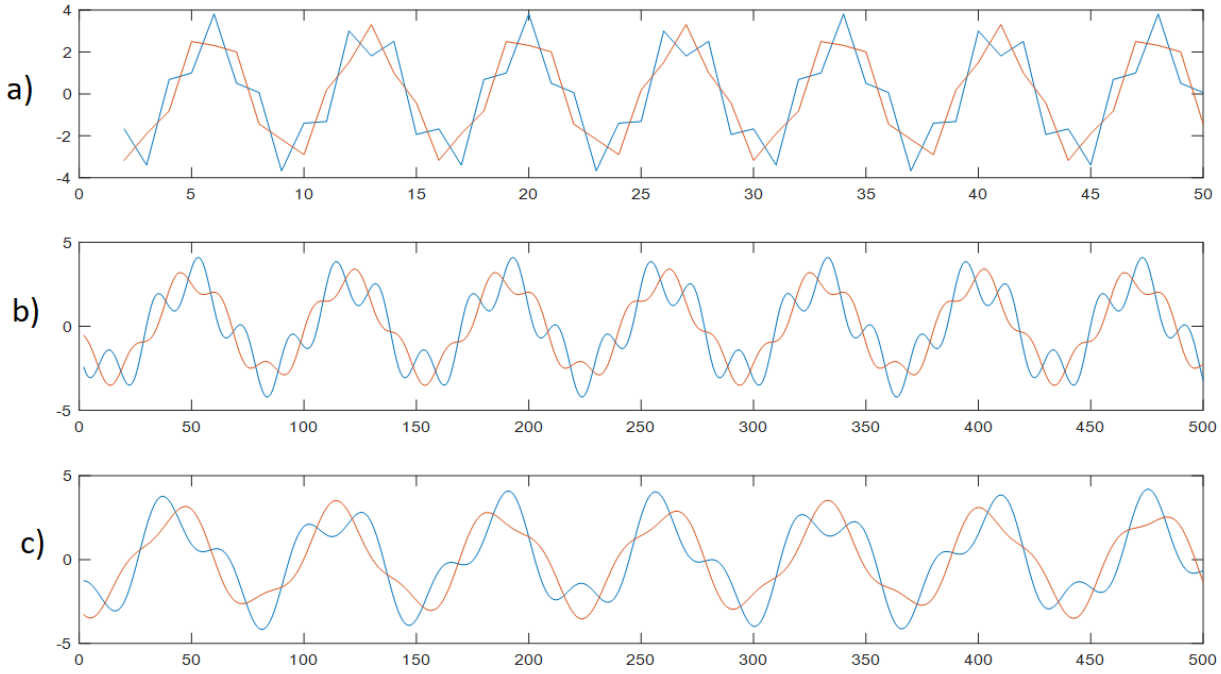

Figure 14. *Comparison of the empirical, theoretical, and multilevel connected mass-spring model detected motion trajectories with* $\omega_1 = \frac{2\pi}{7}$, $\omega_{secondary} = \frac{2\pi}{2}$, *and* $\frac{\kappa_1}{\kappa_2} = 0.9$. *The orange line represents motion of mass 1, which is defined by x(t) in the Equation set (40). The blue line represents motion of mass 2, which is defined by y(t) in the Equation set (40). a) Empirical time series of the motion trajectories with 7 equally spaced observations per cycle joined by straight lines; b) Theoretical time series of the motion trajectories; c) Motion trajectories produced by the system detected by the multilevel connected mass-spring model from the empirical time series, given the same set of initial values. The X-axis represents time units proportional to the measurement occasions.*

The results of this simulation demonstrate that increasing sampling frequency resolves the issue. For instance, the manipulated frequency combination of $\omega_1 = \frac{2\pi}{7}$ and $\omega_{secondary} = \frac{2\pi}{3.5}$ differs from the manipulated frequency combination of $\omega_1 = \frac{2\pi}{70}$ and $\omega_{secondary} = \frac{2\pi}{35}$ only in its sampling rate, which is 10 times higher in the second case. However, the rate of the entire model estimate adequacy increases from 0% to 100% (after exclusion of the inestimable initial value sets discussed above) by introducing this change. The major frequency of $\frac{2\pi}{7}$ was added to the simulation only for the reason of its applicability in daily diary studies (7 daily measures per weekly cycle). It was not expected to produce adequate estimates.

Manipulated parameter sets with $\omega_{secondary} > \frac{2\pi}{7}$ did not produce any adequate κ_1, κ_2, $\omega_{secondary}$ estimates in combination with any manipulated major frequencies/sampling rates. Four observations per secondary cyclic component are not sufficient for accurately capturing the full amplitude of the secondary fluctuations as the peaks are usually skipped over with such a sparse sampling rate. As a result, κ_1 and κ_2 cannot be estimated adequately, which also renders the $\omega_{secondary}$ inadequate, as it contains both κ_1 and κ_2 in its mathematical definition.

Oversensitivity of Acceleration Terms due to High Density of Observations together with Low Coupling Values

The manipulated frequency combination of $\omega_1 = \frac{2\pi}{70}$ *and* $\omega_{secondary} = \frac{2\pi}{69}$ did not always yield adequate estimates of all model parameters. This problem occurred due to acceleration terms being very small and substantially affected by the error in the position trajectories. As was delineated in the Method section, with higher density of the measures, acceleration terms become very small and highly imprecise estimates occur due to the error in the position trajectories. Higher density of the time series implies smaller steps in time between the measures. Smaller steps in time between the measures imply smaller changes in velocity for each step. Smaller changes in velocity per step imply a smaller magnitude of acceleration for each step. Since acceleration terms are derived from the position trajectories, errors that are negligible in the context of position can become magnified and be extraordinarily unreliable in the context of estimating acceleration. The combination of $\omega_1 = \frac{2\pi}{70}$ caused issues specifically with $\omega_{secondary} = \frac{2\pi}{69}$ because $\frac{2\pi}{69}$ is extremely close to the $\omega_1 = \frac{2\pi}{70}$ value. Since $\sqrt{\omega_1^2 + \kappa_1 + \kappa_2} = \omega_{secondary} \rightarrow \kappa_1 + \kappa_2 = \omega_{secondary}^2 - \omega_1^2$, the similarity of these two frequency values causes true values of $\kappa_1$and κ_2 to be extremely small. In the case with the coupling ratio of 1/100, κ_1 is as low as 0.000002. In combination with the increased sensitivity of the acceleration terms to the error in the position terms, it is not surprising that such small magnitudes of the coupling terms were not detected accurately in some cases. When I regenerated all the manipulated value sets with $\omega_1 = \frac{2\pi}{70}$ and $\omega_{secondary} = \frac{2\pi}{69}$ that did not

yield all the model estimates correct with a substantially decreased (but unrealistic in practice) error rate of 0.00000002% (instead of 0.00002%), all the parameter estimates across all the cases were adequate. Thus, the inadequate parameter estimates in case of $\omega_1 = \frac{2\pi}{70}$ with $\omega_{secondary} = \frac{2\pi}{69}$ must have been caused by the increased sensitivity to error.

Coupling coefficient κ_1 was detected inadequately in case of these two manipulated parameter combinations:

1. $\omega_1 = \frac{2\pi}{70}$, $\omega_{secondary} = \frac{2\pi}{50}$, $\frac{\kappa_1}{\kappa_2} = \frac{1}{100}$, initial value set 4 ($p_1 = 1$, $p_2 = 10$, $v_1 = 5$, $v_2 = 5$);

2. $\omega_1 = \frac{2\pi}{35}$, $\omega_{secondary} = \frac{2\pi}{34}$, $\frac{\kappa_1}{\kappa_2} = \frac{1}{100}$, initial value set 4 ($p_1 = 1$, $p_2 = 10$, $v_1 = 5$, $v_2 = 5$);

Since initial value set 4 contains two equal initial velocities, the third term of both motion trajectories cancels out. Plugging the remaining manipulated values into the motion trajectory equations in case of 1) yields:

$$x(t) = 55.7 \sin\omega_1 t + 1.09 \cos \omega_1 t - 0.089 \cos \omega_{secondary} t \qquad (47)$$

$$y(t) = 55.7 \sin\omega_1 t + 1.09 \cos \omega_1 t + 8.91 \cos \omega_{secondary} t$$

Case 2) yields the same x(t) and y(t) equations with an exception of $C_1 = 27.85$ instead of 55.7. The coefficient of the secondary frequency term in Equation set (47), -0.089, is very low in comparison to the combination of the two coefficients of the primary frequency terms. As a result, it is more difficult to discriminate this term from the error, which, in case of $\omega_1 = \frac{2\pi}{70}$ and $\frac{2\pi}{35}$ (sampling rate of 70 and 35 observations per cycle), becomes

sufficiently large in the acceleration terms that serve as an outcome variable. Moreover, very low secondary frequencies, such as $\frac{2\pi}{50}$ and $\frac{2\pi}{34}$ considered here, in combination with the fixed secondary frequency amplitude that is as low as 0.089 are barely detectable as they generate very stretched out fluctuations. To illustrate, $\frac{2\pi}{50}$ will be represented in the motion trajectory x(t) by oscillations that complete a full cycle after 50 observations, with the maximum amplitude of 0.089 displacement units, that is intertwined with the major frequency fluctuations and error. Then, acceleration values that represent change in velocity between each pair of neighboring time points due to the influence of the second mass will be miniscule.

In the case of other initial value combinations (that were not discussed above as dysfunctional), the same primary and secondary frequency combinations with the manipulated coupling ratio of 1/100 yielded adequate estimates because the second secondary frequency representing coefficient (C_3) was not cancelled out. C_3 contains $\omega_{secondary}$ in its denominator (see Equation set 42), which significantly boosts the C_3 estimate, and, in turn, the secondary frequency amplitude when secondary frequencies are as low as $\frac{2\pi}{50}$ and $\frac{2\pi}{34}$.

When I regenerated the two manipulated value sets 1) and 2) with a decreased error rate of 0.00000002% (instead of 0.00002%), all the parameter estimates were adequate. Thus, the inadequate parameter estimates in this case must indeed have been associated with the increased sensitivity to error.

Chapter 5

CONCLUSION

This thesis considered the performance of dynamic models that represent two undamped time-varying variables. These variables followed motion trajectories of two masses that coexist in the same undamped connected mass-spring system with equal natural angular frequencies. This thesis investigated the cyclical forms that the data that represents these variables could take and yield adequate estimates of the multilevel connected mass-spring model, defined as falling within 10% of the true parameter values of the system. First, as the simulation results indicated, the error rate should be extremely low. In the simulation, even when the error rate was only 0.00002% of the total variance of individual trajectories, several cases emerged where the error rate had to be decreased to 0.00000002% to provide adequate parameter estimates. The 10% error rate (comparable to reliability = .90, a high value for self-report measures) yielded only .1% of the parameter sets that met the criterion for adequate estimation. Those .1% of the solutions appeared to be spurious, as they did not yield adequate estimates in the smaller 0.00002% error condition. I selected the 0.00002% error rate for the simulation because it was the largest error rate that I tested in the pilot simulation that yielded adequate estimates for all parameters with the frequencies of interest. When the error rate was increased above 0.00002%, parameter estimate adequacy dropped exponentially, with the majority of estimates becoming inadequate at an error rate of about 2%. Hence, in order to achieve adequate connected mass-spring model estimates, the proportion of the error variance to the total variance should be a minimum of 0.0000002; the 10% error rate that

is commonly deemed high reliability with self-report measures in psychology would certainly not yield adequate estimates of the set of parameters. It is possible that filtering or smoothing might improve the performance of the connected mass spring models, but these approaches have received little attention in psychological literature. A further issue is that my simulation assumed that all individuals have the same underlying signal and there is no between individual variance. If this were not the case, a further increase in the rate of inadequate solutions would be introduced.

Second, the signal of each of the time-varying variables should contain exactly two frequencies, and the two frequencies must be the same across the two variables. As the simulation results have shown, when the primary frequency terms were completely cancelled out by in initial value sets 1., 2., and 3., 0% of the parameter sets were estimated adequately. Similarly, when secondary frequency terms were completely cancelled out by the combination of initial value set 6 along with the coupling ratio of 1/10, 0% of the parameter sets were estimated adequately. Hence, whenever only one frequency was present in the signal of each of the time varying variables, even when the trajectories of the signals were theoretically producible by the connected mass-spring system, the connected mass-spring model in unable to estimate the parameters of that system adequately. This result also means that the trajectory pairs cannot be (a) completely in phase and (b) cannot be collinear: Given the mathematical structure of $x(t)$ and $y(t)$, such instances are producible by the connected mass-spring system only then they contain a single frequency. If more than 2 frequencies are present in the signal of the time varying variables, they will be treated as noise by the connected mass-spring model.

The connected mass-spring model by its design is expected to detect a trajectory pair that is producible by a connected mass-spring system and to estimate the physical parameters of the connected mass-spring system that produced that trajectory pair. The classical connected mass-spring system is capable of producing only single or double-frequency motion trajectories, whether $\omega_1 = \omega_2$ or $\omega_1 \neq \omega_2$. In other words, single or double-frequency motion trajectories are expected whether the natural angular frequencies of the two side components of the system (the left most spring with the left mass, and the right most spring with the right mass) are equal or not (See Appendix B for the mathematical definition of the general motion trajectories with $\omega_1 \neq \omega_2$). Hence, whether the two time-varying variables being examined are expected to be entrained to the cycles of the same or of different length, the connected mass-spring model will attempt to approximate the trajectories with double frequency sinusoidal curves, under the assumption that the time series for both variables are comprised of the same pair of frequencies. This result comes from the mathematical definition of the motion trajectories producible by the connected mass-spring model (see Equation set 40 for cases with $\omega_1 = \omega_2$, and Appendix B for cases with $\omega_1 \neq \omega_2$). If the trajectories of the time varying variables contain any other frequency components in addition to the two described above, these components will be treated as error by the connected mass-spring model. Since the connected mass-spring model cannot handle more than a miniscule amount of error, additional frequencies in the signal of the two time-varying variables would produce inadequate parameter estimates. If the cyclic two-frequency interaction of the two

variables of interest cannot be isolated from other variables that might be affecting either of the cycles, the connected mass-spring model will not estimate the parameters properly.

The simulation results indicated that single frequency trajectories were generated when the initial position and initial velocity pairs were both equal (i.e. $p_1=p_2$ and $v_1=v_2$). When they are equal, they cancel out the secondary frequency terms and yield identical x(t) and y(t) single frequency motion trajectories. That renders the coupling coefficient undetectable since it is a function of the difference between x(t) and y(t), which is in this case is 0 or error. It might appear that this limitation implies that, in order for the connected mass-spring model to work properly, it is necessary for the two time varying variables to have different starting positions or/and different starting velocities. This is not the case. In an undamped connected mass-spring system, initial conditions describe the state of the *physical system* at time 0. The state of the *motion trajectories* at time 0 need not be the same. As delineated in Appendix C, an undamped connected mass-spring system with equal major frequencies repeats its initial conditions every least common multiplier or LCM (denominator of ω_1, denominator of $\omega_{secondary}$; for the repetition pattern when $\omega_1 \neq \omega_2$, see Appendix B). The multilevel connected mass-spring model, by design, is capable of detecting the underlying physical system regardless of where/when the initial conditions occur in the measured trajectories. In practice, it is extremely unlikely that the first measurement occasion of the time-varying variables will coincide with the initial conditions of the system at time 0. Hence, this limitation only indicates that if the trajectories contain only the primary frequency or are identical to each other, then the coupling terms of the underlying system will be inestimable.

Another limitation whose true interpretation might differ from the one suggested by its first impression is the minimum number of observations per secondary cyclic component required to prevent undersampling. The simulation demonstrated that when error variance constitutes 0.00002% of the total individual trajectory variance, a minimum number of 7 equally spaced observations per secondary cyclic component was required to achieve adequate estimates of all parameters. The lowest number of observations per full cycle that yielded adequate estimates of all parameters was 14. These findings lead to the following conclusion: As long as there are at least 7 observations per secondary cyclic component and at least 14 observations per full cycle, the parameter estimates will not be undermined by empirical undersampling. In practice, the lengths of the two cyclic components may be hypothesized or may be a priori unknowns to be estimated from the data. The major frequencies that represent the length of full cycle are more likely to be known from theoretical knowledge about the variables (e.g., weekly cycles), whereas secondary frequencies, which emerge as a consequence of the interaction of the two variables, are far less likely to be known, particularly for cyclic relationships that have not been extensively studied. Thus, the length of the secondary cyclic component will typically be unknown when the multilevel connected mass-spring model is used by researchers. Given that there should be at least 7 observations per potential secondary cyclic component, the researcher should attempt to assure that a sufficient number of observations is collected. However, the full range of secondary frequencies that two interacting time varying psychological variables can produce has no upper bound, i.e. the secondary frequency can be as high as $\lim_{T\to 0^+} \frac{2\pi}{T} = \infty$, where T

represents period). Hence, a sampling design that would accommodate all potential secondary frequencies is impossible. As a practical recommendation that would accommodate the majority of secondary frequencies, a very high sampling rate could be considered when feasible. For instance, a researcher might believe that it is extremely unlikely that the interaction of two variables of interest that follow a biweekly cycle would generate a secondary frequency that is more than 50 times higher than that of the major frequency (full cycle). In such a case, the minimum number of observations required per full cycle of two weeks would be 350 (7 observations multiplied by 50 secondary cyclic components per full cycle).

Very high sampling rates would also require the error rate to be considerably lower than the 0.00002% rate that was used in the simulation. The present simulation was limited to the maximum of 70 observations per full cycle, and even with this sampling rate several cases emerged where the error rate had to be decreased to 0.00000002% to provide adequate parameter estimates. As discussed in the Method section, as the sampling rate increases, the error rate in the measurement of position that will produce imprecise acceleration values becomes smaller. Thus, in cases in which the number of observations per full cycle exceeds 70, it should be expected that even the smaller (tiny) error rate of 0.00002% would produce inadequate parameter estimates.

In summary, in order for two time-varying detrended psychological variables whose fluctuations do not fade over time to have their cycles and their cyclic relationship detected adequately by the connected mass-spring model, their measures would need to meet the following criteria:

a) contain essentially no error;

b) comprise trajectories which each contain exactly 2 interacting frequencies, with the two frequencies being the same in both trajectories, and with no traces or influences of any other frequencies or variables;

c) contain a large number of observations per full cycle.

Chapter 6

FUTURE DIRECTIONS

The conclusions presented in this thesis apply to modeling two detrended time-varying variables that are entrained to cycles of same length with an undamped connected mass-spring model. The key feature of the present simulation study is that all of the data were generated to be consistent with the motion trajectories producible by the connected mass-spring system with equal natural angular frequencies ($\omega_1 = \omega_2$) represented by Equation set (40). The generated variable trajectories represented those produced by this connected mass-spring system to which a tiny (.0000002) or small (.10) random error was added. Thus, the simulated data provided optimal conditions for studying the ability of the estimators to recapture the parameters of the true data generating model. However, the range of trajectory pairs that can be described by Equation set (40) is extremely limited in comparison to the range of all possible sinusoidal trajectory pairs that two psychological variables potentially could produce over time. In order for two psychological processes to produce trajectories that exactly follow Equation set (40), they would need to strictly obey all the laws of mechanics followed by the connected mass-spring model. Even under these conditions, the ability of the estimates to adequately represent the data generating process was limited in the .0000002 error condition and unacceptable in the .10 error condition, a condition which characterizes highly reliable self-report measures. Further, human psychological processes are very unlikely to be restricted by the laws of classical mechanics. Therefore, they are unlikely to always follow the trajectories produced by the mass-spring models defined by Equation set (40).

Future work should further investigate the domains of trajectory pairs that can be potentially studied using the connected mass-spring model. I plan to extend my present work on connected mass-spring models to new cases with equal natural angular frequencies ($\omega_1 = \omega_2$) as well as cases with unequal natural angular frequencies ($\omega_1 \neq \omega_2$) mathematically and graphically. I also plan to conduct a simulation study to examine the performance of the connected mass-spring model under conditions when the trajectories generated by two time-varying variables are theoretically not producible by the connected mass-spring system. Since such trajectories do not have a corresponding set of system parameters that can potentially be detected, they can provide information about the likelihood of potential false positive solutions. Otherwise stated, any parameter estimates produced by this model will be describing a connected mass-spring system that is not capable of reproducing the inputted trajectories under any initial conditions. Taken together with my present simulation study, these future studies will help define the domains under which estimates produced by mass-spring models represent versus do not represent the underlying dynamic processes. Finally, damped connected mass-spring systems, nonlinear connected mass-spring systems, and connected mass-spring systems with external forces should be defined, solved, and examined in studies to define their domain and determine their limitations.

REFERENCES

Abraham, R. H., & Shaw, C. D. (1992). *Dynamics: the geometry of behaviour.* Redwood City, CA: Addison-Wesley.

Armeli, S., Carney, M. A., Tennen, H., Affleck, G., & O'neil, T. P. (2000). Stress and alcohol use: A daily process examination of the stressor–vulnerability model. *Journal of Personality and Social Psychology*, *78*, 979-994.

Assenmacher, I., & Jallageas, M. (1980). Circadian and circannual hormonal rhythms. In A. Epple & M. H. Stentson (Eds.), *Avian Endocrinology*, (pp. 391-441). New York, NY: Academic Press.

Beek, P. J., & Beek, W. J. (1988). Tools for constructing dynamical models of rhythmic movement. *Human Movement Science, 7*, 301-342.

Beek, P. J., Schmidt, R. C., Morris, A. W., Sim, M. Y., & Turvey, M. T. (1995). Linear and nonlinear stiffness and friction in biological rhythmic movements. *Biological Cybernetics*, *73*, 499-507.

Boker, S. M. (2001). Differential structural equation modeling of intraindividual variability. In L. M. Collins & A. G. Sayer (Eds.), *New methods for the analysis of change* (pp. 5-27). Washington DC: American Psychological Association.

Boker, S. M., & Graham, J. (1998). A dynamical systems analysis of adolescent substance abuse. *Multivariate Behavioral Research*, *33*, 479-507.

Boker, S. M., & Laurenceau, J. P. (2007). Coupled dynamics and mutually adaptive context. In T. D. Little, J. A. Bovaird, & N. A. Card (Eds.), *Modeling contextual effects in longitudinal studies* (pp. 299–324). Mahwah, NJ: Lawrence Erlbaum.

Bowerman, B., O'Connell, R., & Koehler, A. (2004). *Forecasting, time series and regression: An applied approach.* Belmont, CA: Thomson Brooks/Cole.

Box, G. E., & Jenkins, G. M. (1976). *Time series analysis: Forecasting and control, (revised ed.).* San Francisco, CA: Holden-Day.

Box, G. E., Jenkins, G. M., Reinsel, G. C., & Ljung, G. M. (2015). *Time series analysis: Forecasting and control*. Hoboken, NJ: John Wiley & Sons.

Brown, K. W., & Moskowitz, D. S. (1998). Dynamic stability of behavior: The rhythms of our interpersonal lives. *Journal of Personality*, *66*, 105-134.

Butner, J., Amazeen, P. G., & Mulvey, G. M. (2005). Multilevel modeling of two cyclical processes: Extending differential structural equation modeling to nonlinear coupled systems. *Psychological Methods*, *10*, 159-177.

Campbell, J. (1986). *Winston Churchill's afternoon nap: A wide-awake inquiry into the human nature of time*. New York, NY: Simon & Schuster.

Chow, S. M., Hamaker, E. L., Fujita, F., & Boker, S. M. (2009). Representing time-varying cyclic dynamics using multiple-subject state-space models. *British Journal of Mathematical and Statistical Psychology*, *62*, 683-716.

Chow, S. M., Ram, N., Boker, S. M., Fujita, F., & Clore, G. (2005). Emotion as a thermostat: Representing emotion regulation using a damped oscillator model. *Emotion*, *5*, 208-225.

Conner, T., & Mehl, M. R. (2015). Ambulatory assessment: Methods for studying everyday life. In R. A. Scott, S. M. Kosslyn & M. Stephen (Eds.), *Emerging Trends in the Social and Behavioral Sciences* (pp. 1-15). Thousand Oaks, CA: SAGE Publications.

Cook, T. D., & Campbell, D. T. (1979). *The design and conduct of true experiments and quasi-experiments in field settings.* Boston, MA: Rand McNally.

Cranford, J. A., Shrout, P. E., Iida, M., Rafaeli, E., Yip, T., & Bolger, N. (2006). A procedure for evaluating sensitivity to within-person change: Can mood measures in diary studies detect change reliably? *Personality and Social Psychology Bulletin*, *32*, 917-929.

Davis, M. C., Zautra, A. J., & Smith, B. W. (2004). Chronic pain, stress, and the dynamics of affective differentiation. *Journal of Personality*, *72*, 1133-1160.

Finan, P. H., Hessler, E. E., Amazeen, P. G., Butner, J., Zautra, A. J., & Tennen, H. (2010). Nonlinear oscillations in pain prediction accuracy: A dynamical systems approach to understanding daily pain prediction. *Nonlinear Dynamics, Psychology, and Life sciences*, *14*, 27-46.

Halberg, F. (1983). Quo vadis basic and clinical chronobiology: Promise for health maintenance. *American Journal of Anatomy*, *168*, 543-594.

Hamaker, E. L., & Wichers, M. (2017). No time like the present: Discovering the hidden dynamics in intensive longitudinal data. *Current Directions in Psychological Science*, *26*, 10-15.

Hamilton, J. D. (1994). *Time series analysis*. Princeton, NJ: Princeton University Press.

Haugh, L. D., & Box, G. E. (1977). Identification of dynamic regression (distributed lag) models connecting two time series. *Journal of the American Statistical Association*, *72*, 121-130.

Haus, E., Lakatua, D. J., Swoyer, J., & Sackett-Lundeen, L. (1983). Chronobiology in hematology and immunology. *American Journal of Anatomy*, *168*, 467-517.

Hessler, E. E., Finan, P. H., & Amazeen, P. G. (2013). Psychological rhythmicities. In J. P. Strumberg & C. M. Martin (Eds.), *Handbook of systems and complexity in health* (pp. 127-146). New York, NY: Springer.

Hilderbrandt, G., & Geyer, F. (1984). Adaptive significance of circo-septan reactive period. *Journal of Interdisciplinary Cycle Res*earch, *15*, 109-117.

Johansson, C., Willeit, M., Smedh, C., Ekholm, J., Paunio, T., Kieseppä, T., ... & Kasper, S. (2003). Circadian clock-related polymorphisms in seasonal affective disorder and their relevance to diurnal preference. *Neuropsychopharmacology*, *28*, 787-793.

Judd, C. M., & Kenny, D. A. (1981). *Estimating the effects of social intervention*. New York, NY: Cambridge University Press.

Kagan, J., Reznick, J. S., & Snidman, N. (1987). The physiology and psychology of behavioral inhibition in children. *Child Development*, *58*, 1459-1473.

Kelly, G. A., Blake, C., Power, C. K., O'Keeffe, D., & Fullen, B. M. (2011). The association between chronic low back pain and sleep: A systematic review. *The Clinical Journal of Pain*, *27*, 169-181.

Kirsch, I., Silva, C. E., Comey, G., & Reed, S. (1995). A spectral analysis of cognitive and personality variables in hypnosis: Empirical disconfirmation of the two-factor model of hypnotic responding. *Journal of Personality and Social Psychology*, *69*, 167-175.

Koopmans, L. H. (1995). *The spectral analysis of time series*. San Diego, CA: Academic Press.

Larsen, R. J., & Kasimatis, M. (1990). Individual differences in entrainment of mood to the weekly calendar. *Journal of Personality and Social Psychology*, *58*, 164-171.

Levi, F., & Halberg, F. (1982). Circaseptan (about-7-day) bioperiodicity—spontaneous and reactive—and the search for pacemakers. *Ricerca in Clinica e in Laboratorio*, *12*, 323-370.

Liu, Y., & West, S. G. (2016). Weekly cycles in daily report data: An overlooked issue. *Journal of Personality*, *84*, 560-579.

Lütkepohl, H. (2005). *New introduction to multiple time series analysis*. New York, NY: Springer.

McCleary, R., & Hay, R. A. (1980). *Applied time series analysis for the social sciences*. Beverly Hills, CA: Sage Publications.

McFarlane, J., Martin, C. L., & Williams, T. M. (1988). Mood fluctuations: Women versus men and menstrual versus other cycles. *Psychology of Women Quarterly*, *12*, 201-223.

Mehl, M., and Conner, T. (2012). *Handbook of Research Methods for Studying Daily Life*. New York, NY: Guilford Press.

Muthén, L. K., & Muthén, B. O. (2002). How to use a Monte Carlo study to decide on sample size and determine power. *Structural Equation Modeling, 9*, 599-620.

Nagle, R. K., Saff, E., & Snider, D. (2010). *Fundamentals of Differential Equations*. Boston, MA: Pearson Education.

Ram, N., Chow, S. M., Bowles, R. P., Wang, L., Grimm, K., Fujita, F., & Nesselroade, J. R. (2005). Examining interindividual differences in cyclicity of pleasant and unpleasant affects using spectral analysis and item response modeling. *Psychometrika, 70*, 773-790.

Raudenbush, S. W., & Bryk, A. S. (2002). *Hierarchical linear models: Applications and data analysis methods*. Thousand Oaks, CA: Sage.

Reid, S., Towell, A. D., & Golding, J. F. (2000). Seasonality, social zeitgebers and mood variability in entrainment of mood: Implications for seasonal affective disorder. *Journal of Affective Disorders*, *59*, 47-54.

Reis, H. T., Sheldon, K. M., Gable, S. L., Roscoe, J., & Ryan, R. M. (2000). Daily well-being: The role of autonomy, competence, and relatedness. *Personality and Social Psychology Bulletin, 26*, 419-435.

Rossi, A. S., & Rossi, P. E. (1977). Body time and social time: Mood patterns by menstrual cycle phase and day of the week. *Social Science Research, 6*, 273-308.

Ruscher, J. B. (2017). Expectations about re-entering the weekly cycle following disruption by familial death or holiday. *Time & Society, 26*, 321-338.

Rusting, C. L., & Larsen, R. J. (1998). Diurnal patterns of unpleasant mood: Associations with neuroticism, depression, and anxiety. *Journal of Personality*, *66*, 85-103.

Ryan, R. M., Bernstein, J. H., & Brown, K. W. (2010). Weekends, work, and well-being: Psychological need satisfactions and day of the week effects on mood, vitality, and physical symptoms. *Journal of Social and Clinical Psychology*, *29*, 95-122.

Ryu, E., West, S. G., & Sousa, K. H. (2012). Distinguishing between-person and within-person relationships in longitudinal health research: Arthritis and quality of life. *Annals of Behavioral Medicine, 43*, 330-342.

Sheldon, K. M., Ryan, R., & Reis, H. T. (1996). What makes for a good day? Competence and autonomy in the day and in the person. *Personality and Social Psychology Bulletin*, *22*, 1270-1279.

Smith, M. T., & Haythornthwaite, J. A. (2004). How do sleep disturbance and chronic pain inter-relate? Insights from the longitudinal and cognitive-behavioral clinical trials literature. *Sleep Medicine Reviews*, *8*, 119-132.

Stone, A. A., Hedges, S. M., Neale, J. M., & Satin, M. S. (1985). Prospective and cross-sectional mood reports offer no evidence of a" blue Monday phenomenon. *Journal of Personality and Social Psychology*, *49*, 129-134.

Stone, A. A., Schneider, S., & Harter, J. K. (2012). Day-of-week mood patterns in the United States: On the existence of 'Blue Monday','Thank God it's Friday'and weekend effects. *The Journal of Positive Psychology, 7*, 306-314.

Studer, J., Baggio, S., Mohler-Kuo, M., Dermota, P., Daeppen, J. B., & Gmel, G. (2014). Differential association of drinking motives with alcohol use on weekdays and weekends. *Psychology of Addictive Behaviors, 28*, 651-658.

Trull, T. J., & Ebner-Priemer, U. (2013). Ambulatory assessment. *Annual Review of Clinical Psychology, 9*, 151-176.

Tuomisto, M. T., Terho, T., Korhonen, I., Lappalainen, R., Tuomisto, T., Laippala, P., & Turjanmaa, V. (2006). Diurnal and weekly rhythms of health-related variables in home recordings for two months. *Physiology & Behavior, 87*, 650-658.

Warner, R. M. (1998). *Spectral analysis of time-series data*. New York, NY: Guilford Press.

White, W. B., Schulman, P., McCabe, E. J., & Dey, H. M. (1989). Average daily blood pressure, not office blood pressure, determines cardiac function in patients with hypertension. *Journal of the American Medical Association, 261*, 873-877.

Wikipedia contributors. (2018, October 15). Damping ratio. In *Wikipedia, The Free Encyclopedia*. Retrieved 19:47, October 17, 2018, from https://en.wikipedia.org/wiki/Damping_ratio

Wilhelm, F. H., & Grossman, P. (2010). Emotions beyond the laboratory: Theoretical fundaments, study design, and analytic strategies for advanced ambulatory assessment. *Biological Psychology, 84*, 552-569.

Wilson, K. G., Eriksson, M. Y., Joyce, L. D., Mikail, S. F., & Emery, P. C. (2002). Major depression and insomnia in chronic pain. *The Clinical Journal of Pain, 18*, 77-83.

Wood, W., Kressel, L., Joshi, P. D., & Louie, B. (2014). Meta-analysis of menstrual cycle effects on women's mate preferences. *Emotion Review, 6*, 229-249.

APPENDIX A

MATHEMATICAL SOLUTION OF THE UNDAMPED CONNECTED MASS-SPRING SYSTEM WITH EQUAL NATURAL FREQUENCIES

Solving the connected mass-spring oscillator system involves solving the system of the two force equations of the moving masses, which are expressed in terms of two 2nd order differential equations. The notation that will be used for derivatives in my solution will be either the classical one – $x'(t) = \frac{dx}{dt} = \frac{d}{dt}x$, or a commonly used simplified notation where differentiation operator $\frac{d}{dt}$ is replaced with the symbol *D*. Second derivatives in terms of this notation will be: $x''(t) = \frac{d^2x}{dt^2} = \frac{d}{dt}\frac{d}{dt}x = D^2x$. A 2nd order differential equation, such as $x'' + 4x' + 3x = 0$ can then be expressed in terms of the *D* notation as

$$D^2x + 4Dx + 3x = (D^2 + 4D + 3)[x] = (D + 3)(D + 1)[x]$$
$$= (D + 1)(D + 3)[x] = 0.$$

As is visible from the set of expressions, this notation is convenient because expressions of the form $aD^2 + bD + c$ can be treated as if they were ordinary polynomials in *D*, as long as *a, b* and *c* are constants (for examples, see Nagle, Saff, & and Snider, 2010, pg. 264 -267).

I will use the *D* notation to implement the elimination method for 2 × 2 differential systems with constant coefficients (Nagle, Saff & Snider, 2017, p. 263-270). It is used to find a general solution to the system of the form

$$\begin{cases} L_1[x] + L_2[y] = f_1 \\ L_3[x] + L_4[y] = f_2 \end{cases},$$

where L_1, L_2, L_3, and L_4 are linear differential operators with constant coefficients (polynomials in *D*), and f_1 and f_2 are some functions of *t* (time), or constants. Given the properties of *D* polynomials with constant coefficients, the *L* operators commute, e.g.,

$L_1L_3 = L_3\,L_1$. Therefore, we can eliminate variables in a basic algebraic way. Variable *y* can be eliminated as follows:

$$(L_1L_4 - L_2L_3)[x] = L_4[f_1] - L_2[f_2]\,. \quad (1)$$

Similarly, variable x is eliminated by

$$(L_1L_4 - L_2L_3)[y] = L_1[f_2] - L_3[f_1]\,. \quad (2)$$

If differential operator $L_1L_4 - L_2L_3$ is of order *n*, then a general solution for equation (1) will contain *n* arbitrary constants; and analogously, a general solution for equation (2) will also contain *n* arbitrary constants, making 2*n* arbitrary constants in total. However, only *n* of these constants are independent, with the remaining *n* being expressions that are dependent on the first *n*. The two general solutions to equations (1) and (2) expressed in terms of the n independent constants are called a *general solution to the system* (Nagle, Saff, & Snider, 2017, p. 267).

As an example, consider a simple system of first order differential equations that are similar in their form to the ones describing a mass-spring system with 2 masses. Suppose the following equation system given:

$$\begin{cases} \frac{dx}{dt} = x - 4y \\ \frac{dy}{dt} = x + y \end{cases}, \quad (1)$$

which we then rearrange into

$$\begin{cases} x - x' - 4y = 0 \\ x + y - y' = 0 \end{cases}. \quad (2)$$

Now the equations are easy to express in terms of operator *D*:

$$\begin{cases} (1 - D)[x] - 4y = 0 \\ x + (1 - D)[y] = 0 \end{cases}. \quad (3)$$

Then we use equation (2) to eliminate x with $L_1 = 1 - D, L_2 = -4,\ L_3 = 1, L_4 = 1 - D,$ $L_1[f_2] = (1 - D)[0] = 0$, and $L_3[f_1] = 1[0] = 0$.

$$(1 - D)(1 - D) - (-4)(1) = 0 - 0 \qquad (4)$$

$$D^2 - 2D + 5 = 0 \qquad (5)$$

The corresponding characteristic equation is

$$r^2 - 2r + 5 = (r - 1 + 2i)(r - 1 - 2i) = 0\ . \qquad (6)$$

(If a review of characteristic equations is needed, please see Nagle, Saff, & Snider, 2010, Section 4.2.) So the roots of the characteristic equation are $r = 1 \pm 2i$. Thus, the general solution for *y* is

$$y = c_1 e^t \cos 2t + c_2 e^t \sin 2t\ . \qquad (7)$$

(If a review of how to get from a characteristic/auxiliary equation to the general solution is needed, please see Nagle, Saff, & Snider, 2010, Sections 4.2 & 4.3.) To get the general solution for *x*, we solve the second equation from the equation system (2) for *x* by substitution. $x = y' - y$

$= c_1 e^t(\cos 2t - 2 \sin 2t) + c_2 e^t(\sin 2t + 2 \cos 2t) - c_1 e^t \cos 2t - c_2 e^t \sin 2t$

$= 2c_2 e^t \cos 2t - 2c_1 e^t \sin 2t$

Hence, the final general solution to the system is

$$x(t) = 2c_2 e^t \cos 2t - 2c_1 e^t \sin 2t$$

$$y(t) = c_1 e^t \cos 2t + c_2 e^t \sin 2t\ .$$

Solution of the Undamped Connected Mass-Spring System with Equal Natural Angular Frequencies

Following Newton's and Hook's laws, the force equations that define the system are:

$$\begin{cases} m_1 \frac{d^2x}{dt^2} = -k_1x + k_2(y-x) \\ m_2 \frac{d^2y}{dt^2} = -k_3y + k_2(x-y) \end{cases}.$$

This can be rearranged into:

$$\begin{cases} \frac{d^2x}{dt^2} + (\frac{k_1}{m_1} + \frac{k_2}{m_1})x - \frac{k_2}{m_1}y = 0 \\ \frac{d^2y}{dt^2} + (\frac{k_3}{m_1} + \frac{k_2}{m_2})y - \frac{k_2}{m_2}x = 0 \end{cases}.$$

Now it can be expressed in terms of operator D:

$$\begin{cases} D^2 + (\frac{k_1}{m_1} + \frac{k_2}{m_1})[x] - \frac{k_2}{m_1}y = 0 \\ -\frac{k_2}{m_2}x + (D^2 + (\frac{k_3}{m_1} + \frac{k_2}{m_2}))[y] = 0 \end{cases}.$$

Since natural angular frequencies are known to be equal, it follows that $\frac{k_1}{m_1} = \frac{k_3}{m_1} = \omega_1^2 = \omega_2^2$. The remaining two stiffness to mass proportions can also be defined as $\frac{k_2}{m_1} = \kappa_1$ and $\frac{k_2}{m_2} = \kappa_2$. Replacing the stiffness to mass proportions by angular velocities and coupling coefficients yields:

$$\begin{cases} D^2 + (\omega_1^2 + \kappa_1)[x] - \kappa_1 y = 0 \\ -\kappa_2 x + (D^2 + (\omega_1^2 + \kappa_2))[y] = 0 \end{cases}.$$

Now, multiplying the first row by κ_2, the second row by $(D^2 + (\omega_1^2 + \kappa_1))$, and adding them up gives:

$$[(D^2 + (\omega_1^2 + \kappa_1))(D^2 + (\omega_1^2 + \kappa_2)) - \kappa_1\kappa_2][y] = 0.$$

Multiplying the terms inside the parentheses results in a 4th degree differential equation:

$$[D^4 + (2\omega_1^2 + \kappa_1 + \kappa_2)D^2 + (\omega_1^4 + \omega_1^2\kappa_1 + \omega_1^2\kappa_2)][y] = 0.$$

This equation can be split into two 2nd degree differential equations:

$$[(D^2 + \omega_1^2)(D^2 + (\omega_1^2 + \kappa_1 + \kappa_2))][y] = 0.$$

Hence, the roots of the auxiliary equation are:

$$r_{1,2} = \pm\omega_1 i \text{ and } r_{3,4} = \pm\sqrt{\omega_1^2 + \kappa_1 + \kappa_2}\, i\,.$$

Using Euler's formula, it follows that:

$$e^{i\omega_1 t} = \cos(\omega_1 t) + i\sin(\omega_1 t) \text{ and}$$

$$e^{i\sqrt{\omega_1^2+\kappa_1+\kappa_2}\,t} = \cos\left(\sqrt{\omega_1^2 + \kappa_1 + \kappa_2}\,t\right) + i\sin\left(\sqrt{\omega_1^2 + \kappa_1 + \kappa_2}\,t\right) \text{ are the}$$

complex-valued solutions to the 4th degree differential equation. Projecting them onto the real plane results in a real-valued solution:

$$y(t) = C_1\cos(\omega_1 t) + C_2\sin(\omega_1 t) + C_3\cos\left(\sqrt{\omega_1^2 + \kappa_1 + \kappa_2}\,t\right) + C_4\sin\left(\sqrt{\omega_1^2 + \kappa_1 + \kappa_2}\,t\right),$$

where C_1, C_2, C_3, C_4 are coefficients that are free to vary, but depend on the initial conditions.

Since the solution for y(t) is now obtained, the solution for x(t) can be achieved by defining x(t) in terms of y(t), and plugging in the relevant expressions. From the initial force equations x can be defined in terms of y in the following way:

$$x = \frac{1}{\kappa_2}\frac{d^2y}{dt^2} + (\frac{\omega_1^2}{\kappa_2} + 1)y.$$

$\frac{d^2y}{dt^2}$ can be easily obtained by taking a second derivative of the y(t) solution with respect to time. Doing so results in:

$$\frac{d^2y}{dt^2} = -\omega_1^2 C_1 \cos(\omega_1 t) - \omega_1^2 C_2 \sin(\omega_1 t)$$

$$- (\omega_1^2 + \kappa_1 + \kappa_2) C_3 \cos\left(\sqrt{\omega_1^2 + \kappa_1 + \kappa_2}\, t\right)$$

$$- (\omega_1^2 + \kappa_1 + \kappa_2) C_4 \sin\left(\sqrt{\omega_1^2 + \kappa_1 + \kappa_2}\, t\right).$$

The remaining terms in the expression of x in terms of y are all known. Plugging them in and simplifying the result yields:

$$x(t) = C_1 \cos(\omega_1 t) + C_2 \sin(\omega_1 t) - C_3 \frac{\kappa_1}{\kappa_2} \cos\left(\sqrt{\omega_1^2 + \kappa_1 + \kappa_2}\, t\right) - C_4 \frac{\kappa_1}{\kappa_2} \sin\left(\sqrt{\omega_1^2 + \kappa_1 + \kappa_2}\, t\right).$$

Thus, the general solution to the force equation system that defines the undamped connected mass-spring system with equal natural angular frequencies is:

$$\begin{cases} y(t) = C_1 \cos(\omega_1 t) + C_2 \sin(\omega_1 t) + C_3 \cos\left(\sqrt{\omega_1^2 + \kappa_1 + \kappa_2}\, t\right) + C_4 \sin\left(\sqrt{\omega_1^2 + \kappa_1 + \kappa_2}\, t\right) \\ x(t) = C_1 \cos(\omega_1 t) + C_2 \sin(\omega_1 t) - C_3 \frac{\kappa_1}{\kappa_2} \cos\left(\sqrt{\omega_1^2 + \kappa_1 + \kappa_2}\, t\right) - C_4 \frac{\kappa_1}{\kappa_2} \sin\left(\sqrt{\omega_1^2 + \kappa_1 + \kappa_2}\, t\right). \end{cases}$$

APPENDIX B

MATHEMATICAL SOLUTION OF THE UNDAMPED CONNECTED MASS-SPRING SYSTEM WITH UNEQUAL NATURAL FREQUENCIES

The motion trajectories of the two masses that belong to the undamped connected mass-spring system with unequal natural angular frequencies are:

$$\begin{cases} y(t) = C_1\cos(gt) + C_2\sin(gt) + C_3\cos(ht) + C_4\sin(ht) \\ x(t) = C_1\frac{\omega_2^2+\kappa_2-g^2}{\kappa_2}\cos(gt) + C_2\frac{\omega_2^2+\kappa_2-g^2}{\kappa_2}\sin(gt) + C_3\frac{\omega_2^2+\kappa_2-h^2}{\kappa_2}\cos(ht) + C_4\frac{\omega_2^2+\kappa_2-h^2}{\kappa_2}\sin(ht) \end{cases},$$

where

$$g = 0.70711\sqrt{(\omega_1^2+\omega_2^2+\kappa_1+\kappa_2) - \sqrt{(\omega_1^2+\omega_2^2+\kappa_1+\kappa_2)^2 - 4(\kappa_1\omega_2^2+\kappa_2\omega_1^2+\omega_1^2\omega_2^2)}},$$

$$h = 0.70711\sqrt{(\omega_1^2+\omega_2^2+\kappa_1+\kappa_2) + \sqrt{(\omega_1^2+\omega_2^2+\kappa_1+\kappa_2)^2 - 4(\kappa_1\omega_2^2+\kappa_2\omega_1^2+\omega_1^2\omega_2^2)}},$$

and initial conditions of the system are periodically revisited every LCM(g,h) measurement units.

The solution is always real as the expressions contained under the square roots in g and h cannot be negative. Given that $\kappa_1 = \frac{k_2}{m_1}$, $\kappa_2 = \frac{k_2}{m_2}$, $\omega_1^2 = \frac{k_1}{m_1}$, and $\omega_1^2 = \frac{k_1}{m_1}$, and that stiffness of the springs (k_i) and mass of the weights (m_i) cannot be negative or zero in classical connected mass-spring systems, the following inequalities are true:

1. $(\omega_1^2+\omega_2^2+\kappa_1+\kappa_2)^2 - 4(\kappa_1\omega_2^2+\kappa_2\omega_1^2+\omega_1^2\omega_2^2)$

   $= (-\omega_1^2+\omega_2^2-\kappa_1+\kappa_2)^2 + 4\kappa_1\kappa_2 > 0$;

2. $(\omega_1^2+\omega_2^2+\kappa_1+\kappa_2) - \sqrt{(\omega_1^2+\omega_2^2+\kappa_1+\kappa_2)^2 - 4(\kappa_1\omega_2^2+\kappa_2\omega_1^2+\omega_1^2\omega_2^2)}$

   > 0

   $\omega_1^2+\omega_2^2+\kappa_1+\kappa_2 > \sqrt{(\omega_1^2+\omega_2^2+\kappa_1+\kappa_2)^2 - 4(\kappa_1\omega_2^2+\kappa_2\omega_1^2+\omega_1^2\omega_2^2)}$

   $(\omega_1^2+\omega_2^2+\kappa_1+\kappa_2)^2 > (\omega_1^2+\omega_2^2+\kappa_1+\kappa_2)^2 - 4(\kappa_1\omega_2^2+\kappa_2\omega_1^2+\omega_1^2\omega_2^2)$

   $0 > -4(\kappa_1\omega_2^2+\kappa_2\omega_1^2+\omega_1^2\omega_2^2)$

   $0 > -4.$

APPENDIX C

SUPPLEMENTAL DISCUSSION AND ILLUSTRATION OF UNDAMPED CONNECTED MASS-SPRING MODEL WITH EQUAL NATURAL ANGULAR FREQUENCIES

The system that is considered in this work is closed. Hence, the amount of energy that is induced into the system by the initial position ($\propto$ initial potential energy, where $\propto$ represents proportional to) and initial velocity ($\propto$ initial kinetic energy) of the masses cannot dissipate, as the sum of all the energies in the system at each point in time must be equal. This implies that the initial conditions will be approximately revisited periodically. The precise values of the initial conditions will also be revisited every least common multiplier or LCM (denominator of ω_1, denominator of $\omega_{secondary}$) measurement occasions, which is evident from the structure of the equations in Equation set 40. Moreover, the exact same oscillation pattern will repeat after every LCM (denominator of ω_1, denominator of $\omega_{secondary}$) measurement occasions. For instance, an equivalent of the seasonal trigonometric model with $\omega_1 = \frac{2\pi}{14}$, and $\omega_{secondary} = \frac{2\pi}{7}$ will have the same fluctuation pattern repeated each LCM (14, 7) = 14 measurement occasions. If the measurement units considered are days, and, accordingly, the major cycle of interest is a biweekly cycle, then each biweekly period will contain an identical fluctuation pattern, and the initial values will be revisited every two weeks (see Figures 15 and 16 for an illustration, and Figures 18 and 20 for an analogous example with the major cycle being weekly). In case of $\omega_1 = \frac{2\pi}{14}$, and $\omega_{secondary} = \frac{2\pi}{10}$, the same fluctuation pattern will be repeated and the initial values will be revisited every LCM (14,10) = 70 days (see Figure 17 for an illustration, and Figure 22 for an analogous example with the major cycle being weekly). The closer the LCM is to the ω_1 denominator, the more stable are the fluctuation pattern and the corresponding attractor are (see Figures 19, 21, and 23).

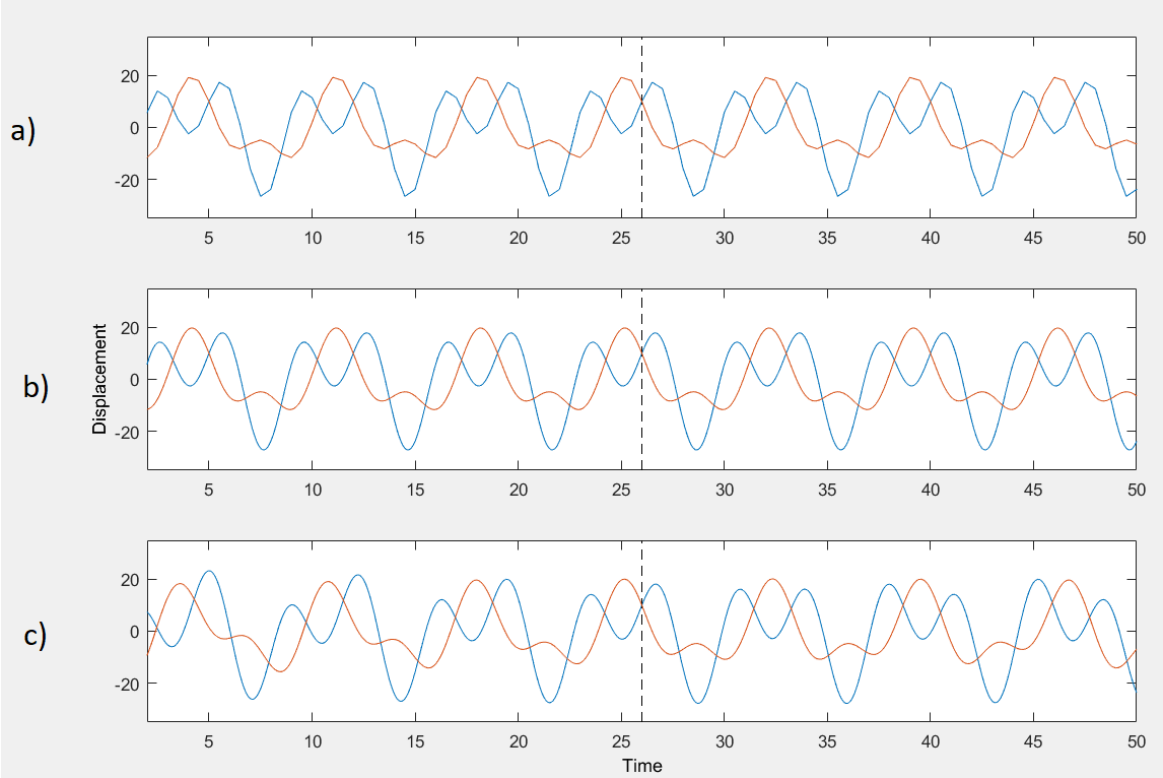

Figure 15. *Comparison of the empirical, theoretical, and multilevel connected mass-spring model detected motion trajectories with* $\omega_1 = \frac{2\pi}{14}$, $\omega_{secondary} = \frac{2\pi}{7}$, $\frac{\kappa_1}{\kappa_2} = \frac{1}{2}$, *and initial value set 9.The orange line represents motion of mass 1, which is defined by x(t) in Equation set (40). The blue line represents motion of mass 2, which is defined by y(t) in Equation set (40). a) Empirical time series of the motion trajectories with 14 equally spaced observations per cycle joined by straight lines; b) Theoretical time series of the motion trajectories; c) Motion trajectories produced by the system detected by the multilevel connected mass-spring model from the empirical time series, given the same set of initial values. The entire set of estimated system parameters was considered adequate. The X-axis represents time units proportional to the measurement occasions. The dashed line marks time zero of the physical system (where the initial values occur).*

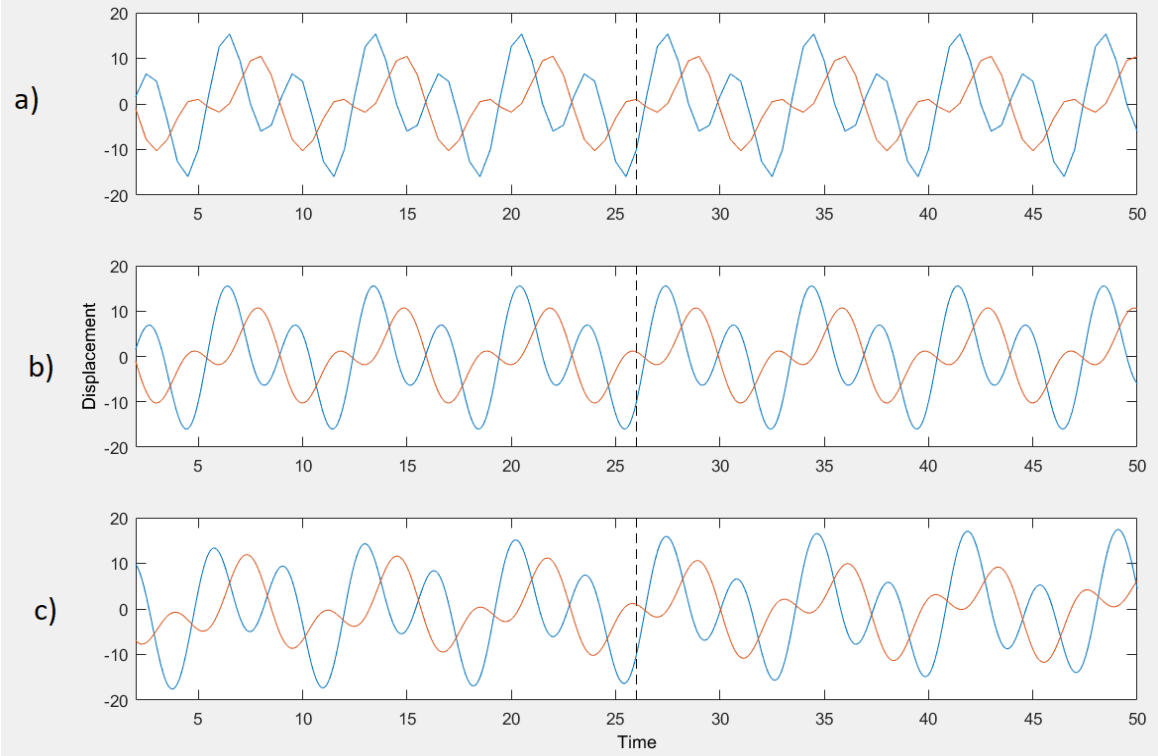

Figure 16. *Comparison of the empirical, theoretical, and multilevel connected mass-spring model detected motion trajectories with* $\omega_1 = \frac{2\pi}{14}$, $\omega_{secondary} = \frac{2\pi}{7}$, $\frac{\kappa_1}{\kappa_2} = \frac{1}{2}$, *and initial value set 6. The orange line represents motion of mass 1, which is defined by x(t) in Equation set (40). The blue line represents motion of mass 2, which is defined by y(t) in Equation set (40). a) Empirical time series of the motion trajectories with 14 equally spaced observations per cycle joined by straight lines; b) Theoretical time series of the motion trajectories; c) Motion trajectories produced by the system detected by the multilevel connected mass-spring model from the empirical time series, given the same set of initial values. The entire set of estimated system parameters was considered adequate. The X-axis represents time units proportional to the measurement occasions. The dashed line marks time zero of the physical system (where the initial values occur).*

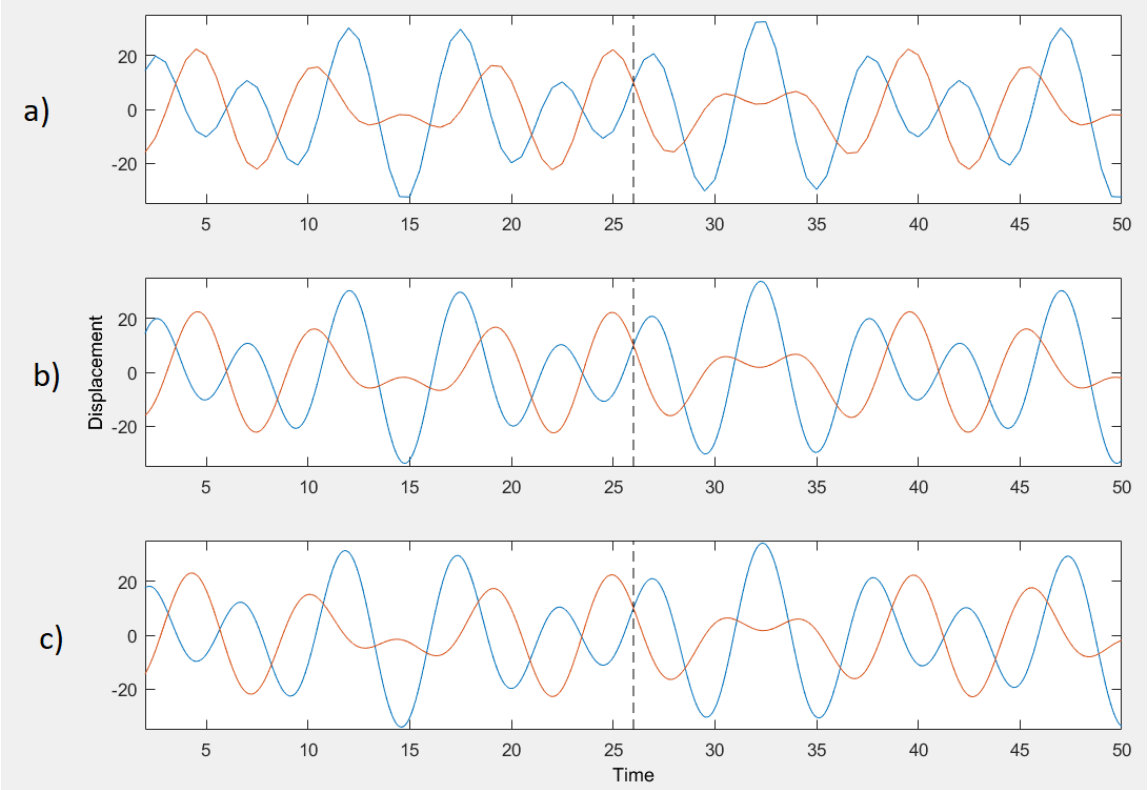

Figure 17. *Comparison of the empirical, theoretical, and multilevel connected mass-spring model detected motion trajectories with* $\omega_1 = \frac{2\pi}{14}$, $\omega_{secondary} = \frac{2\pi}{10}$, $\frac{\kappa_1}{\kappa_2} = \frac{1}{2}$, *and initial value set 9. The orange line represents motion of mass 1, which is defined by x(t) in Equation set (40). The blue line represents motion of mass 2, which is defined by y(t) in Equation set (40). a) Empirical time series of the motion trajectories with 14 equally spaced observations per cycle joined by straight lines; b) Theoretical time series of the motion trajectories; c) Motion trajectories produced by the system detected by the multilevel connected mass-spring model from the empirical time series, given the same set of initial values. The entire set of estimated system parameters was considered adequate. The X-axis represents time units proportional to the measurement occasions. The dashed line marks time zero of the physical system (where the initial values occur).*

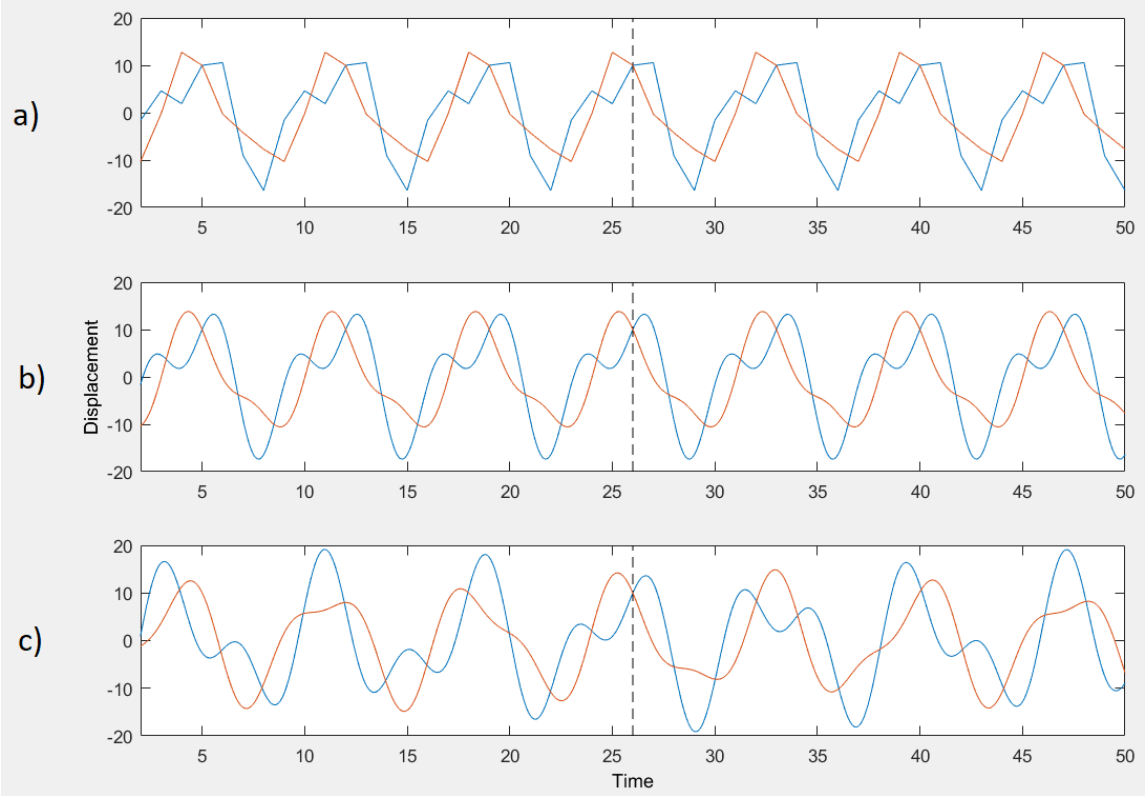

Figure 18. *Comparison of the empirical, theoretical, and multilevel connected mass-spring model detected motion trajectories with* $\omega_1 = \frac{2\pi}{7}$, $\omega_{secondary} = \frac{2\pi}{3.5}$, $\frac{\kappa_1}{\kappa_2} = \frac{1}{2}$, *and initial value set 9. The orange line represents motion of mass 1, which is defined by x(t) in Equation set (40). The blue line represents motion of mass 2, which is defined by y(t) in Equation set (40). a) Empirical time series of the motion trajectories with 7 equally spaced observations per cycle joined by straight lines; b) Theoretical time series of the motion trajectories; c) Motion trajectories produced by the system detected by the multilevel connected mass-spring model from the empirical time series, given the same set of initial values. The entire set of estimated system parameters was considered inadequate. The X-axis represents time units proportional to the measurement occasions. The dashed line marks time zero of the physical system (where the initial values occur).*

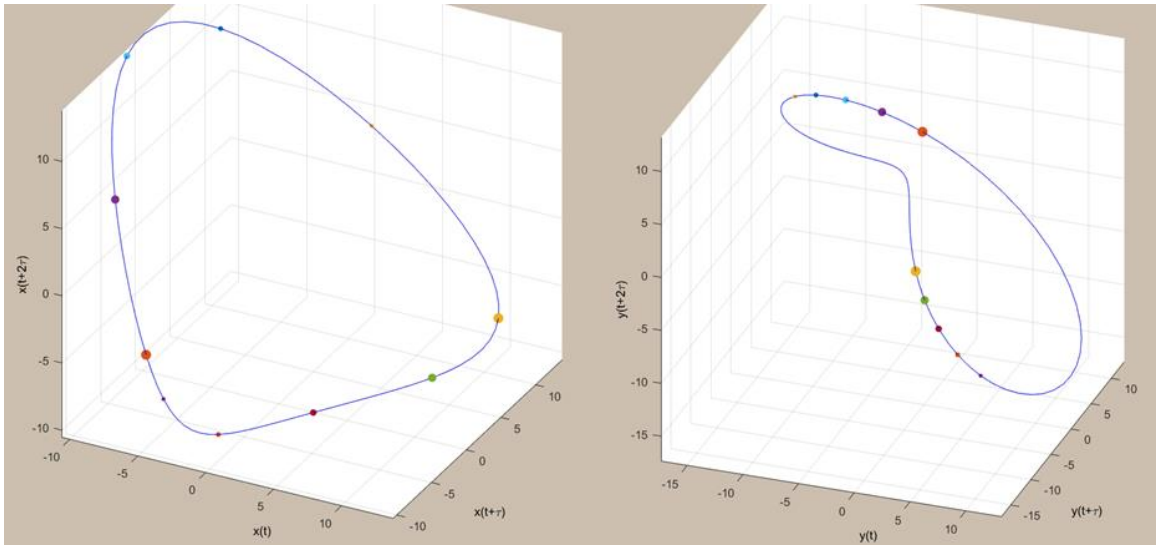

Figure 19. *3D phase portraits of the movement of mass 1, which corresponds to the trajectory x(t) (orange line in Time vs Displacement plots), and mass 2, which corresponds to the trajectory y(t) (blue line in Time vs Displacement plots), in a connected mass-spring system with* $\omega_1 = \frac{2\pi}{7}$, $\omega_{secondary} = \frac{2\pi}{3.5}$, $\frac{\kappa_1}{\kappa_2} = \frac{1}{2}$, *initial value set 9, and* τ*=13.*

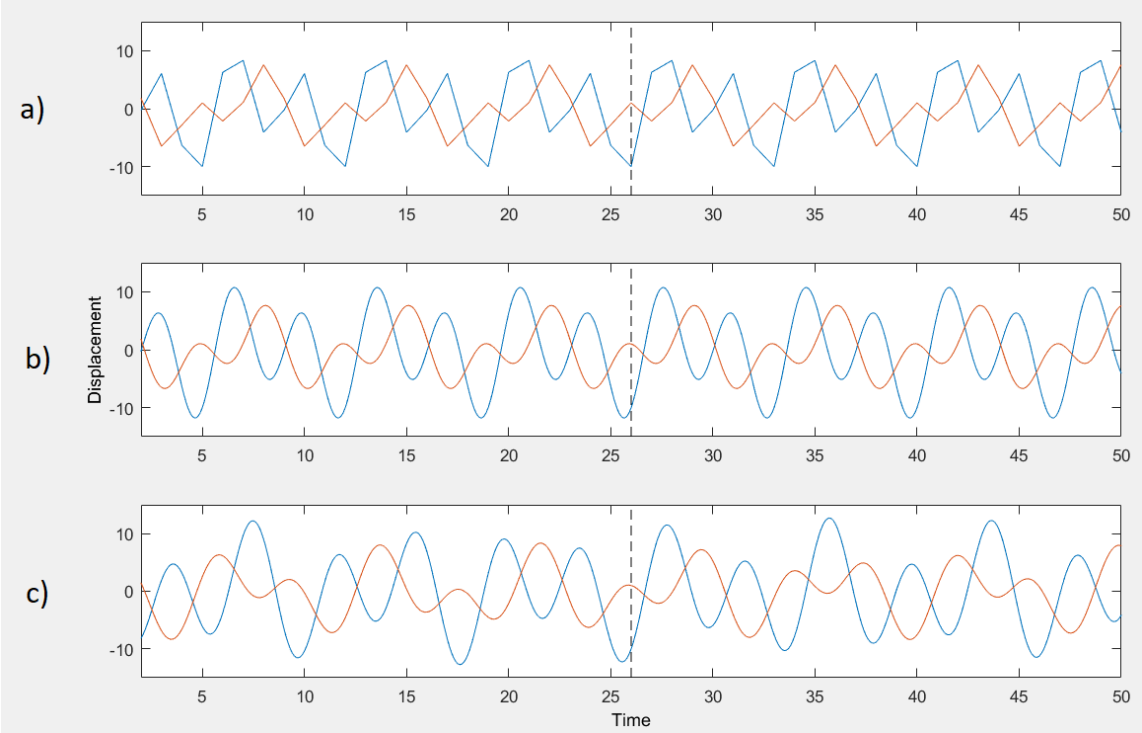

Figure 20. *Comparison of the empirical, theoretical, and multilevel connected mass-spring model detected motion trajectories with* $\omega_1 = \frac{2\pi}{7}$, $\omega_{secondary} = \frac{2\pi}{3.5}$, $\frac{\kappa_1}{\kappa_2} = \frac{1}{2}$, *and*

initial value set 6. The orange line represents motion of mass 1, which is defined by x(t) in Equation set (40). The blue line represents motion of mass 2, which is defined by y(t) in Equation set (40). a) Empirical time series of the motion trajectories with 7 equally spaced observations per cycle joined by straight lines; b) Theoretical time series of the motion trajectories; c) Motion trajectories produced by the system detected by the multilevel connected mass-spring model from the empirical time series, given the same set of initial values. The entire set of estimated system parameters was considered inadequate. The X-axis represents time units proportional to the measurement occasions. The dashed line marks time zero of the physical system (where the initial values occur).

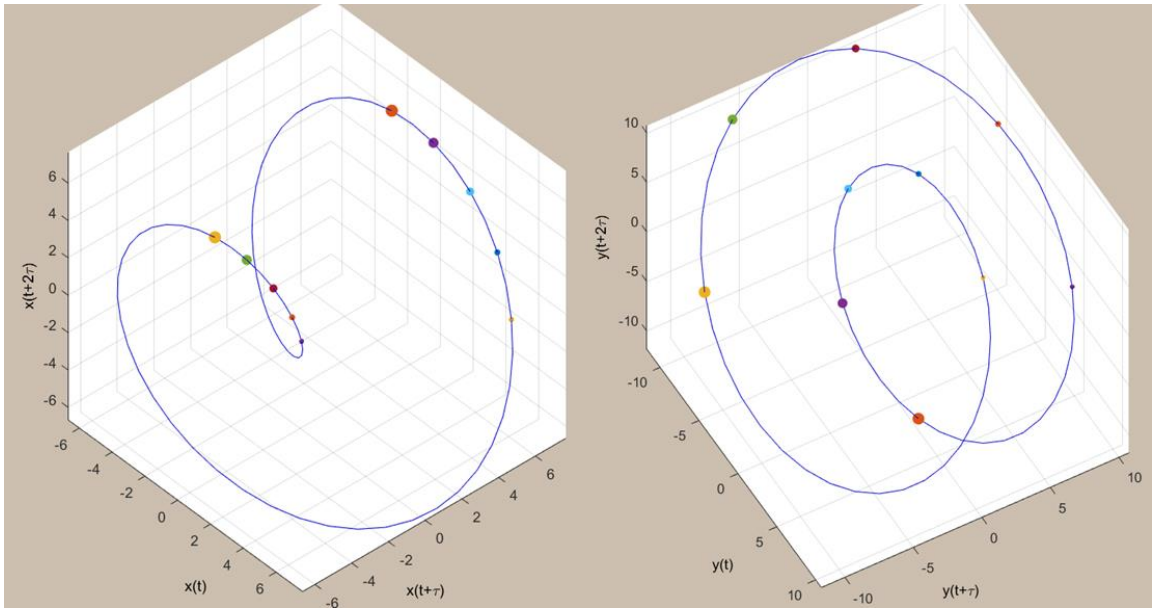

Figure 21. *3D phase portraits of the movement of mass 1, which corresponds to the trajectory x(t) (orange line in Time vs Displacement plots), and mass 2, which corresponds to the trajectory y(t) (blue line in Time vs Displacement plots), in a connected mass-spring system with* $\omega_1 = \frac{2\pi}{7}$, $\omega_{secondary} = \frac{2\pi}{3.5}$, $\frac{\kappa_1}{\kappa_2} = \frac{1}{2}$, *initial value set 6, and* τ*=9.*

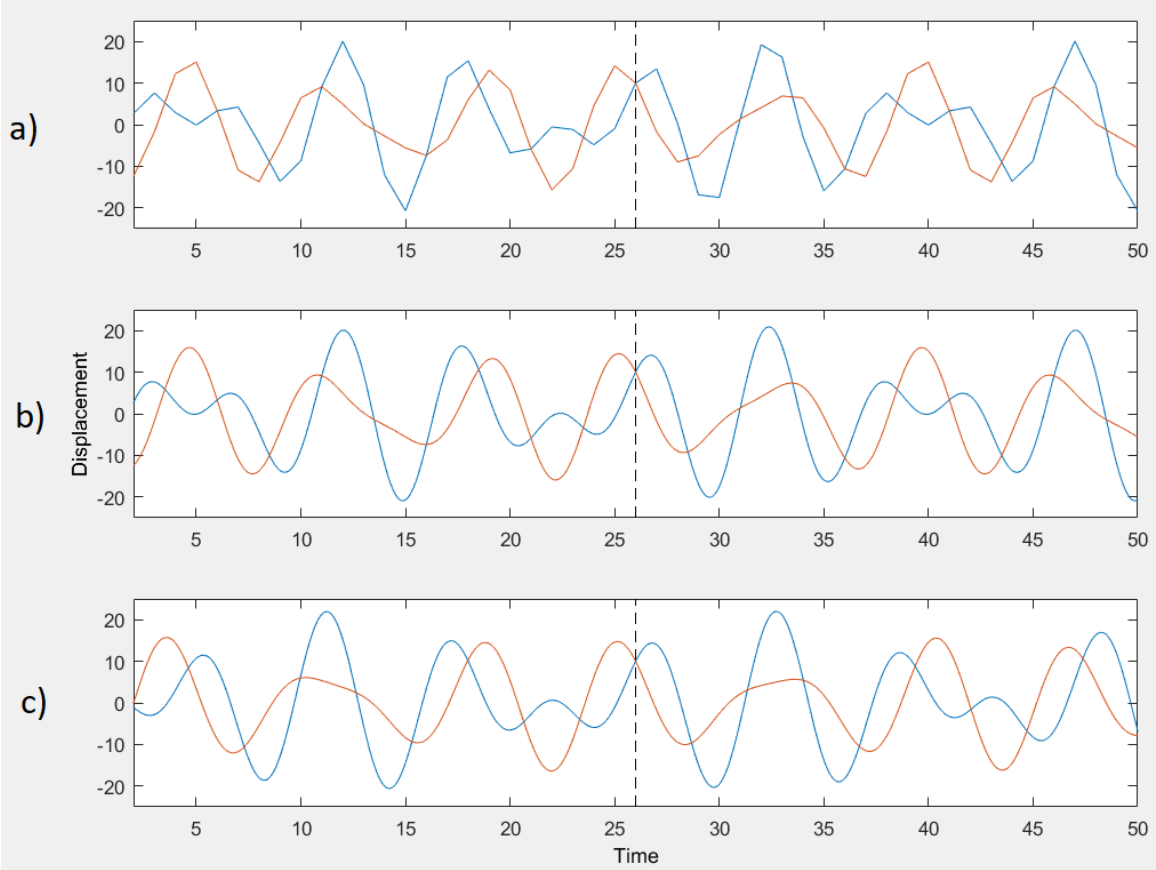

Figure 22. *Comparison of the empirical, theoretical, and multilevel connected mass-spring model detected motion trajectories with* $\omega_1 = \frac{2\pi}{7}$, $\omega_{secondary} = \frac{2\pi}{5}$, $\frac{\kappa_1}{\kappa_2} = \frac{1}{2}$, *and initial value set 9. The orange line represents motion of mass 1, which is defined by x(t) in Equation set (40). The blue line represents motion of mass 2, which is defined by y(t) in Equation set (40). a) Empirical time series of the motion trajectories with 7 equally spaced observations per cycle joined by straight lines; b) Theoretical time series of the motion trajectories; c) Motion trajectories produced by the system detected by the multilevel connected mass-spring model from the empirical time series, given the same set of initial values. The entire set of estimated system parameters was considered inadequate. The X-axis represents time units proportional to the measurement occasions. The dashed line marks time zero of the physical system (where the initial values occur).*

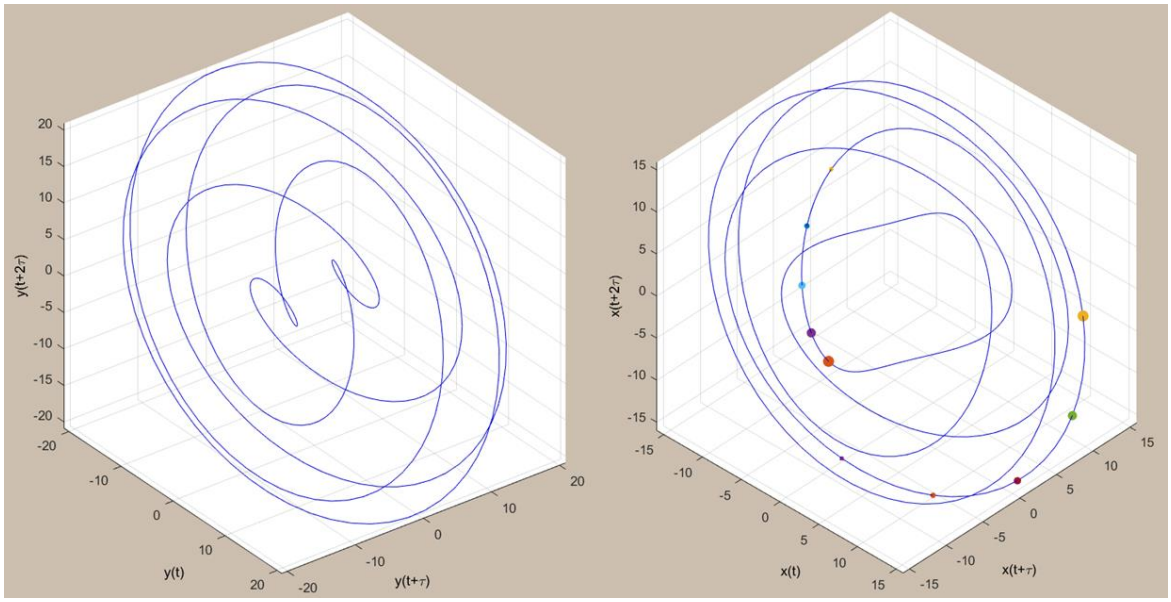

Figure 23. *3D phase portraits of the movement of mass 1, which corresponds to the trajectory x(t) (orange line in Time vs Displacement plots), and mass 2, which corresponds to the trajectory y(t) (blue line in Time vs Displacement plots), in a connected mass-spring system with* $\omega_1 = \frac{2\pi}{7}$, $\omega_{secondary} = \frac{2\pi}{5}$, $\frac{\kappa_1}{\kappa_2} = \frac{1}{2}$, *initial value set 9, and* τ*=13.*

It can be seen in Figures 15 through 23 that different sets of initial conditions produce different motion trajectories. The multilevel connected mass-spring model is designed to detect the parameters of the underlying physical system that produced the imputed trajectories, regardless of the initial conditions. Thus, for instance, the trajectory pair depicted in Figures 18-19 is expected to yield identical parameter estimates to the trajectory pair pictured in Figures 20-21 despite the evident difference in their shape and amplitude. In order to visually inspect the adequacy of the system parameter set estimated by the multilevel model, trajectories of the connected mass-spring system with the estimated parameters were reproduced under the same initial conditions as the original system that produced the imputed trajectories (pictured in section c) of Figures 15-18, 20, and 22). They were visually compared to the original trajectory pair that was analyzed by the model (pictured in sections a) and b) of Figures 15-18, 20, and 22). As can be seen in Figures 18, 20, and 22, when all parameter estimates were adequate, they comprised a system that under the same initial conditions as the original system, produced highly similar trajectories to those of the original system (i.e., c) highly similar to b)). In contrast, as can be seen in Figures 15-17, when some parameter estimates were not adequate, they described a system that under the same initial conditions as the original system produced trajectories that were only somewhat similar to those of the original system (i.e., c) only somewhat similar to b)).

In addition to the multilevel connected mass-spring model detecting the same underlying physical system regardless of the initial conditions, by its design, it should also be capable of detecting the same physical system regardless of where/when the initial conditions occur in the measured trajectories. That is, the same underlying physical system parameters should be detected whether the initial values are present at the first measurement occasion, whether they are present in the middle, or at any other point of the measured piece of trajectories. Since, as explained above, any set of initial conditions in a closed connected mass-spring system will be revisited at some point, it guarantees that initial conditions can occur at any measurement occasion with no discontinuity. The pilot study confirmed this phenomenon by producing either identical or virtually identical parameter estimates under identical conditions, but with different initial value location on the measured time scale.

The simulation presented in this work had all the initial conditions located at the center of the trajectories (marked with a vertical dash-line in Figures 15-18, 20, and 22). Such a location choice was based on two reasons. First, it was the most efficient choice in terms of the simulation programming. Second, if the results follow the mathematical predictions and justifications, then they demonstrate once again that the initial conditions do not have to coincide with the first measurement occasion in order for the connected mass-spring model to correctly detect the underlying physical system. Thus, all theoretical explanations and predictions made in this thesis are applicable regardless of the initial value placement on the measured time scale.

In Figures 15, 17, 18 and 22, where the initial value set is 9 ($p_1 = 10, p_2 = 10, v_1 = -10, v_2 = 10$), the initial position of both masses is 10. Accordingly, all the orange and blue lines in all the trajectory types (a, b, and c) of the listed figures have a displacement value of 10 at the dashed line. v_1, or velocity of mass 1, is negative 10, whereas v_2, or velocity of mass 2 is positive 10. Hence, when the motion trajectories are set to have the initial value set 9, the orange trajectory that belongs to mass 1, and the blue trajectory that belongs to mass 2 should have steep and similar slopes that go in opposite directions with the orange one going down (negative velocity), and the blue one going up (positive velocity) at the dashed line. The slopes around the dashed line (where the x-axis component of the slope is in units of measurement occasions), that represent initial velocity, are not exactly -10 and 10, as whenever time exceeds 0, potential energy stored in the springs starts turning into kinetic energy, which directly contributes to the velocity of the masses. Mass 1's initial position is away from its wall (the spring that connects it to the wall is stretched), and its initial velocity is directed towards its wall (in the direction the mass would move if released with initial velocity 0). As the spring attached to the wall contracts, it produces kinetic energy that is directed to the same direction as the initial velocity. Hence, the two components add up, giving a steeper slope than just the initial velocity itself. Analogously, the initial position of mass 2 is located closer to its wall than its resting position. Hence, the corresponding spring attached to the right wall is compressed. When time exceeds 0, the spring attempts to expand, which

produces kinetic energy in the direction away from the right wall, which is opposite to the initial velocity of the mass 2. Therefore, the initial slope/velocity of the blue trajectory is attenuated. The resting length of the middle spring is not changed by the initial position of the masses and hence it does not contribute to the velocities of the masses around time 0. As one can see, the explicated pattern is present in the theoretical (parts b) and detected (parts c) trajectory pairs, and approximately present in the case of empirical time series trajectories (parts a). That is, in figures that represent trajectories with initial value set 9, the orange trajectory has a negative slope at the dashed line, while the blue trajectory has a positive slope of a similar magnitude, but with the orange slope being steeper than the blue one.

As explained above, the identical components of the trajectories together with the initial conditions repeat themselves each 14 measurement units in Figure 15 (e.g., trajectories in a) and b) at time 5 are identical to the trajectories at time 12, as there are 2 observations per time unit plotted). Analogously, identical components are repeated each 70 measurement occasions in Figure 17 (the initial values are not repeated in the presented segment, as they are outside of it), each 7 measurement units in Figure 18 (e.g., the trajectories in a) and b) at time 10 are identical to the trajectories at time 17), and each 35 measurement units in Figure 22 (e.g., the trajectories in a) and b) at time 5 are identical to the trajectories at time 40). Accordingly, the attractors in Figure 19 that represent 3D phase portraits of the theoretical trajectories in Figure 18 are very stable, representing a single cyclic pattern in the 3D space. This result reflects the fact that each major cycle (defined by ω_1) is repeated identically throughout the generated time series. Similarly, the attractors in Figure 23 that represent 3D phase portraits of the theoretical trajectories in Figure 22, contain 5 differently shaped spiraled cycles, which reflect the fact that each major cycle (of frequency $\omega_1 = \frac{2\pi}{7}$) is repeated identically with a lag of 5 full cycles (35 measurement occasions) throughout the generated time series. Hence, there are 5 differently shaped cycles that are repeated throughout the generated (and infinite) time series.

Similarly, in Figures 16 and 20, where the initial value set is 6 ($p_1 = 1, p_2 = -10, v_1 = -1, v_2 = 10$), the initial position of mass 1 is 1, and the initial position of mass 2 is -10. Accordingly, all the orange lines in all the trajectory types (a, b and c) in the two figures have a displacement value of 1, and all the blue lines have a displacement value of -10 at the dashed line. The slopes of the trajectories (where the x-axis component of the slope is in units of measurement occasions) right after the dashed line are slightly steeper than the ones indicated in the initial conditions (-1 and 10). This increase emerges as the initial positions of both masses are away from their corresponding walls, which causes the side springs to stretch. When time exceeds 0, the potential energy stored in the stretched side springs gradually turns into kinetic energy directed towards the walls, which coincides with the direction of the initial velocities, and therefore positively contributes to the magnitude of the velocity of the masses. Moreover, the middle spring is compressed at time zero. Therefore, when the masses are released, the potential energy

stored in it turns into kinetic energy that is directed to the sides, additionally pushing both masses towards their walls and contributing to the magnitude of the velocities.

The frequency of repetition of identical trajectory components, including initial values, is identical to the ones with the initial value set 9, given that all the other parameters are equal (i.e. repetition frequency is the same in Figures 15 and 15, and Figures 18 and 20). Accordingly, the attractor in Figure 17 that represents a 3D phase portrait of the theoretical trajectories in Figure 20, same as the attractor in Figure 19 that represents the phase portrait of theoretical trajectories in Figure 18, contains a stable single cycle pattern. However, this time with a much more prominent secondary cycle frequency, $\omega_{secondary} = \frac{2\pi}{3.5}$, reflecting component that looks like a loop inside of the bigger cycle. The stable single cycle pattern reflects that each major cycle (defined by ω_1) is repeated identically throughout the generated time series, i.e. there is a single cycle shape that is repeated over and over in each mass 1 trajectory and mass 2 trajectory.

The initial values that comprise initial value dependent coefficients (C_1, C_2, C_3, C_4, which precede all the sine and cosine components of the equations of the trajectories) are directly related to the amplitudes of the trajectories. If all the initial values were increased 10 times, the trajectories would maintain the same shape structures, but would be stretched 10 times along the y-axis (i.e., the amplitude increases 10 times). See Figure 22 for the original plot, and Figure 24 for the plot of the trajectories with all initial values increased 10 times. Analogously, if all the initial values were decreased 10 times, the trajectories would maintain the same shape structures, but would be compressed 10 times along the y-axis (i.e. the amplitude decreases 10 times). See Figure 22 for the original plot, and Figure 25 for the plot of the trajectories with all initial values decreased 10 times.

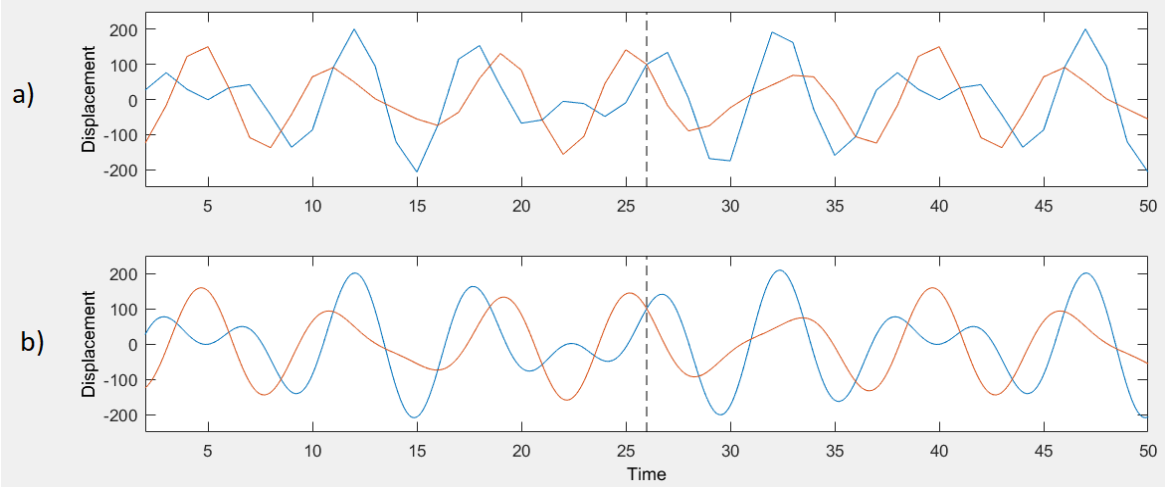

Figure 24. *The empirical and theoretical connected mass-spring model motion trajectories with* $\omega_1 = \frac{2\pi}{7}$, $\omega_{secondary} = \frac{2\pi}{5}$, $\frac{\kappa_1}{\kappa_2} = \frac{1}{2}$, *and initial value set 9 multiplied by*

10. The orange line represents motion of mass 1, which is defined by x(t) in Equation set (40). The blue line represents motion of mass 2, which is defined by y(t) in Equation set (40). a) Empirical time series of the motion trajectories with 7 equally spaced observations per cycle joined by straight lines; b) Theoretical time series of the motion trajectories. The X-axis represents time units proportional to the measurement occasions. The dashed line marks time zero of the physical system (where the initial values occur).

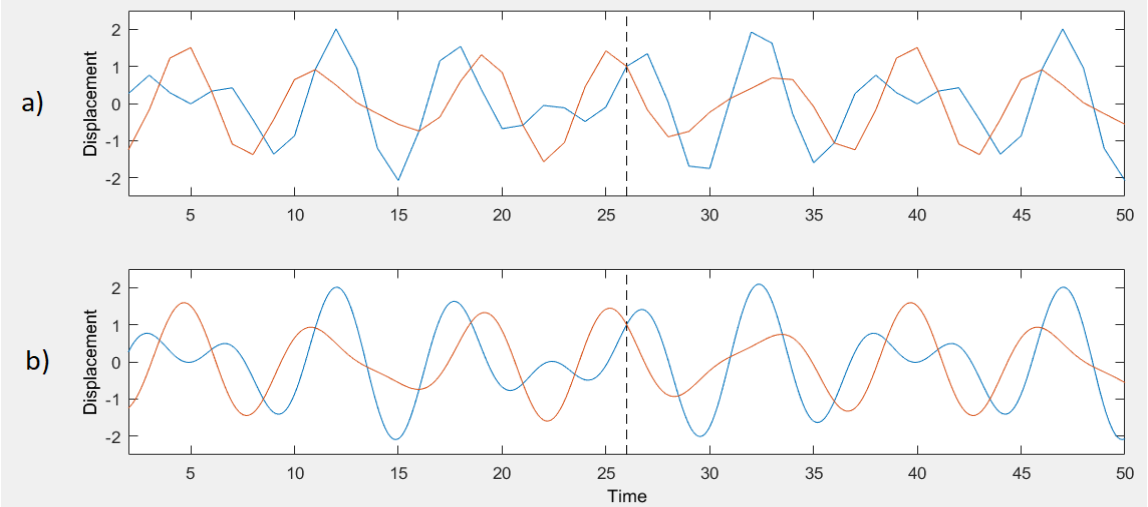

Figure 25. *The empirical and theoretical connected mass-spring model motion trajectories with* $\omega_1 = \frac{2\pi}{7}$, $\omega_{secondary} = \frac{2\pi}{5}$, $\frac{\kappa_1}{\kappa_2} = \frac{1}{2}$, *and initial value set 9 divided by 10.The orange line represents motion of mass 1, which is defined by x(t) in Equation set (40). The blue line represents motion of mass 2, which is defined by y(t) in Equation set (40). a) Empirical time series of the motion trajectories with 7 equally spaced observations per cycle joined by straight lines; b) Theoretical time series of the motion trajectories. The X-axis represents time units proportional to the measurement occasions. The dashed line marks time zero of the physical system (where the initial values occur).*

If all the initial values were increased an infinite number of times, the change in the motion trajectories would be analogous. That is, in the classical connected mass-spring system defined in this thesis there is no point where the behavior of the masses would suddenly change because of physical limitations. The defined system will never reflect masses colliding with the walls or with each other. The defined system does not contain any elements that would restrict the length, the elasticity, or the cross-section area of the springs. The only parameter of the spring that is defined in the classical mass-spring models is stiffness (k). It is known that stiffness, $k = \frac{AE}{l}$, where A represents cross-section area, E represents the modulus of elasticity, and l represents length of the spring. Since stiffness, k, is the only parameter in this formula that is fixed, the interaction of the other 3 parameters can vary without restriction. This means that whatever stiffness of the spring, its length might always be assumed to be as large as

needed for the masses to not collide with each other and with the walls. In theory, A and E can be as large as infinity, allowing the length to be $l = AE / k = \infty / k = \infty$. In order for the connected mass-spring system to reflect certain physical restrictions, they would have to be explicitly defined in the force equations. In the connected mass-spring system whose force equation construction was explicitly delineated in the introduction, no such element was introduced, and therefore, the system behavior detected and produced by the model discussed in this thesis follows an assumption that the distance between the two masses and the walls is always enough to avoid collisions.